

Non collinear magnetic polarization on the basis of Density Functional Theory

D I S S E R T A T I O N

zur Erlangung des akademischen Grades

Doctor rerum naturalium
(Dr. rer. nat.)

vorgelegt

der Fakultät Mathematik und Naturwissenschaften
der Technischen Universität Dresden

von

Vito Domenico Pietro Servedio
geboren am 22. Okt 1966 in Toritto (Italien)

TECHNISCHE UNIVERSITÄT DRESDEN
2000

Contents

Contents	i
List of Figures	iii
List of Tables	v
Introduction	1
1 Short review of Density Functional Theory	5
1.1 Hohenberg-Kohn theory	6
1.2 Extension to spin systems	9
1.3 Lieb's theory	11
1.4 Relativistic Density Functional Theory	12
1.5 Local Spin Density Approximation	16
1.6 The collinear approximation	17
1.7 The self interaction correction	20
2 The Kohn-Sham-Dirac equation	23
2.1 The effective Hamiltonian	24
2.2 The four component spin density matrix	25
2.3 The Kohn-Sham-Dirac equation in the spherical approximation	26
2.4 Introduction of a collinear XC-field	29
2.5 Non spherical KSD equations	32
2.6 Non collinear KSD equations	35
2.7 Transversal XC-field	36
3 Results	39
3.1 Non spherical calculations	39
3.2 Non collinear calculations	50
3.3 Transversal XC-field calculations	58

4 Application of the spherical KSD equations	63
4.1 Relativistic self interaction corrections	63
4.2 Photoemission cross sections	69
Conclusions	79
Bibliography	81
Acknowledgments	87

List of Figures

1	DFT and HF records in INSPEC databases	2
1.1	Example of non collinear magnetization	19
1.2	Example of approximate collinear magnetization	20
2.1	Energy levels of a $3d$ electron in the potential $-30/r$ in a homogeneous magnetic field	30
2.2	Finding the energy eigenvalues in presence of a collinear XC-field	31
3.1	LSDA calculated NoSph-Sph total energy differences for rare- earths	41
3.2	SIC-LSDA calculated NoSph-Sph total energy differences for rare-earths	43
3.3	Rare-earth first ionization energies	45
3.4	Rare-earth second ionization energies	46
3.5	Rare-earth third ionization energies	47
3.6	Rare-earth percentual spin reduction due to a non spherical symmetric XC-field	48
3.7	Calculated quadrupole momenta in rare-earth atoms and +3 ions	49
3.8	Contribution to the Hartree energy of quadrupolar and oc- tupolar momenta in rare-earth +3 ions	49
3.9	SIC-LSDA calculated NsNc-NoSph total energy differences for rare-earths	50
3.10	Collinearity parameter in rare-earths +3 ions	51
3.11	Rare-earth percentual spin reduction due to a non spherical and non collinear XC-field	52
3.12	Non collinear XC-field in Ce^{+3}	54
3.13	Non spherical and collinear XC-field in Pb^{+}	55
3.14	Non spherical and collinear XC-field sources in Pb^{+}	55
3.15	Non spherical and non collinear XC-field in Pb^{+}	56
3.16	Non spherical and non collinear XC-field sources in Pb^{+}	56

3.17	Non spherical and non collinear XC-field in C^+	57
3.18	Source-free XC-field in C^+	59
3.19	Source-free XC-field in Pb^+	60
3.20	Spin magnetization arising from a source-free XC-field in Pb^+	61
3.21	SIC-LSDA calculated SF-NoSph total energy differences for rare-earths	62
3.22	Rare-earth percentual spin reduction due to a source-free XC- field	62
4.1	Bouncing problems of an alternative SIC scheme	67
4.2	Simplified photoemission process in an atom	70
4.3	Pd ($4d$) and (ϵ, f) wave functions	72
4.4	Pd ($4d$) and (ϵ, f) wave functions nearby the Cooper minimum	73
4.5	Pd ($4d$) photoemission cross section	74
4.6	U ($5f$) photoemission cross section	75
4.7	U ($5f$) Cooper minima position as a function of the radial cut-off	75
4.8	Pd ($4d$) photoemission cross section with and without cut-off .	76
4.9	Pd ($4d$) Cooper minima position as a function of the radial cut-off	77
4.10	Pd ($4d$) experimental photoemission scattered electron intensity	78

List of Tables

1.1	Hydrogen ionization energy and atomic radius	21
2.1	Relations among k , j , l_A (angular momentum quantum number of the electronic (large) part) and l_B (angular momentum quantum number of the positronic (small) part)	27
2.2	Order of magnitude of the ratio spin-orbit splitting / XC-field in the outer p shell of carbon-group atoms	31
3.1	Effects of the basis set choice on non-spherical total energy calculations for the Pr^{+3} ion	39
3.2	Self interaction energies in La^{III} $5d$ and La^{II} $4f$ orbitals	42
3.3	IP3 energy for the Pr atom	44
4.1	Hydrogen $1s_{\frac{1}{2}}$, $2s_{\frac{1}{2}}$, $2p_{\frac{1}{2}}$ states	65
4.2	Fm^{+99} $1s_{\frac{1}{2}}$, $2s_{\frac{1}{2}}$, $2p_{\frac{1}{2}}$ states	66
4.3	SIC vs new-SIC total energies	69
4.4	SIC vs hybrid-SIC total energies in heavy atoms and ions	69
4.5	SIC vs hybrid-SIC ionization energies in heavy atoms	69

Introduction

The whole story began thirty-five years ago.

I would not like to diminish the merits of Fermi [1] and Thomas [2], who pioneered in the twenties the possibility to describe the atomic ground state in terms of functionals of the electronic charge density. However Hohenberg and Kohn [3] were the persons who gave the fuel and successively Kohn and Sham [4] those who provided the first engine to move the fantastic apparatus called Density Functional Theory (DFT).

The story culminated with Kohn's Nobel price (1998).

Not just a single man was rewarded with this Nobel price, but those who believed in the future of the DFT. At the end of the sixties, Hartree-Fock (HF) methods were raging in the scientific community, especially among quantum-chemists, (see Fig. 1) and a lot of courage was needed to follow a new branch. Nowadays, DFT based methods are being used largely in many body theory [5, 6, 7, 8, 9, 10, 11, 12, 13, 14]. This is mainly caused by their unsurpassed efficiency, i.e. the ratio between useful output and implementation efforts. One indicator of the increasing use of DFT is the number of records retrieved from the INSPEC databases¹ by searching for the keywords "density", "functional" and "theory". In Fig. 1 this is compared with a similar search for the keywords "Hartree" and "Fock", which parallels the overall growth of the INSPEC databases themselves (for any given year, approximately 0.3% of the records have the Hartree-Fock keywords).

Let me carry on further the metaphor of the engine I have used before. It's well known that an engine cannot have a 100% efficiency. Nevertheless, there are vehicles and even spacecrafts which use it. We cannot produce a perfect engine, but we can use it in its abortive state anyway. We can try to improve our model engine all the time in order to go further with the same amount of fuel. We have to check *any* possibility, any screw and see how far we can go.

In this unorthodox way I wish to present the philosophy which lies behind my work. DFT is an *exact* theory for ground states. It is a theory which

¹See for example: <http://www.fiz-karlsruhe.de/stn/Databases/inspec.html>

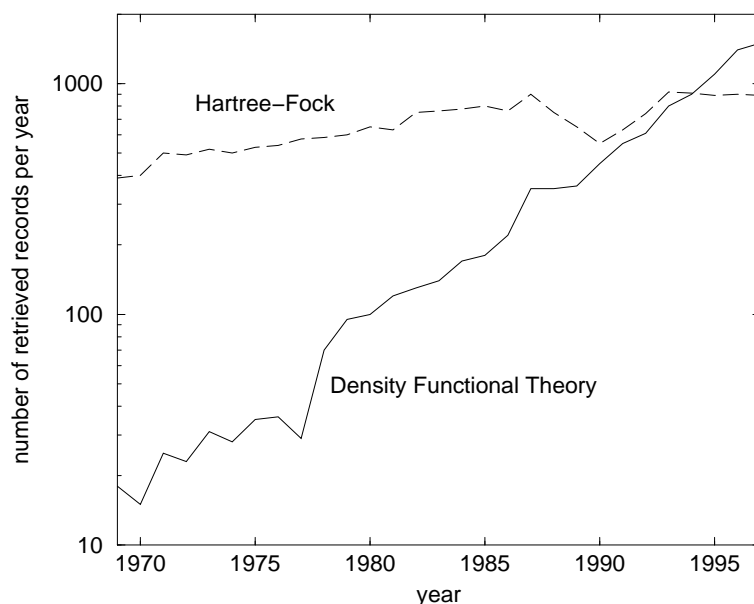


Figure 1: DFT and HF records in INSPEC databases. Data are taken from Ref. [15].

in principle allows, to give a difficult example, to calculate van der Waals energies being very important in organic chemistry and elsewhere [16]. It's the fuel.

But, any fuel needs an engine and in the DFT case there are a lot of, corresponding to which approximation one uses to express the unknown exchange and correlation (XC) energy density functional: LDA (Local Density Approximation), LSDA (Local Spin Density Approximation), GGA (Generalized Gradient Approximation), MGGA (Meta-GGA), ... [17, 18, 19, 20]. These *model* engines are not perfect, such that, to refer to the previous example, they fail to capture the essence of van der Waals energies [16], and one has to improve them in order to approach the equivalent to the Carnot engine, the one with maximum efficiency. What I shall deal with in this work is mainly the LSDA engine which is being tacitly used in the community with the further intra-atomic spin collinear approximation², about which I shall extensively write later. I shall try to remove this rough collinear screw and replace it with the smoother non-collinear one. The price to pay will be a big increase of degrees of freedom which in parallel turns into a big increase of computational effort. For this reason the systems I shall consider will be isolated atoms and ions.

²Remarkable exceptions are given by ref. [21, 22, 23].

In chapter 1 we shall present a brief introduction to the density functional theory, starting from the original Hohenberg and Kohn formulation and landing on the relativistic theory. An overview on the local spin density approximation (LSDA) of the exchange and correlation energy functional closes the chapter.

Chapter 2 is devoted to more technical stuffs. The method we used to solve the Kohn-Sham-Dirac equation is briefly sketched, purposely without being drowned into software details. The non spherical, non collinear and finally the transversal exchange correlation field calculations are explained.

In chapter 3 the methods described in the second chapter are used to produce results. The set of rare-earth atoms and ions is mainly analyzed.

In chapter 4, which can be considered as an appendix, we present two applications of the spherical and collinear approximated functionals.

All over this work atomic units will be used, unless otherwise stated, i.e.

$$|e| = \hbar = m_e = 1$$

As a consequence the speed of light will be equal to the inverse of the fine structure constant: $c = \alpha^{-1}$. Total energies will be presented in rydbergs (1 Hartree = 1 a.u. = 2 Ry $\approx 2 \times 13.6$ eV).

Bold letters usually denote three dimensional vectors. The letter x will be used as a short cut for $(s \mathbf{r})$, denoting both spin and spatial variables. The symbol $\int dx$ is to be read as $\sum_s \int d\mathbf{r}$.

The pictures representing vector and scalar fields were plotted using the program ‘Mathematica ©’³. Other plots were drawn with the help of the shareware program ‘xmgr’⁴.

³cf. <http://www.wolfram.com/products/mathematica/>

⁴cf. <http://plasma-gate.weizmann.ac.il/Xmgr/>

Chapter 1

Short review of Density Functional Theory

Introduction

One crucial problem in modern physics is the determination of the properties of a many-body ground state. Even for the helium atom with a model infinitely massive point nucleus the task is very involved. If one would include quantum electrodynamics effects even hydrogenoid atoms would be very difficult to treat [24]. Still more involved is the situation in molecules and solids, in which also the nuclear motion is to be considered for a complete understanding of the ground state properties. Of course approximations can be made, such to disentangle motions which occur at different time scales (adiabatic approximations).

One would have a quite simple picture if one had a system composed of non interacting particles. Its Hamiltonian would be the sum of single particle Hamiltonians and the difficulty of the problem would be connected to the difficulty of solving the eigenvalue problem for such single particle Hamiltonians. Taking into account the proper symmetry of the total ground state wave function with respect to particles interchange, which for fermions means considering non vanishing determinants and for bosons just a product of the lowest state eigenfunctions, would yield the required ground state wave function without any special effort. It is then logical to think that the determination of the ground state properties of interacting particles would be much more simplified if one could substitute the interacting Hamiltonian with an effective and equivalent non interacting one. This is in fact the main idea which lies behind DFT: to provide the mathematical justification for the use of a fictitious non-interacting system under the action of an effective potential instead of the actual, complicated interacting one.

It is not the purpose of this work to treat deeply the essence of Density Functional Theory. There are a plenty of books and reviews on this topic (see [17, 18, 19] for example). Nevertheless, I shall try to sketch the basic ideas which lie behind this theory, mainly in order to introduce the relativistic extension of it [19, 23] which is necessary to understand the spin-non-collinearity problem. In the next two sections I shall briefly review the Hohenberg-Kohn theory together with the Kohn-Sham scheme in the non relativistic case, and Lieb's theory.

1.1 Hohenberg-Kohn theory

Consider the Hamiltonian in its spatial representation

$$\mathcal{H} = \sum_i^N \mathcal{T}_i + \sum_i^N v(\mathbf{r}_i) + \frac{1}{2} \sum_{i \neq j}^N w(|\mathbf{r}_i - \mathbf{r}_j|) \quad (1.1)$$

of an inhomogeneous fluid of N interacting particles in a static external potential $v(\mathbf{r})$: \mathcal{T} is the kinetic energy operator and $w(|\mathbf{r}_i - \mathbf{r}_j|)$ is an inter-particle interaction term which, for an electron fluid¹, is represented by the usual coulombic repulsion potential $\frac{1}{|\mathbf{r}_i - \mathbf{r}_j|}$.

The ground state energy is by definition:

$$\inf_{\Psi} \langle \Psi | \mathcal{H} | \Psi \rangle \quad | \Psi \rangle \text{ antisymmetric.} \quad (1.2)$$

$\langle \mathbf{r}_1, \dots, \mathbf{r}_N | \Psi \rangle = \Psi(\mathbf{r}_1, \dots, \mathbf{r}_N)$ is the many body wave function in its spatial representation. The infimum is necessary because for a fixed v some of the electrons might be required to flow to infinity (for instance this is the case with $v(\mathbf{r}) = -\frac{1}{r}$ and $N > 2$: a proton can bind only two electrons). Minimizing in the subspace of normalized antisymmetric wave functions one gets the time independent Schrödinger equation:

$$\mathcal{H} | \Psi \rangle = E | \Psi \rangle \quad (1.3)$$

where E is a Lagrange multiplier which is easily shown to be the ground state energy. The direct solution of the latter equation is very complicated even if contemporary numerical methods are used. The difficulty resides in the big amount of degrees of freedom, $3N$, which confines the direct resolution of the eq. (1.3) to few cases with small N .

One defines the spatial density of the ground state Ψ as

$$n(\mathbf{r}) = N \int \Psi(\mathbf{r}, \mathbf{r}_2, \dots, \mathbf{r}_N) \Psi^*(\mathbf{r}, \mathbf{r}_2, \dots, \mathbf{r}_N) d\mathbf{r}_2 \cdots d\mathbf{r}_N. \quad (1.4)$$

¹From now on only electrons will be considered.

Consider the total number of electrons N as fixed. Hohenberg and Kohn showed [3] that *the external potential $v(\mathbf{r})$ is a unique functional of the ground state spatial density $n(\mathbf{r})$* . Namely,

$$v(\mathbf{r}) = v[n(\mathbf{r})] \quad (\text{first theorem}). \quad (1.5)$$

Since the external potential completely determines the ground state via eq. (1.3), also

$$\Psi = \Psi[v[n(\mathbf{r})]] \quad \text{and} \quad E = E[v[n(\mathbf{r})]] \quad (1.6)$$

hold. In the original paper only non degenerate ground states were taken into account. In that particular case even a one-to-one correspondence holds between v and n .

Now consider the functional $E_v[n']$ in which the potential v has been fixed independently from the density. It was demonstrated in the same article, that *the functional $E_v[n']$ assumes its minimum value for the correct ground state density n , rather than for any other density distribution n' with the same total number of particles N* (second theorem).

It is remarkable that a complicated many body ground state depends univocally on the spatial density: it means that one does not really need $3N$ degrees of freedom but can obtain the ground state density and energy with a variational approach that involves a quantity, the $n(\mathbf{r})$, with *only* 3 degrees of freedom, provided that the density functionals to vary are known.

With the help of merely these two theorems, very little can be done. What one can write is a Thomas-Fermi like equation

$$\frac{\delta}{\delta n} E_v[n] = \mu \quad (1.7)$$

with a Lagrange multiplier μ necessary for the fixed particle number condition, and $E_v[n]$ an unfortunately unknown functional. If one would try to make blind approximations at this stage on the functional $E_v[n]$ one would have probably the same problems met by the Thomas-Fermi theory, which is anyway an asymptotically exact theory. In order to overcome these problems, Kohn and Sham [4] proposed a tricky decomposition of the functional $E_v[n]$ in such a way that the atomic shell structure is accounted for:

$$E_v[n] = T_0[n] + E_H[n] + E_{XC}[n] + \int v(\mathbf{r}) n(\mathbf{r}) d\mathbf{r} \quad (1.8)$$

where $T_0[n]$ is the kinetic energy functional of an interaction free electron gas with density n , $E_H[n]$ is the known Hartree energy and $E_{XC}[n]$ is all what remains out.

The trick is now to suppose that $n(\mathbf{r})$ could be derived from a *ground state* determinantal state, i.e. that there exists a non-interacting system with a ground state with the same $n(\mathbf{r})$, such that

$$n(\mathbf{r}) = \sum_i^N |\varphi_i(\mathbf{r})|^2. \quad (1.9)$$

It is then possible to apply the second Hohenberg-Kohn theorem and minimize the eq. (1.8) with respect to the density

$$E_0[v] = \min_n \left\{ \int d\mathbf{r} v n + T_0[n] + E_H[n] + E_{XC}[n] \left| \int n d\mathbf{r} = N \right. \right\} \quad (1.10)$$

or equivalently with respect to the φ_i^* . Taking into account that from eq. (1.9)

$$\frac{\delta}{\delta \varphi_i^*(\mathbf{r})} = \varphi_i(\mathbf{r}) \frac{\delta}{\delta n(\mathbf{r})}, \quad (1.11)$$

one obtains

$$\left(-\frac{\nabla^2}{2} + v + v_H + v_{XC} \right) \varphi_i = \varepsilon_i \varphi_i \quad (1.12)$$

where the ε_i are the usual Lagrange multipliers to ensure the normalization of the orbitals, $v_H(\mathbf{r})$ is the known Hartree potential, $v_{XC}(\mathbf{r})$ is the exchange-correlation potential defined as

$$v_{XC}(\mathbf{r}) = \frac{\delta}{\delta n(\mathbf{r})} E_{XC}[n(\mathbf{r})] \quad (1.13)$$

and it is the only unknown term to be somehow approximated. It contains the exchange potential, as it can be easily seen comparing the eq. (1.12) with the usual Hartree-Fock equations, the correlation potential and the correction to the non interacting kinetic energy operator necessary to have the actual one.

The appearance of a non local Laplacian operator is caused by the replacement of the density-functional of the kinetic energy by an orbital-functional. This is an important term which is absent in the Thomas-Fermi theory and leads to a correct description of the shell structure in atoms.

Of course, in order to have the same density of the interacting fluid, the interaction-free gas must feel a different effective external potential

$$v_{\text{eff}} = v + v_H + v_{XC}. \quad (1.14)$$

Solving self-consistently the eqs. (1.12), occupying the lowest N states (aufbau principle), together with eq. (1.9) yields the density of the ground state

as well as its total energy.

The crucial assumption that $n(\mathbf{r})$ can be generated by a *ground state* determinantal state *cannot* be proved. What can be demonstrated is that a physical density can be represented by a determinantal state but not that this state is also a ground state [25]. Hence, the Hohenberg-Kohn theory must be adjusted in order to overcome this representability problem (see sect. 1.3).

1.2 Extension to spin systems

Hohenberg-Kohn theory delivers the ground state density $n(\mathbf{r})$ of an inhomogeneous electron fluid. No mention is given to spin polarization. One recovers from the theory the total charge density $n(\mathbf{r})$ which is in fact the sum of $n_+(\mathbf{r})$ and $n_-(\mathbf{r})$, the spin up and the spin down charge density respectively. In the general case it is unclear how to extract separately each of the $n_{\pm}(\mathbf{r})$. To have the possibility to deal explicitly with spin polarization an extension of the theory is needed.

When taking into account spin, the relevant quantity is the spin-density matrix $n_{ss'}$ defined in analogy with the eq. (1.4) as

$$n_{ss'}(\mathbf{r}) = N \int \Psi(s\mathbf{r}, x_2, \dots, x_N) \Psi^*(s'\mathbf{r}, x_2, \dots, x_N) dx_2 \cdots dx_N. \quad (1.15)$$

It is a 2×2 Hermitian matrix, which then contains informations about four real quantities: one scalar quantity, the charge density $n(\mathbf{r})$, and one vector quantity, the vector spin density $\mathbf{m}(\mathbf{r})$. Namely

$$\hat{n}(\mathbf{r}) = n_{ss'}(\mathbf{r}) = \begin{pmatrix} n_{++}(\mathbf{r}) & n_{+-}(\mathbf{r}) \\ n_{-+}(\mathbf{r}) & n_{--}(\mathbf{r}) \end{pmatrix} \quad (1.16)$$

gives

$$n(\mathbf{r}) = n_{++}(\mathbf{r}) + n_{--}(\mathbf{r}) = \text{tr}(\hat{n}) \quad (1.17)$$

and

$$\begin{cases} m_x(\mathbf{r}) = 2 \text{Re}(n_{-+}(\mathbf{r})) \\ m_y(\mathbf{r}) = 2 \text{Im}(n_{-+}(\mathbf{r})) \\ m_z(\mathbf{r}) = n_{++}(\mathbf{r}) - n_{--}(\mathbf{r}) \end{cases} \quad \text{i.e.} \quad \mathbf{m} = \text{tr}(\hat{n}\boldsymbol{\sigma}) \quad (1.18)$$

where $\boldsymbol{\sigma} = (\sigma_x, \sigma_y, \sigma_z)$ is a vector which has its components equal to the Pauli matrices. The spin magnetization density is readily obtained multiplying the eqs. (1.18) by a factor $\mu_B = \frac{e\hbar}{2m} = -\frac{1}{2}(\text{a.u.})$.

Note that the equations (1.18) are the link between SU(2) and SO(3) transformations. A rotation in the three dimensional space would change

the components of the vector \mathbf{m} and accordingly also the spin density matrix in correspondence to a unitary transformation (see Ref. [26] for related formulae). This means that if one by incidence, diagonalizes the matrix \hat{n} , one would equivalently rotate the three dimensional space such that the vector \mathbf{m} is finally directed along the z-axis.

A reformulation of the Hohenberg and Kohn theorems in terms of the spin density matrix was readily considered [27]. The ground state properties are now unique functionals of the spin density matrix or equivalently of both the charge density and magnetization density, and the Kohn-Sham scheme can be easily reimplemented. The total energy would be decomposed in this way now, in absence of an external magnetic field:

$$E[\hat{n}] = T_0[\hat{n}(\mathbf{r})] + E_H[n(\mathbf{r})] + E_{XC}[n_{ss'}(\mathbf{r})] + \int v[n(\mathbf{r})]n(\mathbf{r})d\mathbf{r} \quad (1.19)$$

and the spin density matrix of a determinantal state would be

$$\hat{n}(\mathbf{r}) = \sum_i^N \langle \mathbf{r} | \varphi_i \rangle \langle \varphi_i | \mathbf{r} \rangle \quad \text{with} \quad \langle \mathbf{r} | \varphi_i \rangle = \begin{pmatrix} \varphi_{i+}(\mathbf{r}) \\ \varphi_{i-}(\mathbf{r}) \end{pmatrix} = \langle \varphi_i | \mathbf{r} \rangle^\dagger, \quad (1.20)$$

while the kinetic energy is

$$T_0[\hat{n}] = \min_{\{\varphi_i\}} \left\{ \sum_i^N \left\langle \varphi_i \left| -\frac{\nabla^2}{2} \right| \varphi_i \right\rangle \left| \sum_i^N \langle \mathbf{r} | \varphi_i \rangle \langle \varphi_i | \mathbf{r} \rangle = \hat{n}(\mathbf{r}); \langle \varphi_i | \varphi_j \rangle = \delta_{ij} \right\} \quad (1.21)$$

Note that once the kinetic energy has been written as above, the functional dependence on \mathbf{m} is present explicitly in E_{XC} , and in T_0 only via the orbitals φ_i . Using the eqs. (1.20) it is simple to obtain the variation with respect to $\varphi_{i\pm}^*$:

$$\frac{\delta}{\delta \varphi_{i\pm}^*(\mathbf{r})} = \varphi_{i\pm}(\mathbf{r}) \frac{\delta}{\delta n} + \varphi_{i\mp}(\mathbf{r}) \frac{\delta}{\delta m_x} \mp i \varphi_{i\mp}(\mathbf{r}) \frac{\delta}{\delta m_y} \pm \varphi_{i\pm}(\mathbf{r}) \frac{\delta}{\delta m_z} \quad (1.22)$$

or in a more compact way

$$\frac{\delta}{\delta \langle \varphi_i |} = |\varphi_i\rangle \frac{\delta}{\delta n} + \boldsymbol{\sigma} |\varphi_i\rangle \cdot \frac{\delta}{\delta \mathbf{m}}. \quad (1.23)$$

One immediately realizes that in the spin dependent Kohn-Sham equations, an effective vector field, which couples to the spin only, appears

$$\mathbf{B}_{XC}(\mathbf{r}) \stackrel{\text{def}}{=} \frac{\delta}{\delta \mathbf{m}(\mathbf{r})} E_{XC}[n(\mathbf{r}), \mathbf{m}(\mathbf{r})] \quad (1.24)$$

and the one particle spin dependent effective potential can be written as

$$v_{\text{eff}}^{ss'} = v + v_H + v_{XC} + \mathbf{B}_{XC} \cdot \boldsymbol{\sigma} \quad (1.25)$$

1.3 Lieb's theory

With Lieb's theory and the idea in ref. [19] to enclose the system in a box of finite volume, the representability problems present in the Hohenberg-Kohn theory are solved. The key to a clean theory relies on the theory of convex functions and Legendre transforms.

The Legendre transform of a functional $f[c]$ is defined as:

$$f^*[x] = \sup_{c \in \mathbf{X}} \{ (x|c) - f[c] \} \quad (1.26)$$

with $(x|c) = \int x c d\mathbf{r}$.

The functional $f[c]$ can be as general as one can imagine. Nevertheless its Legendre transform $f^*[x]$ will be convex and lower semi-continuous [19].² The Legendre transform of $f^*[x]$, namely $f^{**}[c]$, is generally not the $f[c]$ itself. Being a Legendre transform, f^{**} will be the "best" convex lower semi-continuous functional "near" f . That is f^{**} is the maximal lower semi-continuous convex minorant of f . If f is itself convex and lower semi-continuous then: $f^{**} \equiv f$. The variables c and x are said to live in dual spaces, \mathbf{X} and \mathbf{X}^* respectively. For our purposes c and x will be the spatial density n and the external potential v . The space $\mathbf{X} \ni n$ can be shown to be $\mathbf{L}^3(\mathbf{T}^3)$, namely the set of power 3 integrable functions in a finite three dimensional torus. Its dual is $\mathbf{X}^* \equiv \mathbf{L}^{3/2}(\mathbf{T}^3)$ (the dual to \mathbf{L}^p is \mathbf{L}^q with $\frac{1}{p} + \frac{1}{q} = 1$). Moreover, $\mathbf{X}^{**} \equiv \mathbf{X}$ (reflectivity).

It is easy to show that $E[v]$ is a concave functional of $v \in \mathbf{X}^*$. Thus $-E[v]$ is convex (finite, thus continuous) and can be thought as the Legendre transform of a functional $\mathcal{F}[n]$ with $n \in \mathbf{X}$. Namely

$$-E[v] = \sup_{n \in \mathbf{X}} \left\{ \int n v dx - \mathcal{F}[n] \right\} \quad (1.27)$$

or equivalently

$$E[v] = \inf_{n \in \mathbf{X}} \left\{ \int n v dx + F[n] \right\} \quad (1.28)$$

where n has been renamed into $-n$ and $\mathcal{F}[-n]$ into $F[n]$. Conversely

$$F[n] = \sup_{v \in \mathbf{X}^*} \left\{ E[v] - \int n v dx \right\} \quad (1.29)$$

although convex, needs not to be continuous but is surely lower semi-continuous. The search for the infimum in eq. (1.28) can be constrained into a sphere

²A bounded convex function is also continuous. If a convex function has a discontinuity the latter must be an infinite step. Lower semi-continuous means that the value the function assumes on the discontinuity is the lowest. Extension to functionals requires an extension of the concept of limes in an infinite dimensional space. Details in [28].

$\|n\|_3 < C$. This constraint and the reflexivity of the space \mathbf{X} assures the existence of the minimum $n = n_0$. Moreover, the first Hohenberg-Kohn theorem affirms that there is only one v_0 in correspondence. Such that $v_0 = \frac{\delta F}{\delta n}|_{n=n_0}$ is the functional derivative of F . The same can be written for the interaction free system. In this case we know that the functional $F[n]$ reduces to the kinetic energy functional $T[n]$, namely

$$E[v] = \inf_{n \in \mathbf{X}} \left\{ \int nv \, dx + T[n] \right\} \quad (1.30)$$

As a consequence the functional

$$E_{\text{XC}}[n] \stackrel{\text{def}}{=} F[n] - T[n] - E_{\text{H}}[n] \quad (1.31)$$

has also a unique well defined functional derivative

$$v_{\text{XC}} = \frac{\delta E_{\text{XC}}[n]}{\delta n} \quad (1.32)$$

which lives in \mathbf{X}^* and is a local potential.

1.4 Relativistic Density Functional Theory

The relativistic generalization of DFT appeared already at the beginning of the seventies [29]. The crucial role played by the particle density in the non polarized case and later by the spin density matrix in the spin dependent theory, had to be assigned to a four-vector quantity, the four-current density, whose time-like component is indeed proportional to the charge density. The affine-linear dependence of the relativistic Hamiltonian, describing a quantum electrodynamical system in an external classical field, on the external four-potential A^μ (via the term $\int d\mathbf{r} \hat{j}_\mu A^\mu$ with $\hat{j}^\mu = \hat{\psi} \gamma^\mu \hat{\psi}$ the four-current operator; $\hat{\psi} = \hat{\psi}^\dagger \gamma^0$; the γ^μ are the Dirac 4×4 matrices), is sufficient to extend the non relativistic Hohenberg-Kohn theorem also to the relativistic case: *the external four-potential A^μ is a unique functional of the ground state four-current density J^μ .*

Moreover, the Kohn-Sham scheme can be invoked with the aid of a relativistic non interacting electron gas, such that a Kohn-Sham-Dirac effective one particle Hamiltonian can be introduced. In complete analogy with the non relativistic case, the fictitious relativistic non interacting gas will feel an effective four-potential in addition to the external one. One could claim about representability problems also at this stage, but the extension of Lieb's theory to the relativistic case, plus a finite torus containing the physical system,

solve definitely this problem [23] (see ref. [19] for a complete and rigorous derivation).

As in the non relativistic case, a variational principle can be cast for the ground state energy involving now, the ground state four-current:

$$E[A, Q] = \inf_J \left\{ H[J] - \int d^3r A^\mu(\mathbf{r}) J_\mu(\mathbf{r}) \left| -\frac{1}{c} \int d^3r J^0(\mathbf{r}) = Q \right. \right\}; \quad (1.33)$$

here $H[J]$ plays the same role as $F[n]$ of eq. (1.28) and can be analogously split in a wise way. The constant total charge condition substitutes the total particle number conservation of the non relativistic case, for in a relativistic theory the total number of particles can vary because of pair creation. Calling $K[J]$ the functional $H[J]$ in the special case of a non interacting relativistic gas, one can write:

$$H[J] = K[J] - \frac{1}{2} \int d^3r J^\mu a_\mu^{\text{H}} + E_{\text{XC}}[J] \quad (1.34)$$

where a_μ^{H} , the Hartree four-potential, is related to J^μ by the Maxwell equations. The final Kohn-Sham-Dirac equations read:

$$\left[-ic\boldsymbol{\alpha} \cdot \boldsymbol{\nabla} + \beta mc^2 - c\beta\gamma^\mu (A_\mu + a_\mu^{\text{H}} + a_\mu^{\text{XC}}) \right] \psi_k = \psi_k \varepsilon_k, \quad (1.35)$$

with the Kohn-Sham exchange and correlation four-potential

$$a_\mu^{\text{XC}} \stackrel{\text{def}}{=} \frac{\delta E_{\text{XC}}[J]}{\delta J^\mu}. \quad (1.36)$$

Relativistic effects enter the Kohn-Sham equations in two different ways. One is via the Dirac equation, which is used instead of the Schrödinger equation. This brings automatically into consideration scalar relativistic effects (Darwin terms, velocity terms) and spin-orbit effects. The other way is via the XC-energy functional, which includes orbital magnetism together with relativistic corrections to the homogeneous interacting fluid. For the latter an estimation exists [30], while unfortunately, the former must be neglected, up to now, since their intrinsic non local character (undetermined gauge) poses an hard barrier to their treatment. An attempt was tried to include them in the XC-energy functional in a non relativistic way [31], but it does not lead to systematic improvements of the orbital magnetic moment of $3d$ elements [32]. In order to explain better this problem one can introduce the Gordon decomposition of the three-current

$$\mathbf{J} = \mathbf{I} + \boldsymbol{\nabla} \times \mathbf{S} + \frac{\partial \mathbf{G}}{\partial t}, \quad (1.37)$$

into the orbital current density

$$\mathbf{I} = \frac{1}{2} \sum_{k=1}^N \bar{\psi}_k (-i \overleftarrow{\nabla} + i \nabla + 2\mathbf{A}) \psi_k, \quad (1.38)$$

and the spin current density derived from the spin density

$$\mathbf{S} = \frac{1}{2} \sum_{k=1}^N \bar{\psi}_k \boldsymbol{\Sigma} \psi_k, \quad \Sigma_l = \begin{pmatrix} \sigma_l & 0 \\ 0 & \sigma_l \end{pmatrix}, \quad (1.39)$$

where σ_l are the Pauli matrices and the ψ_k are bispinor functions. The last term of (1.37) vanishes in a stationary situation.

The total stationary current density must have zero divergence due to charge conservation. Since the divergence of the spin current density vanishes by its very structure as a curl, the orbital current density must also be divergence free: $\nabla \cdot \mathbf{I} = 0$. Once more we take the advantage of including our system in a finite torus with periodic boundary conditions: the charge flux through its surface is zero, such that \mathbf{I} vanishes here. As a consequence it may be expressed as a curl of some vector field \mathbf{L} , to be visualized as an ‘angular momentum density’:

$$\mathbf{I} = \frac{1}{2} \nabla \times \mathbf{L}. \quad (1.40)$$

(Recall that an orbital angular momentum *density* cannot really figure in quantum mechanics because position and momentum cannot be simultaneously measured at the same time. Accordingly, (1.40) defines \mathbf{L} only up to an arbitrary additive gradient term.)

The total electric current density may then be expressed as

$$\mathbf{J} = \nabla \times \mathbf{M} = \frac{1}{2} \nabla \times (\mathbf{L} + 2\mathbf{S}) \quad (1.41)$$

where \mathbf{M} has the dimension of a ‘magnetization density’.

The four-current density is now given by $J^\mu = (nc, \nabla \times \mathbf{M})$, and hence the functional $E_{\text{XC}}[J]$ may be rewritten as a functional $E_{\text{XC}}[n, \mathbf{M}]$ of the electron density n and the ‘magnetization density’ \mathbf{M} . It yields the mechanical exchange and correlation potential acting on an electron

$$v^{\text{XC}} = ca_0^{\text{XC}} = \frac{\delta E_{\text{XC}}}{\delta n} \quad (1.42)$$

and the magnetic exchange and correlation field

$$\mathbf{b}^{\text{XC}} = \nabla \times \mathbf{a}^{\text{XC}} = \int d^3r' \frac{\delta \mathbf{J}(\mathbf{r}')}{\delta \mathbf{M}} \frac{\delta E_{\text{XC}}}{\delta \mathbf{J}(\mathbf{r}')} = \frac{\delta E_{\text{XC}}}{\delta \mathbf{M}}. \quad (1.43)$$

The interaction terms $-J^\mu A_\mu$ are cast into

$$J^0 A_0 = nV \quad (1.44)$$

and

$$J^k A_k = \mathbf{J} \cdot \mathbf{A} = \mathbf{A} \cdot \nabla \times \mathbf{M} \hat{=} -\mathbf{M} \cdot \nabla \times \mathbf{A} = -\mathbf{B} \cdot \mathbf{M}. \quad (1.45)$$

The sign $\hat{=}$ means equivalence under the spatial integral after integration by parts. V and \mathbf{B} are the mechanical potential and the magnetic field corresponding to A^μ .

With

$$\frac{\delta \mathbf{M}(\mathbf{r})}{\delta \bar{\psi}_k(\mathbf{r}')} = \frac{1}{2} \left(\frac{\delta \mathbf{L}(\mathbf{r})}{\delta \bar{\psi}_k(\mathbf{r}')} + \delta(\mathbf{r}' - \mathbf{r}) \Sigma \psi_k(\mathbf{r}) \right) \quad (1.46)$$

an alternative way of writing down the general Kohn-Sham-Dirac equation is

$$\begin{aligned} & \left[-ic\boldsymbol{\alpha} \cdot \nabla + \beta c^2 + V(\mathbf{r}) + v^{\text{H}}(\mathbf{r}) + v^{\text{XC}}(\mathbf{r}) \right] \psi_k(\mathbf{r}) - \\ & - \beta \int d^3 r' \left(\mathbf{B}(\mathbf{r}') + \mathbf{b}^{\text{H}}(\mathbf{r}') + \mathbf{b}^{\text{XC}}(\mathbf{r}') \right) \cdot \frac{\delta \mathbf{M}(\mathbf{r}')}{\delta \bar{\psi}_k(\mathbf{r})} = \psi_k(\mathbf{r}) \varepsilon_k. \end{aligned} \quad (1.47)$$

At the price of replacing the four-current, local in terms of the Kohn-Sham orbitals ψ_k , by a ‘magnetization density’ \mathbf{M} , non-locally depending on the ψ_k and whose orbital part \mathbf{L} is subject to another gauge (undetermined gradient term), the vector potential with its unpleasant far-ranging character has been eliminated. The crucial problem remaining to be solved is to find a suitable expression for $\delta \mathbf{L}(\mathbf{r}) / \delta \bar{\psi}_k(\mathbf{r}')$.

By completely neglecting the orbital current \mathbf{I} , that is

$$\frac{\delta \mathbf{M}(\mathbf{r})}{\delta \bar{\psi}_k(\mathbf{r}')} = -\frac{1}{2} \Sigma \psi_k \delta(\mathbf{r} - \mathbf{r}') \quad \text{for} \quad \mathbf{I} = 0, \quad (1.48)$$

one ends up with the simple form of the Kohn-Sham-Dirac equation of spin-density functional theory (SDFt)

$$\left[-ic\boldsymbol{\alpha} \cdot \nabla + \beta c^2 + V + v^{\text{H}} + v^{\text{XC}} + \frac{1}{2} \beta \Sigma \cdot (\mathbf{B} + \mathbf{b}^{\text{H}} + \mathbf{b}^{\text{XC}}) \right] \psi_k = \psi_k \varepsilon_k, \quad (1.49)$$

where the magnetic field couples to the spin only. The Kohn-Sham exchange and correlation field \mathbf{b}^{XC} is non-collinear even in the widely used local spin-density approximation (LSDA), an important issue which has been taken into account only in recent years [21, 22, 23]. An important defect of the LSDA

is, however, that \mathbf{b}^{XC} obtained from this approximation is not source-free as it should be because of the first equality in (1.43).

What we learn from the previous derivation of SDFT from RDFT is that the XC-field must be a transversal field (its sources must vanish everywhere) and the hope is that, once a new XC-field with this property is achieved, things like orbital magnetization could be described more satisfactorily and easily, treating it as a Zeeman field entering the effective one particle Hamiltonian with the term $\mathbf{b}^{\text{XC}}(\hat{\ell} + \hat{\sigma})$ ($\hat{\ell}$ is the one particle angular momentum operator).

Just here transpires the aim of the present work. A transversal field cannot be both collinear and possess a spherical symmetry at the same time, unless it is a constant (still collinear and non constant is mathematically possible: $\mathbf{B} = (0, 0, B_z(x))$). Hence, the new wanted functional must be searched without the collinear and spherical approximations restrictions.

1.5 Local Spin Density Approximation

Once again I stress the point that the DFT is an exact theory. But in order to use it one has to provide approximations for the energy functional. The latter can be decomposed into three distinct functionals (the Hartree energy, the exchange-correlation energy and the kinetic energy of a model non interacting system), and Lieb's theory shows that the functional derivative of them with respect to the spin density is a well defined local functional. In the Kohn-Sham scheme, this functional derivative is performed considering its projection onto a set of occupied single particle orbitals.

The price to be paid for a description of the ground state of an inhomogeneous interacting electron fluid in terms of a spin density matrix, i.e. with 3×4 degrees of freedom instead of $6N$, is represented by an unavoidable approximation to be done on the exchange-correlation energy functional. The most natural to be thought, at least as a starting point, is a local density approximation of the type

$$E_{\text{XC}}[\hat{n}] \approx \int n(\mathbf{r}) \varepsilon_{\text{XC}}[n_{\uparrow}(\mathbf{r}), n_{\downarrow}(\mathbf{r})] d\mathbf{r} = \int n(\mathbf{r}) \varepsilon_{\text{XC}}[n(\mathbf{r}), \zeta(\mathbf{r})] d\mathbf{r} \quad (1.50)$$

$$n(\mathbf{r}) = n_{\uparrow}(\mathbf{r}) + n_{\downarrow}(\mathbf{r}) \quad \zeta(\mathbf{r}) \stackrel{\text{def}}{=} \frac{n_{\uparrow}(\mathbf{r}) - n_{\downarrow}(\mathbf{r})}{n(\mathbf{r})} \quad (1.51)$$

where ε_{XC} is the exchange-correlation energy functional per particle of a known model system, usually chosen as the homogeneous interacting electron gas; $n_{\uparrow}, n_{\downarrow}$ are the spin up and spin down particle densities respectively, which will be dealt with in the next section; $\zeta(\mathbf{r})$ is the degree of polarization. The

exchange part of the ε_{XC} can be easily calculated; the correlation part requires numerical quantum Monte Carlo methods and can be estimated at any order of accuracy [33]. Throughout this work we shall use the ε_{XC} parameterization given by Perdew and Zunger [34]. The formula (1.50) is indeed exact in an homogeneous situation, where \hat{n} does not depend on the position. Conversely, it can be thought not to perform correctly in an inhomogeneous situation, such as in isolated atoms. This is, in fact, not quite the case. What happens is that the approximation (1.50) assures that the exchange-correlation hole around each electron has still the value of a positive electron charge, as it should always be. Its shape is not reproduced correctly, but the integrated value all over the space is still $+e$. This fact is sufficient to have reasonable results even in inhomogeneous systems. That is why it is widely used: it does not require a big computational effort and leads to good results.

Other approximations are also being used, essentially trying to improve the exchange-correlation functional, including a functional dependence on the gradient of the density (GGA) and, recently, on the kinetic energy functional (Meta GGA). These approximations will not be treated in this work.

1.6 The collinear approximation

In the local density approximation the exchange-correlation energy of an homogeneous electron gas is used. An homogeneous electron gas can be spin polarized by means of an homogeneous magnetic field. The total particle density n is then the sum of a spin up density and a spin down density $n = n_{\uparrow} + n_{\downarrow}$. This means that there exist sets of cartesian coordinate axis in which the spin density matrix of the homogeneous electron gas is in the diagonal form

$$\hat{n} = \begin{pmatrix} n_{\uparrow} & 0 \\ 0 & n_{\downarrow} \end{pmatrix}, \quad (1.52)$$

namely the ones with the z axis along the magnetic field.

Consider the case of an electron in an external spherical symmetric potential. If one completely neglects relativistic effects, in absence of an external magnetic field, the spin up and spin down parts of the electron spinor are not mixed with each other, in the sense that one can fix a z axis in order to have only one component different from zero. As soon as spin orbit interaction is switched on, the σ_z operator does not commute with the Hamiltonian any more. Rather, the electron states are now eigenvectors of $j_z = l_z + \frac{1}{2}\sigma_z$ such that up and down spinor components are now mixed. As a result, a non collinear magnetization density is achieved, i.e. there is a non zero component perpendicular to the z axis and no global rotation of the three-dimensional

space can let it vanish in all points in space.

As an example consider the so called $p_{+1/2}^*$ state, i.e. the eigenstate of J^2, J_z with $j = l - s = \frac{1}{2}$, $l = 1$ and $j_z = +\frac{1}{2}$ (generally denoted as $\mathcal{Y}_{jl}^{j_z}$):

$$\mathcal{Y}_{\frac{1}{2}1}^{+1/2}(\theta, \phi) = \begin{pmatrix} -\sqrt{\frac{1}{3}} Y_{10}(\theta, \phi) \\ +\sqrt{\frac{2}{3}} Y_{11}(\theta, \phi) \end{pmatrix} = -\frac{1}{\sqrt{4\pi}} \begin{pmatrix} \cos \theta \\ \sin \theta e^{i\phi} \end{pmatrix} \quad (1.53)$$

with Y_{lm} the usual spherical harmonics. Since we are interested in a qualitative picture, let's assume the spatial part to be a constant. The spin density matrix for such state is then proportional to

$$\hat{n}(\theta, \phi) \propto \begin{pmatrix} \cos^2 \theta & \cos \theta \sin \theta e^{-i\phi} \\ \cos \theta \sin \theta e^{i\phi} & \sin^2 \theta \end{pmatrix} \quad (1.54)$$

which corresponds to the magnetization vector

$$\mathbf{m}(\theta, \phi) \propto (\sin 2\theta \cos \phi, \sin 2\theta \sin \phi, \cos 2\theta) \quad (1.55)$$

Since the state is eigenfunction of J_z , the densities have azimuthal symmetry along the z axis (as can also be seen by the $\cos \phi, \sin \phi$ dependence of m_x, m_y). This magnetization density is, by construction, scale invariant, depending only on the spherical angles θ and ϕ . Only a cut in the xz plane is shown in the figure 1.1. For this state, it is easy to calculate the mean values

$$\langle \mathcal{Y}_{\frac{1}{2}1}^{+1/2} | \boldsymbol{\sigma} | \mathcal{Y}_{\frac{1}{2}1}^{+1/2} \rangle = (0, 0, -\frac{1}{3}) \quad (1.56)$$

In general one has

$$\langle \mathcal{Y}_{jl}^{j_z} | \sigma_x | \mathcal{Y}_{jl}^{j_z} \rangle = \langle \mathcal{Y}_{jl}^{j_z} | \sigma_y | \mathcal{Y}_{jl}^{j_z} \rangle = 0 \quad (1.57)$$

just because the spherical harmonics in the spinors get different sign if one changes the direction of the z axis ($\cos \theta \rightarrow -\cos \theta$). As a result the x, y components of the magnetization are antisymmetric with respect to the $z = 0$ plane, while the z component is symmetric.

The approximation tacitly used in the collinear approximation is to neglect the density matrix off-diagonal terms, which means imposing the m_x, m_y components of the magnetization density to be zero everywhere. In figure 1.2, the collinear magnetization density as resulting from the magnetization density of picture 1.1 is shown. In this collinear case the mean values in eq. (1.56) are obviously the same.

When applying the local spin density approximation in connection with a spin collinear approximation, one neglects the functional dependence of the

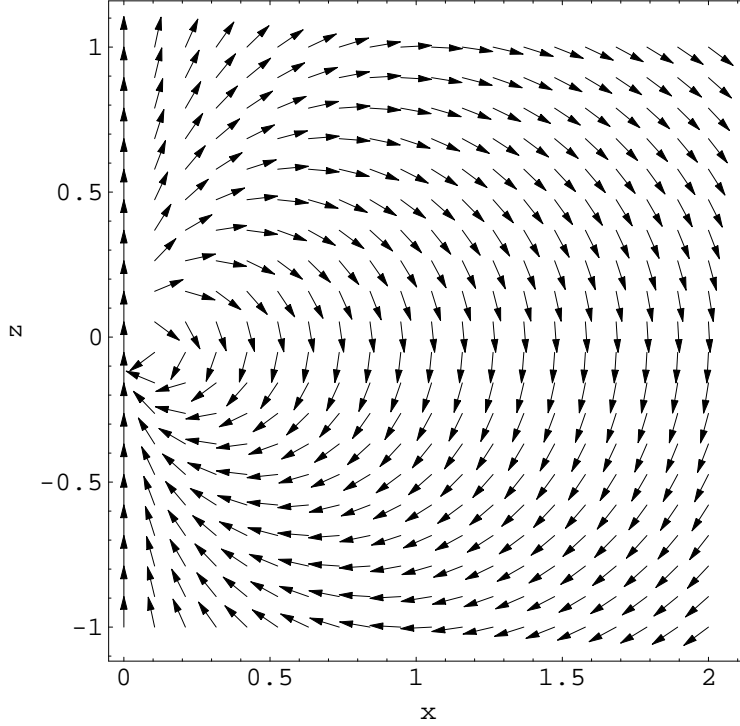


Figure 1.1: Spin magnetization generated by the state $\mathcal{Y}_{\frac{1}{2}1}^{+1/2}$

homogeneous electron gas exchange-correlation energy ε_{XC} , on the m_x, m_y components of the magnetization density. Such that the functional derivatives in eq. (1.24) with respect to m_x, m_y vanish, and the only component of the exchange-correlation field to be different from zero, is the $B_{z,\text{XC}}$ one. This results in an enormous simplification of the equations to be solved. That's why it is being used.

What is nice in the LSDA is really the fact that it is *local*. This means that in a non collinear situation, one is still allowed to treat each point in the space separately. One can sit down at a point \mathbf{r} , diagonalize the spin density matrix via an $\text{SU}(2)$ transformation, find the eigenvalues $n_{\uparrow}(\mathbf{r}), n_{\downarrow}(\mathbf{r})$ and construct the potential.

Using simple algebra and the relations (1.18) one obtains:

$$n_{\uparrow}(\mathbf{r}) = \frac{1}{2}(n(\mathbf{r}) + |\mathbf{m}(\mathbf{r})|) \quad \text{and} \quad n_{\downarrow}(\mathbf{r}) = \frac{1}{2}(n(\mathbf{r}) - |\mathbf{m}(\mathbf{r})|) \quad (1.58)$$

The degree of polarization in each point is

$$\zeta(\mathbf{r}) = \frac{n_{\uparrow}(\mathbf{r}) - n_{\downarrow}(\mathbf{r})}{n(\mathbf{r})} = \frac{|\mathbf{m}(\mathbf{r})|}{n(\mathbf{r})} \quad (1.59)$$

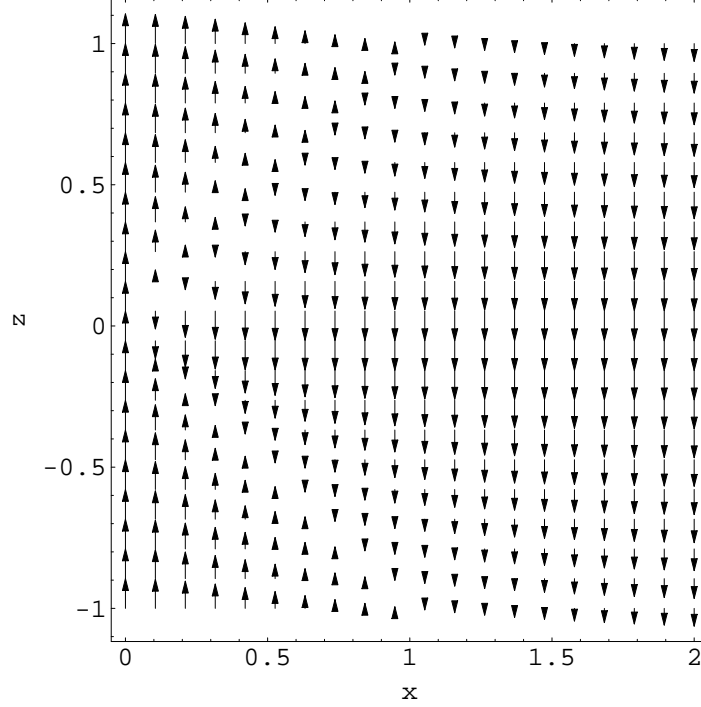


Figure 1.2: Approximate collinear spin magnetization generated by the state $\mathcal{Y}_{\frac{1}{2}1}^{+1/2}$

while the exchange-correlation field is

$$\mathbf{B}_{\text{XC}} = \frac{\delta E_{\text{XC}}}{\delta \mathbf{m}(\mathbf{r})} \stackrel{\text{LSDA}}{=} n \frac{\delta \varepsilon_{\text{XC}}}{\delta \mathbf{m}} = n \frac{\delta \varepsilon_{\text{XC}}}{\delta \zeta} \frac{\delta \zeta}{\delta \mathbf{m}} = \frac{\mathbf{m}}{|\mathbf{m}|} \frac{\delta \varepsilon_{\text{XC}}}{\delta \zeta}. \quad (1.60)$$

Hence, the exchange-correlation field \mathbf{B}_{XC} has, in LSDA, the same direction as the magnetization density.

1.7 The self interaction correction

Usually, the exchange energy is defined to be the non local expression present in the Hartree-Fock variational scheme:

$$E_{\text{X}} = -\frac{1}{2} \sum_{ij} \langle \varphi_i \varphi_j | w | \varphi_j \varphi_i \rangle \quad (1.61)$$

where the φ_i are the one particle wave functions of the best Slater determinant approximation of the ground state, and w the interaction term in the

	Ioniz. energy (Ryd)	Atomic radius (a_0)
LSDA	0.957	1.58
exact	1.000	1.50

Table 1.1: Hydrogen ionization energy and atomic radius $\langle r \rangle$ as estimated by LSDA and by exactly solving the corresponding one particle Schrödinger equation.

Hamiltonian. It appears naturally in connection with the Hartree energy

$$E_{\text{H}} = \frac{1}{2} \sum_{ij} \langle \varphi_i \varphi_j | w | \varphi_i \varphi_j \rangle \quad (1.62)$$

such that the non physical contribution of one particle interacting with itself ($i = j$), cancels out.

When using LSDA, the exchange energy functional is written in an approximate form, borrowing it from the model homogeneous interacting electron gas system. As a result, the previously mentioned cancellation is not achieved any more. This effect is the more evident the more localized a one particle state is. In table 1.1, the ionization energy and the atomic radius are shown for the hydrogen atom. Here, the spurious self interaction of the hydrogen electron results in a fictitious net repulsion which in turn is responsible for the increase of the atomic size and for the decrease of the extraction potential.

In order to overcome these problems, a practical calculational scheme was suggested by Perdew and Zunger [34]. An orbital dependent correction to the total energy functional was added, with the only purpose of reducing, ad hoc, the unphysical self interaction. The self interaction corrected (SIC) total energy functional reads [35]:

$$E_{\text{SIC}} = \Theta[\hat{n}] + E_{\text{H}}[n] + E_{\text{XC}}[n_{\uparrow}, n_{\downarrow}] + \int v n \, d\mathbf{r} \quad (1.63)$$

with the functional Θ defined in analogy with T_0 of eq. (1.21) as

$$\Theta[\hat{n}] = \min_{\{\varphi_{\alpha\sigma}\}} \left\{ \sum_{\alpha\sigma} \langle \varphi_{\alpha\sigma} | -\frac{1}{2} \nabla^2 | \varphi_{\alpha\sigma} \rangle - E_{\text{H}}[n_{\alpha\sigma}] - E_{\text{XC}}[n_{\alpha\sigma}, 0] \left| \sum_{\alpha} \langle \mathbf{r} | \varphi_{\alpha} \rangle \langle \varphi_{\alpha} | \mathbf{r} \rangle = \hat{n}(\mathbf{r}); \langle \varphi_{\alpha} | \varphi_{\beta} \rangle = \delta_{\alpha\beta} \right. \right\} \quad (1.64)$$

with $n_{\alpha\sigma}$ denoting the density of the orbital α with spin σ . The term $E_{\text{XC}}[n_{\alpha\sigma}, 0]$ accounts for the exchange-correlation self interaction and assumes that the orbital α is fully spin polarized. If not, there is not a complete cancellation of the self exchange-correlation part which can produce an energy

shift for states in the j - j coupling regime, as we shall discuss later in section 4.1. Hence, this scheme yields exact results for hydrogen like ions, if no relativity effects are taken into account, i.e. neither spin-orbit terms, nor small component corrections.

Applying the Kohn-Sham scheme to the functional E_{SIC} , one obtains the effective potential

$$v_{\text{eff},\sigma\sigma'}^{\text{SIC},\alpha} = v_{\text{ext}} + v_{\text{H}} + v_{\text{XC}} + \mathbf{B}_{\text{XC}} \cdot \boldsymbol{\sigma} - v_{\text{H}}^{\alpha} - v_{\text{XC}}^{\alpha} - B_{z,\text{XC}}^{\alpha} \quad (1.65)$$

which is orbital dependent. This causes the Kohn-Sham eigenfunctions not to be automatically orthogonal. One needs to introduce non diagonal Lagrange multipliers to achieve orthogonality, as in Hartree-like methods [36]. Since this effect was shown to be of almost no importance on the calculation of total energies and ionization potentials [34], we never took care of such problem. Unlike the Hartree-Fock eigenvalues and LSDA eigenvalues, the SIC ones are a good approximation to the removal energies [34, 37]. Moreover, the SIC potential manages to describe the minus one charged ions, which in LSDA are found to be in an unbound state.

Chapter 2

The Kohn-Sham-Dirac equation

Our final goal will be to describe systems allowing for a non collinear spin magnetization, that would arise because of the transversal (i.e. source-free) character of the exchange-correlation field, as stated at the end of section 1.4. We have already seen in section 1.6, that spin non collinearity also arises simply, when a quantum state is not an eigenfunction of the spin projection operator along a given direction. What mainly causes this feature in isolated systems as atoms, is the presence of a spin-orbit interaction.

One could think either to include spin-orbit in a perturbative way or try to solve numerically the Kohn-Sham-Dirac equation (1.49), in order to take into account all relativistic features without approximation. A perturbative treatment would be justified in atoms with a low nuclear charge, up to $3d$ elements say, whereas we would like to focus our attention mainly on rare-earths, which present an intriguing phenomenology connected with the spin properties of the $4f$ orbitals. Also scalar effects due to the Lorentz contraction of orbitals nearby large Z nuclei are of great importance: s and p^* states have diverging amplitudes approaching the nucleus, so that they are more affected by the Lorentz contraction (or mass increase, it is the same) with respect to other states; as a result they are more localized, screen better and push other states outwards. We were amazed by realizing that the two outer $6p$ electrons in the Pb atom are in a j - j coupling regime! Comparison with data in literature made us more confident about our calculations [38]. Animated by these physical arguments and by a feeling of challenge toward the Dirac equation, we decided to write a program to solve it numerically, first in a spherical approximation in order to provide a suitable basis set, and secondly in a non spherical non collinear fashion.

Solving the four component Dirac equation requires special attention to few problems which are not present in the Schrödinger formalism. One problem is represented by the fact that the Dirac operator is not bounded from

below, allowing for the existence of negative energy states. Such a problem can be solved imposing to the stationary bound electronic solution the correct asymptotic behavior. Another problem which one encounters in atoms is connected to the finite dimension of the nucleus. A point like nucleus causes the Dirac operator to be no more self adjoint as soon as Z is greater than 118 and even no stable solutions are possible if $Z > \alpha^{-1} \approx 137$, where the electrostatic potential nearby the nucleus starts to be able to create electron-positron pairs from the vacuum. This problem is easily removed considering nuclei with a finite extension. Anyway, since our analysis concerned atoms with a nuclear charge not greater than 103 and finite nucleus corrections do affect core levels, but practically do not affect valence electrons [39], we did not take them into account.

2.1 The effective Hamiltonian

The simplest conceivable Dirac Hamiltonian to be used in connection with quantum chemistry methods, describing a system with N electron is:

$$H = \sum_i^N H_D^i + \frac{1}{2} \sum_{i \neq j}^N \frac{1}{|\mathbf{r}_i - \mathbf{r}_j|} \quad (2.1)$$

where the

$$H_D^i = \boldsymbol{\alpha}_i \cdot [c\mathbf{p}_i + \mathbf{A}(\mathbf{r}_i)] + \beta_i c^2 - \phi(\mathbf{r}_i) \quad (2.2)$$

are Dirac single electron Hamiltonians; \mathbf{A} and ϕ denote the vector and scalar potential of any electro-magnetic field acting on the electron, including the nuclear potential; the $\boldsymbol{\alpha}$ and β are the four by four Dirac matrices:

$$\boldsymbol{\alpha} = \begin{pmatrix} 0 & \boldsymbol{\sigma} \\ \boldsymbol{\sigma} & 0 \end{pmatrix} \quad \beta = \begin{pmatrix} I & 0 \\ 0 & -I \end{pmatrix} \quad (2.3)$$

Again atomic units were used.

The Hamiltonian (2.1) suffices many purposes, even though the Coulomb interaction $1/r_{ij}$ is not Lorentz covariant. However, the Coulomb interaction appears as the leading term in an expansion of the interaction energy in powers of the fine structure constant obtained by the methods of quantum electrodynamics. The successive term in the expansion, which behaves as $(\alpha Z)^2$, is the Breit term, which involves scalar products of the $\boldsymbol{\alpha}$ matrices. It describes the emission of a virtual photon by one electron and its absorption by a different one. If the emitting electron and absorbing one would be the same, one would have the process responsible for the Lamb shift.

As we already discussed in the previous chapter, a Kohn-Sham scheme can be cast in terms of the Dirac Hamiltonian. An effective Hamiltonian,

which can be found in the left part of the eigenvalue problem (1.49), can be justified within the already discussed approximations. We write it again in atomic units, neglecting external and internally condensed magnetic fields, which are 2-3 orders of magnitude weaker than the exchange-correlation field:

$$H_{\text{KSD}} = -i\mathbf{c}\boldsymbol{\alpha} \cdot \boldsymbol{\nabla} + \beta c^2 + V_{\text{ext}} + v_{\text{H}} + v_{\text{XC}} + \frac{1}{2}\beta\boldsymbol{\Sigma} \cdot \mathbf{B}_{\text{XC}} \quad (2.4)$$

where $V_{\text{ext}}(\mathbf{r})$ is the external potential ($-Z/r$ for isolated atoms in the adiabatic approximation); v_{H} the Hartree potential generated by the electronic clouds repulsion; v_{XC} and \mathbf{B}_{XC} are the exchange-correlation potential and field respectively. The Breit interaction discussed above as well as retardation effects have been included in a local way multiplying the LDA exchange potential by the factor

$$f_v = \frac{1}{2} \left(3 \frac{\text{asinh}\beta}{\beta\sqrt{1+\beta^2}} - 1 \right) \quad (2.5)$$

with $\beta = (3\pi^2 n(\mathbf{r}))^{1/3}/c$ the relativistic strength parameter [30]. Relativistic corrections involving the correlation part of the potential can be introduced [40], but at the high densities where relativistic effects are important, those corrections can be neglected in view of other approximations to be made.

Our final goal will be to solve the eigenvalues problem

$$H_{\text{KSD}}\psi_k = \varepsilon_k\psi_k \quad (2.6)$$

with the four component wave functions ψ_k . We shall solve this problem in three steps. First in a collinear and spherical approximation (i.e. with $B_{\text{XC},x} = B_{\text{XC},y} = 0$, $B_{\text{XC},z}(r)$, $v_{\text{H}}(r)$ and $v_{\text{XC}}(r)$; this will provide a basis set), then in a collinear non spherical way and finally in a non collinear and non spherical way.

2.2 The four component spin density matrix

A crucial role in solving self consistently the Kohn-Sham-Dirac equation is the construction of a spin density matrix. In some sense one has to link the space of the four component wave function to the simpler single spinor one, where one knows it is possible to perform SU(2) transformations which have a correspondence with an SO(3) one. The simplest way to achieve such a link is presented in the following.

We introduce a 4×4 bispinor density matrix

$$\hat{n}_4 = \sum_{k=1}^N \psi_k \psi_k^\dagger, \quad n(\mathbf{r}) = \text{tr} \hat{n}_4(\mathbf{r}), \quad \mathbf{M}(\mathbf{r}) = \text{tr} (\beta\boldsymbol{\Sigma}\hat{n}_4(\mathbf{r})). \quad (2.7)$$

Since the relevant quantities depend only on the two 2×2 diagonal blocks of \hat{n}_4 , we write it as

$$\hat{n}_4 = \begin{pmatrix} \hat{n}_L & \text{n.i.} \\ \text{n.i.} & \hat{n}_S \end{pmatrix} \quad (2.8)$$

where \hat{n}_L is a 2×2 spin density matrix constructed by means of the large components of the bispinor ψ_k , \hat{n}_S with the small components, “n.i.” stands for *not important*. The charge density is then

$$n(\mathbf{r}) = \text{tr } \hat{n}_4(\mathbf{r}) = \text{tr } \hat{n}_L + \text{tr } \hat{n}_S, \quad (2.9)$$

while the magnetization is

$$\mathbf{M}(\mathbf{r}) = \text{tr}(\beta \boldsymbol{\Sigma} \hat{n}_4(\mathbf{r})) = \text{tr}(\hat{n}_L \boldsymbol{\sigma}) - \text{tr}(\hat{n}_S \boldsymbol{\sigma}). \quad (2.10)$$

From these two quantities one may build an ordinary 2×2 spin density matrix, simply inverting the relations (1.18), namely

$$\hat{n}(\mathbf{r}) = \begin{pmatrix} n_{++}(\mathbf{r}) & n_{+-}(\mathbf{r}) \\ n_{-+}(\mathbf{r}) & n_{--}(\mathbf{r}) \end{pmatrix} \quad \text{with} \\ n_{++} = \frac{1}{2}(n + M_z) \quad n_{--} = \frac{1}{2}(n - M_z) \quad n_{-+} = \frac{1}{2}(M_x + iM_y). \quad (2.11)$$

This spin density matrix has, by construction, all the properties necessary to deliver the effective one particle potential to insert in the self consistent scheme.

Note that the electron system, even an $s_{1/2}$ state, which has vanishing spin-orbit effects, cannot be fully spin polarized if a nonzero small component of the wave function is present.

2.3 The Kohn-Sham-Dirac equation in the spherical approximation

As a first task, it is of crucial importance to solve the Kohn-Sham-Dirac equations in a spherical approximation. If one would not include spin polarization effects, one would have the effective Hamiltonian without the exchange-correlation field, which after algebraic manipulation can be rewritten as:

$$H_{\text{KSD}}^{\text{Sph}} = i c \gamma_5 \sigma_r \left(\frac{\partial}{\partial r} + \frac{1}{r} - \frac{\beta}{r} K \right) + (\beta - I_4) c^2 - \frac{Z}{r} + v_{\text{H}}(r) + v_{\text{XC}}(r) \quad (2.12)$$

where the energy was shifted downwards by the constant c^2 (electron rest energy) and

$$\gamma_5 = \begin{pmatrix} 0 & -I \\ -I & 0 \end{pmatrix} \quad \sigma_r = \boldsymbol{\sigma} \cdot \frac{\mathbf{r}}{r} \quad K = \beta(\boldsymbol{\Sigma} \cdot \mathbf{L} + I_4); \quad (2.13)$$

	l_A	l_B
$k = j + \frac{1}{2}$	$j + \frac{1}{2}$	$j - \frac{1}{2}$
$k = -(j + \frac{1}{2})$	$j - \frac{1}{2}$	$j + \frac{1}{2}$

Table 2.1: Relations among k , j , l_A (angular momentum quantum number of the electronic (large) part) and l_B (angular momentum quantum number of the positronic (small) part)

I_4 is the 4×4 unity matrix; K is called spin-orbit operator. The Hamiltonian (2.12), being spherically symmetric, commutes with the total angular momentum operator squared \mathbf{J}^2 , its projection along, say, the z axis as well as with the spin-orbit operator K . Moreover, the operator K commutes with all components of the vector operator \mathbf{J} . Thus, for an electron in a central potential, we can construct a simultaneous eigenfunction of H , K , \mathbf{J}^2 and J_z . The corresponding eigenvalues are denoted by E , $-k$, $j(j+1)$ and j_z . Note that because of the presence of the operator K , which contains the β matrix, the operator \mathbf{L}^2 does not commute with the Hamiltonian. The bispinors, eigenfunctions of \mathbf{J}^2 , J_z , K , can be represented as follows:

$$\Upsilon_{jk}^{j_z}(\theta, \phi) = \begin{pmatrix} \mathcal{Y}_{j l_A}^{j_z}(\theta, \phi) \\ \mathcal{Y}_{j l_B}^{j_z}(\theta, \phi) \end{pmatrix} \quad (2.14)$$

with

$$K \Upsilon_{jk}^{j_z} = -k \Upsilon_{jk}^{j_z}, \quad \mathbf{J}^2 \Upsilon_{jk}^{j_z} = j(j+1) \Upsilon_{jk}^{j_z}, \quad J_z \Upsilon_{jk}^{j_z} = j_z \Upsilon_{jk}^{j_z}. \quad (2.15)$$

The $\mathcal{Y}_{jl}^{j_z}(\theta, \phi)$ are the eigenfunctions of \mathbf{J}^2 , \mathbf{L}^2 and J_z already introduced in section 1.6, for which we use the following expressions [41]:

$$\mathcal{Y}_{jl}^{j_z} = \begin{cases} -\sqrt{\frac{l-j_z+\frac{1}{2}}{2l+1}} Y_l^{j_z-\frac{1}{2}} \begin{pmatrix} 1 \\ 0 \end{pmatrix} + \sqrt{\frac{l+j_z+\frac{1}{2}}{2l+1}} Y_l^{j_z+\frac{1}{2}} \begin{pmatrix} 0 \\ 1 \end{pmatrix} & \text{if } j = l - \frac{1}{2} \\ \sqrt{\frac{l+j_z+\frac{1}{2}}{2l+1}} Y_l^{j_z-\frac{1}{2}} \begin{pmatrix} 1 \\ 0 \end{pmatrix} + \sqrt{\frac{l-j_z+\frac{1}{2}}{2l+1}} Y_l^{j_z+\frac{1}{2}} \begin{pmatrix} 0 \\ 1 \end{pmatrix} & \text{if } j = l + \frac{1}{2}. \end{cases} \quad (2.16)$$

The eigenvalue k is connected to j , l_A , l_B , according to the table (2.1). Pictorially speaking, the sign of k determines whether the spin is antiparallel ($k > 0$) or parallel ($k < 0$) to the total angular momentum in the nonrelativistic limit.

Finally, the operator σ_r has the following property:

$$\sigma_r \mathcal{Y}_{j l_A}^{j_z} = -\mathcal{Y}_{j l_B}^{j_z} \quad (2.17)$$

and vice versa, since $\sigma_r^2 = I$.

The eigenfunctions of the Hamiltonian (2.12) will be, then, a product of a radial part with an angular part given by the quantities (2.14). Writing as an ansatz for such eigenfunctions

$$\psi(r, \theta, \phi) = \begin{pmatrix} g(r) \mathcal{Y}_{j_A}^{j_z}(\theta, \phi) \\ if(r) \mathcal{Y}_{j_B}^{j_z}(\theta, \phi) \end{pmatrix} \quad (2.18)$$

one decouples the angular degrees of freedom from the radial part in the KSD-equations. As a result, one can finally write the following system of two equations, which involve the large and small radial parts only:

$$\begin{cases} \frac{\partial}{\partial r} P = -\frac{k}{r} P + [\frac{E-V}{c^2} + 2] Q \\ \frac{\partial}{\partial r} Q = +\frac{k}{r} Q + [E - V] P \end{cases} \quad (2.19)$$

with $P = rg(r)$, $Q = crf(r)$, V the effective scalar potential and E the corresponding eigenvalue.

The numerical solution of the previous system of differential equations does not require special efforts. I wish not to focus too much into technical details at this stage:

- an initial starting energy eigenvalue E is guessed;
- a power expansion of the potential (starting from the power -1, to account for the nuclear attraction), and the wavefunction nearby the nucleus is performed to have a set of four points from which to start a predictor-corrector integration outwards;
- analogously an inwards integration is performed starting from infinity, where an exponentially decaying behaviour is imposed (this is also sufficient to discriminate the positron-like solutions from the electron ones);
- both integrations are performed until the point r_0 , defined by the solution of $V(r_0) = E$;
- the value of E is updated until the inward and outward solutions join continuously in r_0 .

2.4 Introduction of a collinear XC-field

The introduction of a further term in the KSD-Hamiltonian, which represents the interaction with a collinear field, for example the exchange-correlation field coupled to the spins,

$$H_{\text{KSD}}^{\text{Coll}} = H_{\text{KSD}}^{\text{Sph}} + \frac{1}{2}B_z\beta\Sigma_z, \quad (2.20)$$

complicates considerably the simple picture we had in the previous section. The operators K and \mathbf{J}^2 do not commute with the KSD-Hamiltonian any more. Because of the preferred direction chosen, the system has lowered its symmetry from a spherical to a cylindrical one, around the z axis. For this reason the j_z is still a good quantum number. The matrix elements

$$\langle nkj_z|B_z\beta\Sigma_z|n'k'j'_z\rangle, \quad (2.21)$$

where n is the principal quantum number, are then different from zero only if $j_z = j'_z$ for symmetry reasons. One would have instead of eqs. (2.19), an infinite system of coupled equations involving all states with the same j_z . Fortunately, atomic states with a different principal quantum number as well as states with different l_A have negligible matrix elements with $\beta\Sigma_z$. The function $B_z(r)$ is not so wild to increase the order of magnitude of the matrix elements, so that only couplings of states with the same n and l_A (only two) can be considered. This turns out to be an approximation of the order B_z/c^2 [42]. In picture (2.1) we show the energy levels of a $3d$ electron ($l_A = 2$) subject to the potential $-30/r$ and experiencing a homogeneous magnetic field along the z axis. The Hamiltonian (2.20) was used, so that there is no explicit orbital momentum dependence (in particular, these energy levels are not connected to the observed spectroscopic lines in an external magnetic field). Hence, the slope of the energy levels equals the mean value of the spin magnetization $\langle\beta\Sigma_z\rangle$. The coupled states with the same j_z , ranging from $-3/2$ to $+3/2$ are shown by dotted arrows. As one can see, the existence of a coupling between the previous mentioned states is important to have the correct description of electronic spin states. Imagine to have an atom with more than two electrons in absence of an external magnetic field. The field which multiplies the spin magnetization operator in the Hamiltonian (2.20) is then, according to the approximations introduced in the previous chapter, the exchange-correlation field, which is no more a homogeneous field. Consider then, the horizontal axis in fig. 2.1 to be the effective value of the exchange-correlation field. If it is much greater than the spin-orbit splitting Δ_{SO} (divided by μ_B for dimensional reasons), one has fully polarized electronic states, i.e. the projection of the spin on the z axis is a good quantum number,

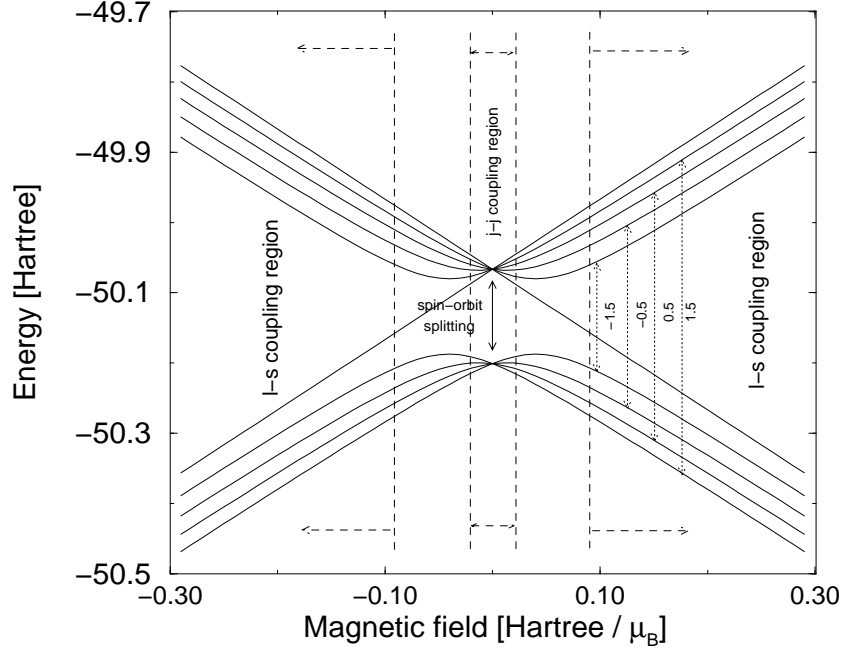


Figure 2.1: Energy levels of a $3d$ electron in the potential $-30/r$ in a homogeneous magnetic field. According to the Hamiltonian (2.20), no coupling of the field to the orbital momentum is considered. The numbers at dotted arrows give the j_z values.

and one is in the non relativistic limit where states fulfil a Russel-Saunders coupling (outer regions in the figure). If the exchange-correlation field is much smaller than Δ_{SO} , one has, on the contrary a j - j coupling (region in the middle). This is not only the case which occurs in core states, but also in the $6p$ states of Pb as shown in table (2.2). Notice also the spin magnetization values $\pm\frac{1}{3}$ in Pb as expected from eq. (1.56).

The introduction of a collinear magnetic field term in the Hamiltonian, leads to a supplementary subtle problem. As it was already said, up to the order B/c^2 one has a coupling between the two states with the same principal quantum number, same l_A and same j_z . This means that one has to solve four coupled equations. Two for the small components and two for the large ones. However, these equations are connected with one energy eigenvalue only. This means that the same set of four differential equations has two solutions, one for the state labeled with $k > 0$ ($j = l_A - \frac{1}{2}$) and one for the $k < 0$ ($j = l_A + \frac{1}{2}$). It happens that the numerical solution of this system is highly dependent on the starting guessed energy eigenvalues. In picture (2.2) is shown the error function whose zeroes are the requested

	C (2 <i>p</i>)	Si (3 <i>p</i>)	Ge (4 <i>p</i>)	Sn (5 <i>p</i>)	Pb (6 <i>p</i>)
$\Delta_{\text{SO}}/\mu_{\text{B}}B_{\text{XC}}$	10^{-2}	10^{-1}	1	10^1	10^2
$\langle\beta\Sigma_z\rangle[p_{-\frac{1}{2}}^*]$	-0.99995	-0.99965	-0.98591	-0.85014	+0.33336
$\langle\beta\Sigma_z\rangle[p_{+\frac{1}{2}}^*]$	-0.99998	-0.99969	-0.98869	-0.91780	-0.33336

Table 2.2: Order of magnitude of the ratio spin-orbit splitting / XC-field in the outer *p* shell of carbon-group atoms followed by the calculated mean value of the projection of the spin moment along the *z* axis for the two occupied states $j = \frac{1}{2}$ (except for Pb, this is a mere label), $j_z = \pm\frac{1}{2}$.

eigenvalues of the problem. This error function arises from an algebraic treatment of the matching conditions at the point r_0 defined at the end of the previous section. One can clearly see that if we would like to have the solution for $k > 0$ and start with the guess x_1 , using a Newton-Raphson method, we would not get it, since the point x_2 would yield the solution for $k < 0$. It is then crucial to have good guesses of the energy eigenvalues, such to pick the correct attraction basin.

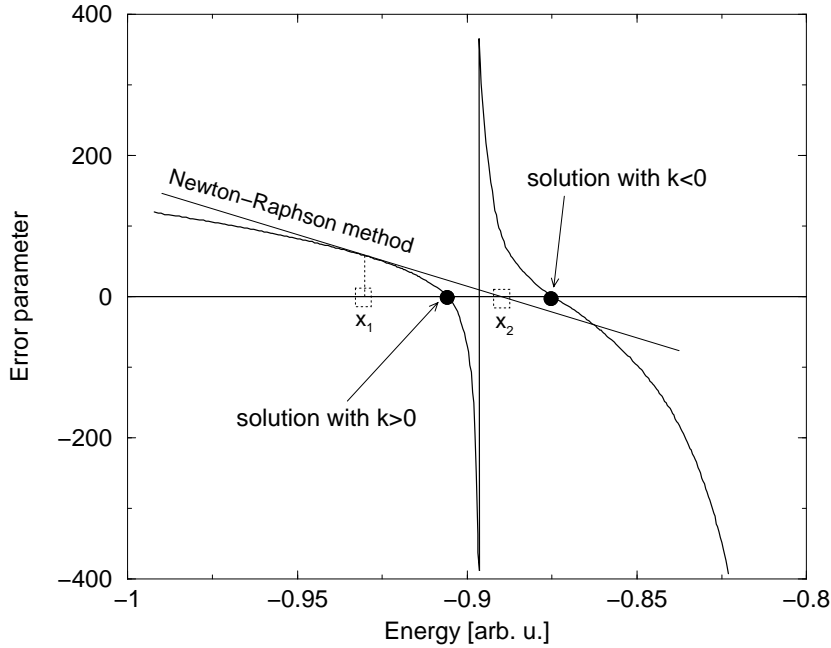


Figure 2.2: Error function whose zeroes are the energy eigenvalues of the four coupled differential equations arising in the presence of a collinear XC-field. The vertical line between the two branches represents an asymptote.

To summarize, the method used to calculate eigenvalues and eigenfunc-

tions in presence of a collinear magnetic field is pretty identical to the one described in the previous section. The only change is connected to the number of equations and to the attraction basin of the solutions, mentioned above:

- Proceed as in previous section;
- Supplementary calculation is needed to have an estimate of the eigenvalues, such to pick an initial energy guess in the correct attraction basin;
- The spin of the resulting state *must* be always checked.

2.5 Non spherical KSD equations

It is the rule rather than the exception that isolated atoms are found not to possess a spherical symmetry in their ground state. Only closed shell or closed subshell (e.g. Gd^{+3} , Pb) atoms and ions have a spherically symmetric ground state in an isotropic environment. Although the Hamiltonian of an isolated atom has indeed a spherical symmetry, its ground state needs not to be spherical. There occurs a spontaneous symmetry breaking due to the electron-electron Coulomb interaction. However, the direction of the total angular momentum \mathbf{J} must be conserved, so that in fact, a cylindrical symmetry is present. In terms of the KS scheme, the effective potential inside the KSD equations is not spherical, but possesses a cylindrical symmetry, which we shall choose along the z axis.

With the help of the eigenfunctions of the effective non interacting system, one can write the particle density as

$$\rho(\mathbf{r}) = \sum_i^N \bar{\psi}_i(\mathbf{r})\beta\psi_i(\mathbf{r}) = \sum_i^N \psi_i^\dagger(\mathbf{r})\psi_i(\mathbf{r}) \quad (2.22)$$

with $\psi_i(\mathbf{r})$ equal to the product of a radial dependent part with an angular dependent one (see eq. (2.18)). In the spherical approximation, the particle density is approximated by its angular integrated $\rho(r) = \int \rho(\mathbf{r}) d\Omega$. Using LSDA, from a non spherical density a non spherical effective potential arises, which in the collinear approximation can be written as

$$W[\rho(\mathbf{r})] \stackrel{\text{def}}{=} v_{\text{eff}}^{\tau\tau'}(\mathbf{r}) = v(r) + v_{\text{H}}(\mathbf{r}) + v_{\text{XC}}(\mathbf{r}) + \frac{1}{2}B_{\text{XC},z}(\mathbf{r})\beta\Sigma_z \quad (2.23)$$

where the external potential v was assumed spherically symmetric in atoms, being generated by a point-like nucleus. The non spherical effective KSD

Hamiltonian will be

$$H_{\text{nsph}} = \mathcal{T} + W[\rho(\mathbf{r})] = H_{\text{sph}} + W[\rho(\mathbf{r})] - W[\rho(r)] = H_{\text{sph}} + \Delta W(\mathbf{r}) \quad (2.24)$$

with $\Delta W(\mathbf{r})$ a diagonal 4×4 matrix. The non spherical KSD equations to be solved self-consistently are now

$$H_{\text{nsph}} \tilde{\psi}_i(\mathbf{r}) = \tilde{\varepsilon}_i \tilde{\psi}_i(\mathbf{r}). \quad (2.25)$$

The solution of the spherically symmetric problem offers a complete set of orthonormal wave functions, such that the $\tilde{\psi}_i$ can be written as:

$$\tilde{\psi}_i(\mathbf{r}) = \sum_j c_{ij} \psi_j(\mathbf{r}). \quad (2.26)$$

We have in mind to solve the previous eigenvalue problem variationally, such that the variation of the functional

$$\langle \tilde{\psi}_i | H_{\text{nsph}} | \tilde{\psi}_i \rangle \quad (2.27)$$

under the normalization constraints $\langle \tilde{\psi}_i | \tilde{\psi}_i \rangle = 1$, has to vanish. Introducing the Lagrange multipliers $\tilde{\varepsilon}_i$ one obtains

$$\delta \left(\langle \tilde{\psi}_i | H_{\text{nsph}} - \tilde{\varepsilon}_i | \tilde{\psi}_i \rangle \right) = 0 \quad (2.28)$$

for each $i = 1 \dots N$.

Using the expressions (2.24) and (2.26), these equations become

$$\delta \left(\sum_{jk} c_{ij}^* c_{ik} \langle \psi_j | H_{\text{sph}} + \Delta W(\mathbf{r}) - \tilde{\varepsilon}_i | \psi_k \rangle \right) = 0 \quad (2.29)$$

and the variation can be done with respect to the set of c_{ij}^* . Hence, taking into account that $\langle \psi_j | H_{\text{sph}} - \tilde{\varepsilon}_i | \psi_k \rangle = (\varepsilon_k - \tilde{\varepsilon}_i) \delta_{jk}$, one gets

$$\sum_k c_{ik} (\Delta W_{jk} + (\varepsilon_k - \tilde{\varepsilon}_i) \delta_{jk}) = 0 \quad \forall j \quad (2.30)$$

with the matrix elements ΔW_{jk} explicitly given by

$$\Delta W_{jk} = \int d\Omega \int r^2 dr \psi_j^*(\mathbf{r}) \Delta W(\mathbf{r}) \psi_k(\mathbf{r}). \quad (2.31)$$

This means that we have finally to diagonalize the matrix $\{\Delta W_{jk} + \varepsilon_k \delta_{jk}\}$ to have the new KSD eigenfunctions and eigenvalues of the non spherical problem. Since the matrix $\{\Delta W_{jk}\}$ is Hermitian, the set of diagonalizing

c_{ij} 's forms a unitary matrix, so that the resulting $\tilde{\psi}_i$ are automatically orthonormal, provided that the KSD spherical eigenfunctions are orthogonal as well (this is not the case if, for instance, one uses non orthogonalized SIC orbitals, but in this case the effect is negligible).

Because of the cylindrical symmetry, only the matrix elements between two states with the same quantum number j_z , eigenvalue of the projection of the total angular momentum along the symmetry axis, can be different from zero. The scalar potential and the z component of the XC-field are even functions with respect to the $z = 0$ plane. Namely, $V(z) = V(-z)$ and $B_z(z) = B_z(-z)$. These properties pose further restrictions on the matrix elements which are not vanishing if the sum of the angular momentum quantum numbers of the large parts of the two involved wave functions is an even number. Hence, the matrix $\{\Delta W_{jk}\}$ is a sparse matrix. The integrals (2.31) have to be evaluated over the whole three-dimensional space, so that we decided to introduce a three-dimensional grid as in ref. [43], instead of solving the KSD equations by expanding all functions into spherical harmonics. The method we used is straightforward to implement also if no cylindrical symmetry is present, as for atoms embedded in a solid, where also matrix elements between states with different j_z can differ from zero.

For the purpose of investigating isolated atoms and ions, due to the cylindrical symmetry, only a bidimensional grid was used: a radial mesh identical to the one used for the numerical calculation of the spherical approximation; and an angular Gauss-Legendre mesh [44] for the latitudinal angle θ . The Hartree energy and potential were calculated by expanding the particle density and the Hartree potential in sums of Legendre polynoms:

$$\rho(r, \theta) = \sum_l \rho_l(r) P_l(\cos \theta) \quad \text{and} \quad V_H(r, \theta) = \sum_l V_{H,l}(r) P_l(\cos \theta) \quad (2.32)$$

together with the definition

$$\rho_l(r) = \frac{2l+1}{2} \int_{-1}^1 \rho(r, x) P_l(x) dx \quad \text{with} \quad x = \cos \theta. \quad (2.33)$$

Actually, since we never considered wave functions with a large component angular momentum quantum number larger than 3 (f states), the sum was taken to run up to $l = 6$ (the density is a sum of squared wave functions) and the angular grid was chosen such to exactly integrate expressions containing terms up to $l = 12$ (energies are products of two densities).

From the $\rho_l(r)$ it is possible to define the multipolar electronic momenta. Namely the $2l$ -pole is defined as

$$Q_l = l! \frac{4\pi}{2l+1} \int_0^\infty r^{l+2} \rho_l(r) dr. \quad (2.34)$$

The Poisson equation to calculate the Hartree potential reads

$$\nabla^2 V_{\text{H}}(\mathbf{r}) = -4\pi\rho(\mathbf{r}) \quad (2.35)$$

which after substituting the expressions (2.32) and an algebraic simplification becomes:

$$\left(\partial^2 + \frac{2}{r}\partial - \frac{l(l+1)}{r^2} \right) V_{\text{H},l}(r) = -4\pi\rho_l(r) \quad \text{with} \quad \partial \stackrel{\text{def}}{=} \frac{d}{dr}. \quad (2.36)$$

The solution to the previous equation can be found with the ansatz

$$\frac{1}{r^{n+k}} \partial(r^n \partial(r^k V_{\text{H},l})) = -4\pi\rho_l \quad (2.37)$$

which yields the values

$$k = l + 1, n = -2l \quad \text{or} \quad k = -l, n = 2 + 2l. \quad (2.38)$$

Although they are equivalent, the second set of values leads to expressions numerically simpler to integrate, so we chose this one. Finally,

$$V_{\text{H},l}(r) = \frac{4\pi}{2l+1} \left(\frac{1}{r^{l+1}} \int_0^r t^{l+2} \rho_l(t) dt + r^l \int_r^\infty t^{1-l} \rho_l(t) dt \right). \quad (2.39)$$

2.6 Non collinear KSD equations

As already mentioned at the end of section 1.6, the local character of LSDA allows to handle in a relative easy way the spin non-collinearity as well. Once a spin density matrix is known at any point in space, it is possible, by means of two SO(3) transformations (one is the inverse of the other), to calculate the LSDA XC-field at any point. The final result was summarized by the chain of equations (1.60), which, together with the definitions (1.18), gives an easy and fast way to compute the XC-field. As a generalization of the non spherical implementation, the KSD equations in presence of an effective potential given by

$$v_{\text{eff}}^{\tau\tau'}(\mathbf{r}) = v(r) + v_{\text{H}}(\mathbf{r}) + v_{\text{XC}}(\mathbf{r}) + \frac{1}{2} \mathbf{B}_{\text{XC}}(\mathbf{r}) \cdot \beta \boldsymbol{\Sigma} \quad (2.40)$$

are solved variationally, with the functional basis set given by the spherical and collinear KSD eigenfunctions. The non collinear and non spherical correction to the spherical potential is now no more diagonal in the spin. It still

does not mix large and small components of the wave function. Therefore, calling it ΔW as in the previous non spherical case:

$$\Delta W = \begin{pmatrix} \Delta V + \Delta B_z & B_\rho & & 0 \\ B_\rho & \Delta V - \Delta B_z & & \\ & 0 & \Delta V - \Delta B_z & -B_\rho \\ & & -B_\rho & \Delta V + \Delta B_z \end{pmatrix} \quad (2.41)$$

where V indicates the scalar parts of the potential and $B_{\rho/z}$ the XC-field components perpendicular and parallel to the z axis respectively.

2.7 Transversal XC-field

In this section we present a simple non local method to extract an *ad hoc* transversal XC-field from the non collinear LSDA one. The main idea is that any continuous and differentiable vector field can be decomposed as the sum of one longitudinal vector field and a transversal one. Namely

$$\mathbf{B}(\mathbf{r}) = \mathbf{B}_L(\mathbf{r}) + \mathbf{B}_T(\mathbf{r}) \quad \text{with} \quad \begin{cases} \text{rot } \mathbf{B}_L(\mathbf{r}) = 0 \\ \text{div } \mathbf{B}_T(\mathbf{r}) = 0 \end{cases}. \quad (2.42)$$

This means that

$$\text{div } \mathbf{B}(\mathbf{r}) = \text{div } \mathbf{B}_L(\mathbf{r}) \stackrel{\text{def}}{=} \rho_L(\mathbf{r}). \quad (2.43)$$

The condition of longitudinality, $\text{rot } \mathbf{B}_L(\mathbf{r}) = 0$ assures the existence of a scalar function $V_L(\mathbf{r})$ such that (notice the analogy with the electrostatic field)

$$\mathbf{B}_L(\mathbf{r}) = \text{grad } V_L(\mathbf{r}) \quad (2.44)$$

which substituted into eq. (2.43) gives

$$\nabla^2 V_L(\mathbf{r}) = \rho_L(\mathbf{r}). \quad (2.45)$$

By a direct numerical differentiation of the non collinear XC-field it is easy to obtain the source density ρ_L in principle at any point in space according to eq. (3.2), below. It is then a routine to solve the Poisson equation (2.45) to have the potential function V_L . In fact, the same method used to obtain the non spherical Hartree potential can be easily adapted here. The difference is that now only odd Legendre polynoms compose the XC-field source density. Once V_L is known, again a numerical derivative would do the final job to get the longitudinal field \mathbf{B}_L . With a certain lack of fantasy, we propose as a source free XC-field the difference

$$\mathbf{B}_T(\mathbf{r}) = \mathbf{B}(\mathbf{r}) - \mathbf{B}_L(\mathbf{r}). \quad (2.46)$$

This method turns out to be a non local one, because of the Poisson equation (2.45) to be solved. Notice that the spin magnetization vector needs not to be parallel to the XC-field any more, as it was the case in LSDA (cf. eq. (1.60)).

The equation the transversal field must obey are then (in a static condition):

$$\operatorname{div} \mathbf{B}_T = 0 \quad \text{and} \quad \operatorname{rot} \mathbf{B}_T = \mathbf{j} \quad (2.47)$$

with \mathbf{j} its vortices. The second of eqs. (2.47) implies $\operatorname{div} \mathbf{j} = 0$, which is automatically fulfilled since the only non vanishing component of \mathbf{j} is $j_\phi(\rho, z)$ (ρ , ϕ and z are the cylindrical coordinates). The same equation implies also that \mathbf{B}_T is defined unless a gradient of an arbitrary function f . The first of eqs. (2.47) would then imply that $\nabla^2 f = 0$ everywhere in the space, i.e. ∇f is constant in space. Since \mathbf{B}_T is vanishing at infinity, $\nabla f = 0$ everywhere.

Remark

Sometimes, in the following, we shall refer to a ‘zero-step’ energy, which can be used in the non spherical, the non collinear and transversal field case, as well. It is just the energy which comes out from the non spherical spatial density and new XC-field, before any self-consistent calculation. Just after the calculation of the spherical basis set, one can associate to each KSD wavefunction its angular part and get the zero-step spin density matrix and the zero-step XC-field (which can be cleaned from its sources or not) in correspondence. Then, one can calculate the zero-step energy:

$$E^0 = E_{\text{Sph}} + \Delta E_{\text{H}} + \Delta E_{\text{XC}} \quad (2.48)$$

with E_{Sph} the energy in the spherical symmetric case and the last two terms representing the difference of Hartree energy and XC-energy with respect to the corresponding spherical energies. This zero-step energy is obtained before that the $\{\Delta W_{jk}\}$ is calculated. We shall see in the following that this zero-step energy gives already a good estimation of the self-consistent calculated one. This is because the non diagonal matrix elements of $\{\Delta W_{jk}\}$ remain small, with respect to the diagonal ones, during all the self-consistent cycles.

Chapter 3

Results

3.1 Non spherical calculations

As already mentioned in section 2.5, the non spherical KSD equations are solved variationally using the bispinor wave functions solution of the spherical atomic problem as a basis set. In any variational method, special attention must be paid to the choice of the basis set. The infinite sum in eq. (2.26) has to be practically cut to a finite number of terms. In all calculations, all occupied orbitals are included in the sum, allowing for a non spherical description of core levels as well. Table 3.1 shows the influence of the chosen set of basis functions on the total energy calculation of the Pr^{+3} ion. First of all, LSDA used in connection with the spherical approximation gives lower total energies than the non spherical ground state. This does not mean that the

Pr^{+3}	
$E_{\text{Sph}} = -18460.2370 \text{ Ryd}$	$\langle \beta \Sigma_z \rangle_{\text{Sph}} = 1.95$

Basis	$\Delta E_{\text{NoSph}}^0$ [mRy]	ΔE_{NoSph} [mRy]	$\langle \beta \Sigma_z \rangle_{\text{NoSph}}$
[Xe] $4f^2$ (only occ.)	32.7	32.7	1.95
[Xe] 4f	32.7	28.0	1.82
[Xe] 4f 5d 6sp 7s	32.7	27.0	1.83
[Xe] 4f 5df 6spd 7sp	32.7	26.6	1.83

Table 3.1: Effects of the basis set choice on non-spherical total energy calculations for the Pr^{+3} ion. E_{NoSph}^0 is the zero-step energy explained in the text, while E_{NoSph} results from a self-consistent calculation using the basis set shown in the first column. Both values refer to the spherical one. The last column shows the effect of non-sphericity on the spin magnetization projection along the z axis.

ground state of Pr^{+3} is spherical in reality, but that LSDA, which we should not forget to be an approximation, delivers such result. Again, DFT is an exact theory. If one knew the exact functional dependence of the XC-energy functional on the electron density, one would get the correct answer applying it. The zero-step energy ($\Delta E_{\text{NoSph}}^0$ column in table 3.1, cf. pg. 38 for its definition) already gives a good estimation of non-spherical effects on total energy, being ca. 6 mRy away from the self-consistent value calculated with the largest basis set we considered. Unfortunately, because of its definition, it yields an unchanged spin projection along the total angular momentum direction, with respect to the spherical calculated one, whereas we find in most rare-earths a reduction and in few cases an enhancement if we treat them self-consistently. This is because, in this zero-step, no matrix elements are involved.

The row indicated with a ‘non occ.’ refers to a calculation performed with all occupied states as basis set. Here, the two $4f$ electrons, which are chosen to have $j_z = \frac{5}{2}$ and $\frac{3}{2}$ according to the aufbau principle, are coupled with the occupied d and p levels with the same j_z (actually the matrix elements between d and f states are always vanishing for symmetry reasons). They are not coupled, then to the unoccupied $4f$ states which have the same j_z but opposite s_z . As a result, since the matrix elements f - p are small and no coupling with f states with opposite spin is considered, the resulting energy is almost equal to the zero-step one and there occurs no spin reduction.

Our different choice of the basis set affects the total energy with tiny changes (as, for instance, compared with the ionization potential mismatch with experimental values in rare-earths) of the order of 1 mRy, such that in the following, only the occupied shells will be considered in the self-consistent cycle (corresponding to the second row of table 3.1). Releasing the spherical approximation and introducing an angular dependent XC-field projection along the z axis, yields a reduction of the spin moment of Pr^{+3} as large as 7% (we will see in fig. 3.6 that this is the highest spin-reduction among all rare-earth +3 ions due to asphericity).

In fig. 3.1 the difference between the non-spherical total energy and the spherical one, calculated with LSDA, is shown for the whole rare-earth series of atoms and up to three fold positively charged ions. The atomic electronic configurations were chosen as $[\text{Xe}] 4f^n 6s^2$, with n being the difference between the atomic number and 56. Singly and doubly ionized atoms were created by removing the two $6s$ electrons; three-plus ions by removing an f electron. The only exceptions to this scheme were:

- La: $[\text{Xe}] 5d^1 6s^2$; La⁺: $[\text{Xe}] 4f^1 6s^1$; ...
- Ce: $[\text{Xe}] 4f^1 5d^1 6s^2$; Ce⁺: $[\text{Xe}] 4f^1 5d^2$; Ce⁺²: $[\text{Xe}] 4f^2$; ...

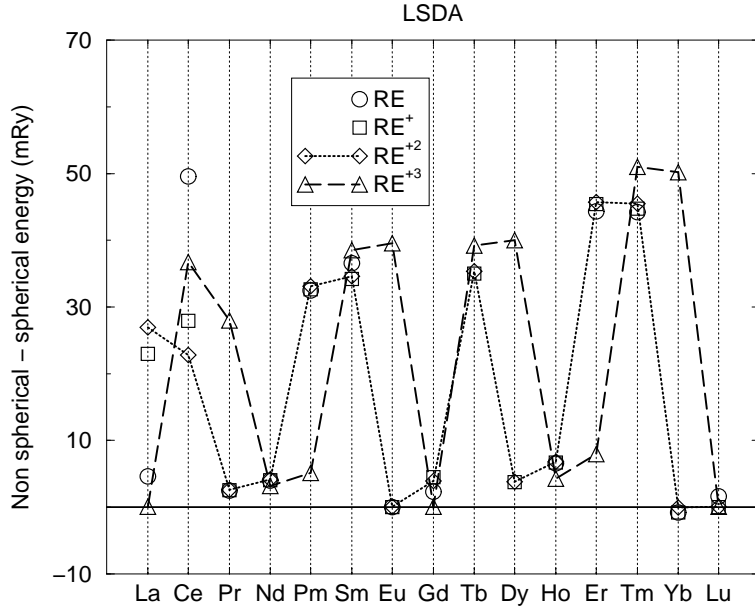


Figure 3.1: LSDA calculated non-spherical - spherical total energy differences for rare-earths (RE) atoms and ions.

- Gd: $[\text{Xe}] 4f^7 5d^1 6s^2$; Gd^+ : $[\text{Xe}] 4f^7 5d^1 6s^1$; ...
- Lu: $[\text{Xe}] 4f^{14} 5d^1 6s^2$; Lu^+ : $[\text{Xe}] 4f^{14} 6s^2$.

The terbium and dysprosium atoms did not converge in the spherical- and LSD-approximation. The reason is that the XC-field generated by the half filled $4f$ shell, is so strong to push the 8-th and 9-th electrons with opposite spin close to the continuum, extending their wave functions out of the numerical grid. This peculiar behaviour can be healed either by introducing an ad hoc integration grid, or a positive step in the potential at some large distance, or, as we did, using SIC-LSDA.

The LSDA effective potential of a neutral atom decays exponentially away from the nucleus. Hence, it is numerically difficult to compute eigenfunctions corresponding to unoccupied bound states. Since the SI-corrected LSDA effective potential has the correct asymptotic behaviour, it is convenient to use the set of SIC eigenfunctions as a basis set. Unoccupied states will be calculated in the effective field of the outermost corresponding occupied state, which we define in the following. Since the non spherical potential contains only even Legendre polynomials contributions, only levels with the large component angular momentum quantum numbers which differ by an even number will have non vanishing matrix elements with the non spherical potential correction and will be coupled. These ones we define to correspond to each

other. Hence, for example an unoccupied g level will have non vanishing non spherical matrix elements with an occupied s (octupolar contributions) or d (quadrupolar) or g . We chose to use as the effective potential for the unoccupied states, the one felt by the outermost occupied corresponding coupled level. Again as an example, take the Pr^{+3} ion calculated in table 3.1, with the basis set of the last row: unoccupied $[4f, 5f, 6p, 7p]$ will be calculated in the effective potential of the highest occupied $4f$, while $[5d, 6sd, 7s]$ in the effective potential of the highest occupied $5s$.

When we use such a scheme in any non-spherical calculation, we will use the term SIC-LSDA. Notice, that it is not a self-interaction-corrected method as in the spherical case, but only using the SIC orbitals of the spherical approximation to build the basis set. Namely, the variation in eq. (2.29) is now

$$\delta \left(\sum_{jk} c_{ij}^* c_{ik} \langle \psi_j^{\text{SIC-LSDA}} | H_{\text{sph}}^{\text{SIC-LSDA}} + \Delta W(\mathbf{r}) - \tilde{\epsilon}_i | \psi_k^{\text{SIC-LSDA}} \rangle \right) = 0 \quad (3.1)$$

with $H_{\text{sph}}^{\text{SIC-LSDA}} | \psi_k^{\text{SIC-LSDA}} \rangle = \epsilon_k^{\text{SIC-LSDA}} | \psi_k^{\text{SIC-LSDA}} \rangle$. This leads to the diagonalization of the matrix $\{ \Delta W_{jk}^{\text{sic-lsda}} + \epsilon_k^{\text{SIC-LSDA}} \delta_{jk} \}$ with the elements $\Delta W_{jk}^{\text{sic-lsda}}$ calculated as in eq. (2.31), but by means of the spherical SIC-LSDA eigenfunctions. This procedure does not cancel the non spherical self interaction contained in the $\Delta W_{jk}^{\text{sic-lsda}}$ (that is why we write a lowercase sic-lsda as index). Just as an estimation, one can compute this non spherical self interaction for each occupied orbital, outside the self-consistent cycle. It is composed by the sum of the Hartree self energy, a positive quantity and the XC self energy, a negative quantity. Table 3.2 shows these quantities for the occupied $5d$ orbital of three-valent lanthanum and the $4f$ of divalent lanthanum.

Energies for the $4f$ in La^{II} are higher than the $5d$ of La^{III} because the

	$E_{\text{H}}^{\text{NoSph}}$ [mRy]	$E_{\text{H}}^{\text{Sph}}$ [mRy]	$E_{\text{XC}}^{\text{NoSph}}$ [mRy]	$E_{\text{XC}}^{\text{Sph}}$ [mRy]
$\text{La}^{\text{III}} (5d)$	322.6	310.5	-334.5	-306.1
$\text{La}^{\text{II}} (4f)$	775.4	738.3	-780.8	-684.0

Table 3.2: Self interaction energies in $\text{La}^{\text{III}} 5d$ and $\text{La}^{\text{II}} 4f$ orbitals.

former is more contracted than the latter and consequently, has an higher density. As a crude estimation of the non spherical self interaction energies, let's consider the difference between columns 2 and 3 (Hartree energies) and between columns 4 and 5 (XC-energies). One gets:

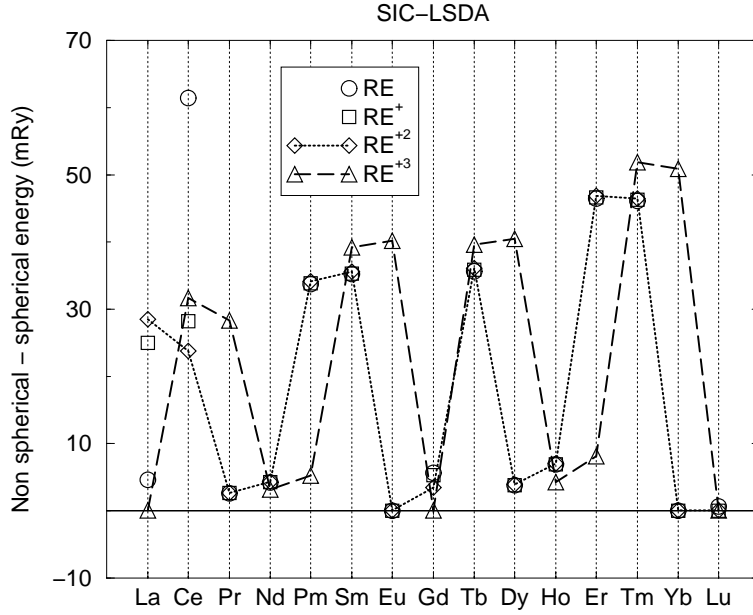


Figure 3.2: SIC-LSDA calculated non-spherical - spherical total energy differences for rare-earths (RE) atoms and ions.

	$E_{\text{H}}^{\text{NoSph-Sph}}$ [mRy]	$E_{\text{XC}}^{\text{NoSph-sph}}$ [mRy]
$\text{La}^{\text{III}} (5d)$	12.1	-28.4
$\text{La}^{\text{II}} (4f)$	37.1	-96.8

The sum of these two contribution is then negative with values -16.3 mRy and -59.7 mRy for La^{III} and La^{II} respectively¹. These numbers are of comparable magnitude with the values in fig. 3.1 and 3.2.

It is in principle easy to develop a method which is self-interaction free also in the more general non-spherical and non-collinear case, but the computational effort would be so time consuming to mine the main idea of DFT to be a fast tool to prefer it to quantum chemical methods.

The relative change of the total energy values with respect to the spherical basis set used, is for this SIC-LSDA the same as shown in table 3.1 for the LSDA case. The same quantities of figure 3.1 calculated with SIC-LSDA are now plotted in fig. 3.2. One can see practically no change in the values, except that now the Tb and Dy atoms could be calculated and the Ce atom where SIC gives an energy difference increased of ca. 10 mRy. This stems from the Ce 5d and 4f electrons, which in LSDA are more extended than in

¹Since self interaction energies have to be subtracted from the total energy, these two values tend to prefer the three-valent state as the ground state of the isolated La atom, as experimentally verified.

SIC (KS-eigenvalues: -0.26 Ry and -0.44 Ry in LSDA, -0.48 Ry and -1.14 Ry in SIC-LSDA respectively). It is not a surprise that values in figure 3.1 and in fig. 3.2 are practically the same: the non spherical part of the potential $\Delta W(\mathbf{r})$ is treated in the same way.

In table 3.3, the ionization energy is shown which is needed to produce a Pr^{+3} ion from the isolated Pr atom, calculated with different approximations. As one can see, the spherical approximation gives an IP3 for Pr, which is 4%

Pr	Sph	NoSph	Sph-SIC	NoSph-SIC	NoSph-SIC+orb	Exp
IP3	2.88	2.90	2.93	2.95	2.88	2.78

Table 3.3: IP3 energy in Rydbergs, for the Pr atom. Sph = LSD-spherical approximated potential; NoSph = LSD-non spherical potential; Sph-SIC = spherical SIC-LSDA; NoSph-SIC = non spherical with SIC-LSDA basis set; NoSph-SIC+orb = non spherical with SIC-LSDA basis set + non spherical contribution to the self interaction (as described for table 3.2).

away from the experimental one, and there is no improvement using other approximations. Considering the effect of the self interaction non spherical part in a rough way, as described before in the case of lanthanum, drives the non spherical calculated value towards the correct direction (cf. the sixth column in table 3.3). For all lanthanides, as far as $4f$ electrons are involved, this negative shift in the IP3 is around 50 mRy. Thus, figure 3.5, depicting the IP3 in lanthanides, would not be dramatically changed if we take them into consideration. We suggest that this mismatch of calculated IP3 with respect to the experimental ones is connected with the LSDA approximation itself. Even for the IP3 of beryllium, which involves no aphericity at all and the ground state of the three-fold positive charged ion is analytically computable, we find a 15% discrepancy with experiments (calculated IP3: 182 eV, exp.: 154 eV). The complete calculated and experimental data on rare-earth ionization energies are presented in figs 3.3, 3.4, 3.5. Calculated energies were obtained as total energy differences. Similar tables were published in [45], but calculated with the von Barth and Hedin [27] parameterization of the correlation energy functional, while we used the one suggested by Perdew and Zunger [34]. This choice yields substantial improvements to the calculated ionization potentials.

As one can see, the first and second ionization potentials are somewhat improved by SIC, as already noticed in [37] and [45]. No appreciable differences are found between spherical SIC and non-spherical SIC in IP1 and IP2 in those atoms which ionize losing one s electron, as expected. More intriguing is the situation as regards the third ionization potential. Spherical SIC is not

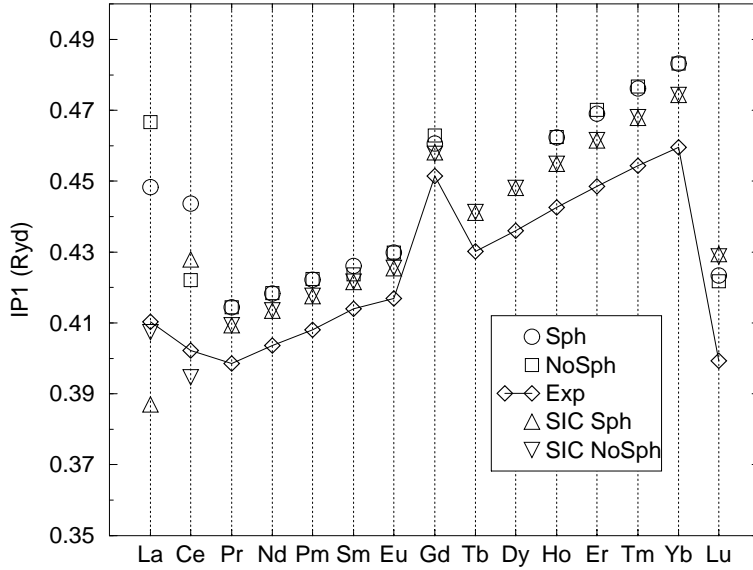


Figure 3.3: Rare-earth first ionization energies. Circles are calculated with LSDA spherical and collinear approximation; squares with LSDA non spherical and collinear; Up and down triangles with SIC-LSDA described in the text. LSDA for Tb and Dy did not converge.

performing as well as in IP1 and IP2. This fact was explained in ref. [37] as due to non-sphericity, since to get a rare-earth plus three ion, one f electron must be removed. Our calculation shows no systematic improvement taking asphericity into account. It leads even to a worse estimation of IP3 in most cases and only in four cases (Ce, Pm, Dy, Er) the IP3 was slightly driven to the experimental value².

In fig. 3.6, the reduction of the spin projection along the total angular momentum direction, due to the non spherical correction to the XC-field, is shown. This quantity is defined as the ratio $-(\langle s_z \rangle_{\text{NoSph}} - \langle s_z \rangle_{\text{Sph}}) / \langle s_z \rangle_{\text{Sph}}$ and zero if both spin projections vanish. Negative values are of course, connected to a spin increase. The greatest spin reduction occurs when two f electrons are in the shell, while the greatest increase corresponds to two f holes. Calculations were performed with SIC-LSDA. A spin reduction indicates a tendency of the system to exhibit spin non collinearity, while a spin increase (Ho, Er, Er^{+3} and Tm^{+3}) on the contrary the tendency of non spherical corrections to drive the system into a more spin collinear displacement. This fact we should remember when dealing with non collinear corrections. Due to convergence problems, La, La^+ , Ce^{+3} and Gd were calculated with

²Atomic data were taken from <http://www.webelements.com>

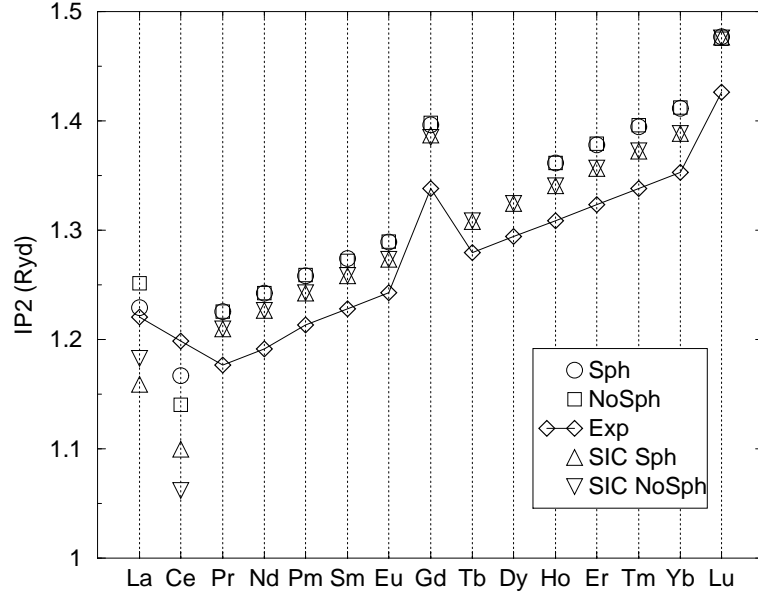


Figure 3.4: Rare-earth second ionization energies. Cf. previous figure caption.

the minimum basis set: only occupied spherical states (not shells! Cf. first column in table 3.1) were taken to form the basis set in the self-consistent non spherical cycles. As a result the spin reduction shown in fig. 3.6 for these atoms and ions can be heavily underestimated (because of the forced absence of matrix elements between the occupied and unoccupied $4f$ states with the same j_z), while their total energies will be almost unaffected (cf. table 3.1). Probably this convergence problems could be solved in the future allowing for fractional occupation numbers.

Finally, in fig. 3.7, a list of electronic quadrupole momenta calculated self-consistently for the lanthanides according to eq. (2.34) are shown for further reference. They could be useful for the calculation of cristall field parameters as well as for an estimation of electric quadrupole effects due to the electron cloud in NMR spectra [46]. Negative values correspond to an oblate charge density, while positive values to a prolate one. Pictures of the $4f$ charge densities can be found in ref. [47]. The nucleus was always considered as point-like, with no multipole momenta, so that no induced multipolar effects of the nucleus are considered. In particular no Sternheimer antishielding factors were analyzed [46, 48]. For the ions, multipolar momenta were defined with respect to a system of coordinates centered at the nucleus. The La, Ce, Gd and Lu atoms have a higher quadrupole momentum because of the more extended d electrons. The quadrupolar momenta of the three-fold positive

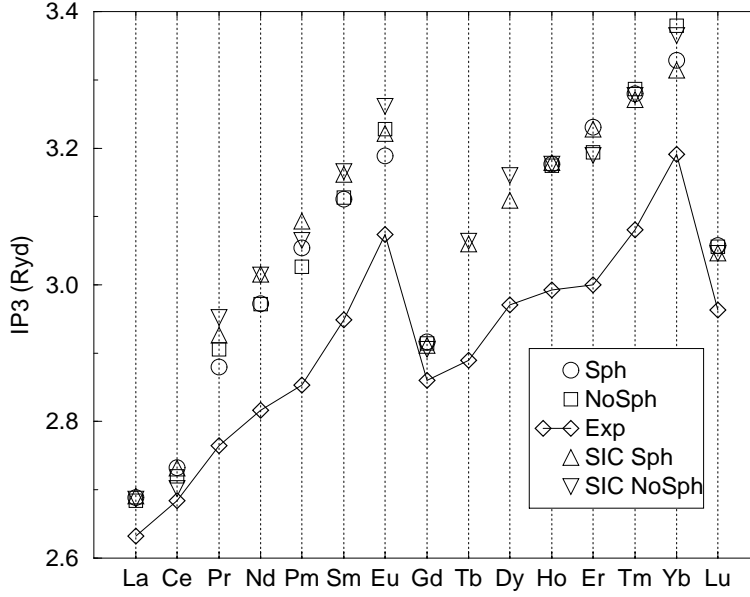


Figure 3.5: Rare-earth third ionization energies. Cf. caption of fig. 3.3.

charged ions stem only from the $4f$ charge density. Here, a point symmetry with respect to Gd^{+3} , which has a half filled $4f$ shell, is visible. It is due to electron states to its left and hole states (not positrons!) to its right. A small decrease in the corresponding electron and hole states of the quadrupolar momenta stems from the lanthanide contraction. In fig. 3.8, the contribution of the quadrupolar and octupolar momenta to the Hartree energy is shown for rare-earth $+3$ ions. The smaller values at Nd^{+3} and Pm^{+3} and symmetrically at Ho^{+3} and Er^{+3} stem from the $4f$ shell to be one fourth occupied (unoccupied). This generates an almost spherical state, because of the second Hund's rule way of occupying orbitals. The values at Ce and Yb are strongly influenced by the non spherical contribution to the self interaction. Here, one has one f electron (hole) and the only physical contribution to the Hartree energy is the small interaction between the aspherical $4f$ charge density and the core electrons. This large Hartree self interaction energy value finds no XC-energy counterpart because of the LSD-approximation to be introduced for the XC-energy functional [43], and because we do not consider truly non spherical SIC. The slight energy increase with atomic number is again an effect of the lanthanide contraction.

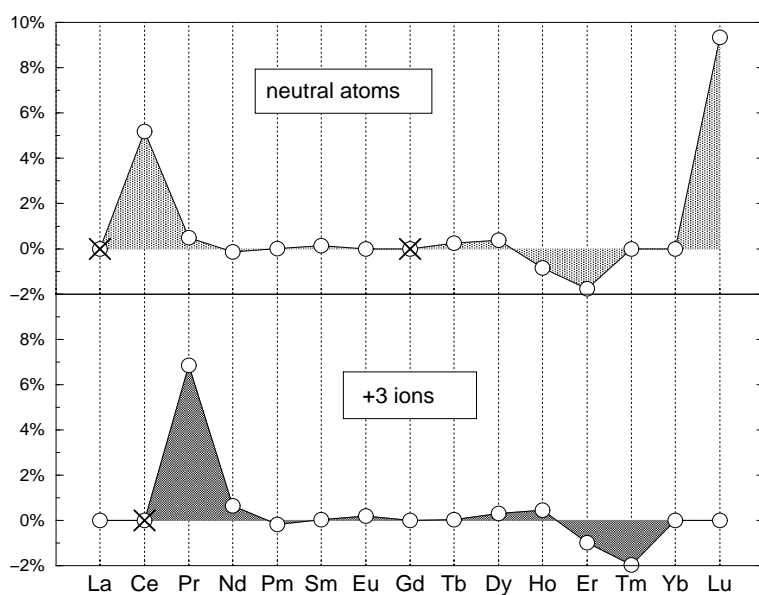


Figure 3.6: Percentual reduction with respect to the spherical approximation, of the z projection of the spin, driven in rare-earth atoms and +3 ions, by a non spherical symmetric, but still collinear, XC-field. Negative values correspond to an increase of s_z , instead. Big crosses indicate that those atoms and ions were calculated with a minimum basis (cf. text) and their spin reduction can be underestimated.

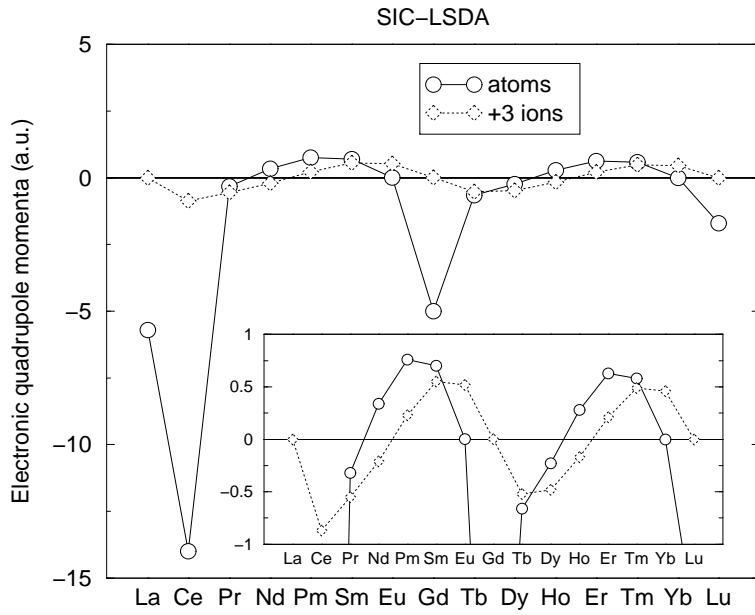


Figure 3.7: Calculated quadrupole momenta in rare-earth atoms and +3 ions. ($1 \text{ a.u.} = ea_{\text{Bohr}}^2$). The inset focuses to a narrower vertical axis region.

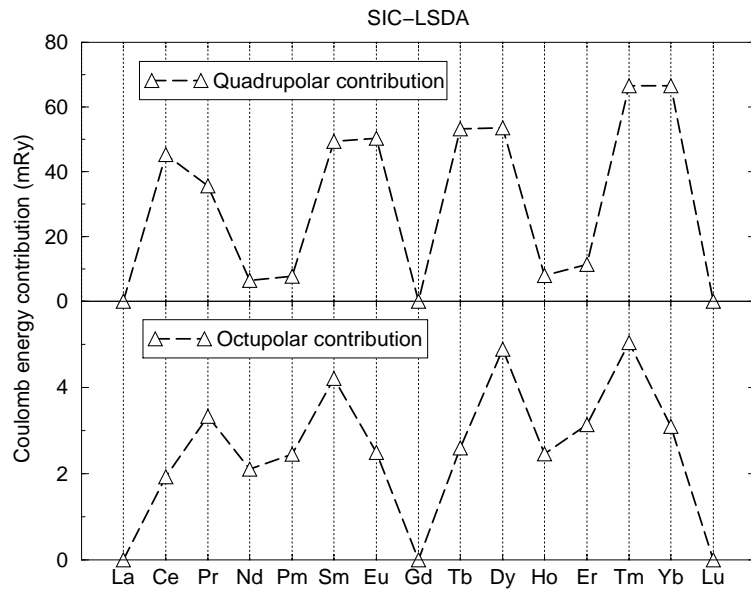


Figure 3.8: Contribution to the Hartree energy of quadrupolar and octupolar momenta in rare-earth +3 ions.

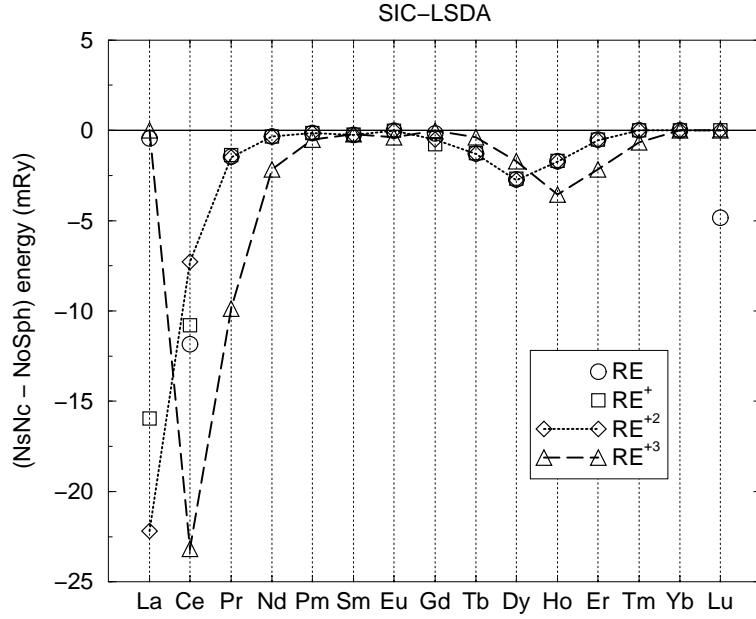


Figure 3.9: SIC-LSDA calculated [non-spherical-and-non-collinear - non-spherical] total energy differences for rare-earths (RE) atoms and ions.

3.2 Non collinear calculations

As in the previous non spherical case, spin non collinearity is taken into account variationally, with the eigensolutions of the spherical problem as basis set. In fig. 3.9 the difference of total energies calculated in the non spherical and non collinear effective potential with respect to the non spherical and collinear one, are shown for rare-earth atoms and ions. In most cases this energy difference is below 5 mRy. The non collinear potential lowers the total energy with respect to the collinear one, but since the effect is small, still the spherical LSDA gives a lower ground state energy. In section 1.6 it was mentioned that the spin-orbit interaction is responsible for the non collinearity in isolated systems described within the LSDA, since it is the only effect that mixes the up and down spin components, if dipole effects are neglected (Hartree magnetic field). On the contrary there is the XC-field which tries to align spins. This counter play game was somehow shown in fig. 2.1, where the region of large non collinearity was shown in the middle as j - j coupling region and the collinear one at the left and right edges as l - s coupling regions. The slope indicated the spin projection along the z axis. The less the slope, the less the collinearity. In picture 3.10 we show the value of the ratio $\langle B_{XC} \rangle_{4f} / \Delta_{SO}$ (effective XC-field, in atomic units, felt by the $4f$ electrons divided the spin-orbit energy splitting between the $j = \frac{5}{2}$

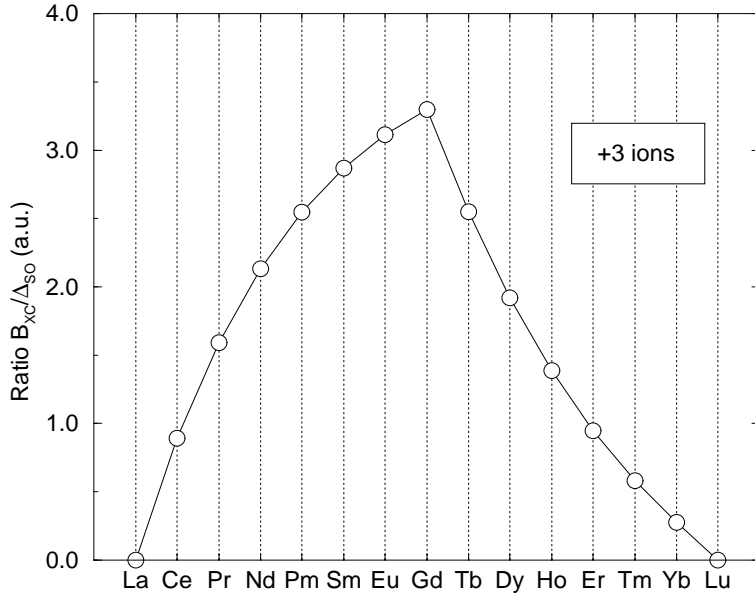


Figure 3.10: Collinearity parameter in rare-earths +3 ions, i.e. the ratio between the effective XC-field felt by the $4f$ electrons divided their spin-orbit splitting.

and the $j = \frac{7}{2}$ multiplets in absence of XC-field), calculated in the spherical approximation for the $4f$ levels of lanthanides +3 ions. The less the ratio, the more non collinear the system should be. One sees, comparing then fig. 3.9 and 3.10, that for Ce^{+3} and Pr^{+3} this is true also in terms of total energy contributions. Then, it would be also expected for Er^{+3} , Tm^{+3} and Yb^{+3} . Here, no big deviation from collinearity does occur instead, because as we have seen in fig. 3.6, non sphericity acts for these ions as another source to enhance the collinearity. Moreover, in Yb^{+3} there is an hole with $j_z = j = \frac{7}{2}$ in the $4f$ shell, which has a collinear spin density.

The effect of interplay between spin-orbit and XC-field can also be seen comparing fig. 3.15 and fig. 3.17. In the former the XC-field of Pb^+ is shown, which has a large non-collinear parameter with respect to the C^+ ion (cf. table 2.2: there are 4 order of magnitudes of difference). The latter shows clearly a larger collinearity.

In fig. 3.11 the spin reduction with respect to the spherical case is shown. The atoms La, Ce and Gd required a minimum basis to converge. Hence, their almost zero spin reduction can be underestimated. Due to non collinearity, which is treated self-consistently, the spin projection along the z axis undergoes a more pronounced reduction than in the collinear case. We even find a spin reversion in the case of Ce^{+3} . The qualitative explanation of this

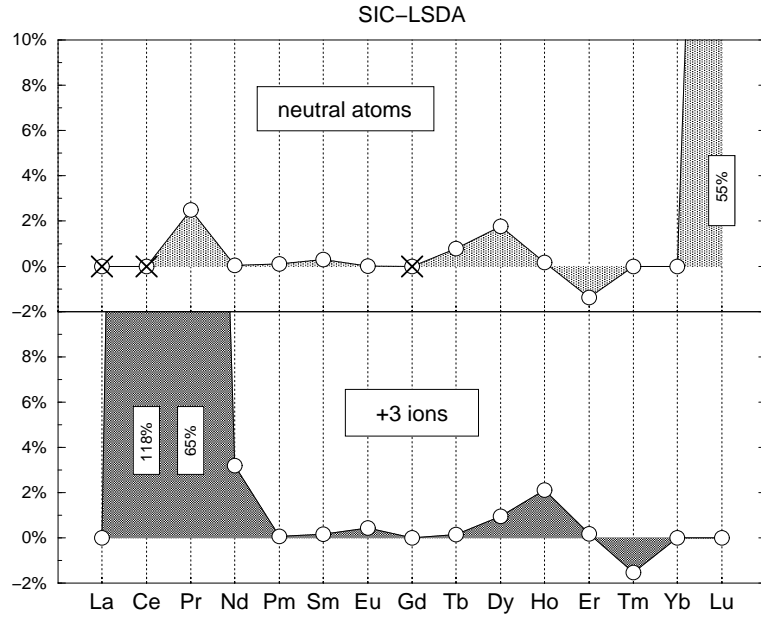


Figure 3.11: Percentual reduction with respect to the spherical approximation, of the z projection of the spin, driven in rare-earth atoms and +3 ions, by a non spherical symmetric and non collinear XC-field. Negative values correspond to an increase of s_z , instead. The value over 100% in Ce^{+3} indicates a spin reversion. Data at crosses can be underestimated.

effect is clear if considering fig. 3.12 where the resulting XC-field for this ion is shown. Since we showed that in LSDA the spin magnetization is parallel to the XC-field, fig. 3.12 can be thought to represent also the spin magnetization. Length of vectors, would of course change in a non linear way. Here, a cut in the x,z plane, with the nucleus at the middle of the left edge (nearby the axis label 'z') is displayed. Cylindrical symmetry is present such that the full three dimensional representation is obtained rotating by 2π this picture along the left edge. Both edge lengths are 3.5 a.u. Starting from the nucleus and going along the x axis, the field is found to be directed toward the positive z . This is, qualitatively, the positive XC-field which is considered in the spherical and collinear calculations, which yields $\langle\beta\Sigma_z\rangle \approx -0.97$. But now, treating the problem in a non spherical and non collinear way, the XC-field projection along z turns to negative values rather near the x,y plane, because of the large oblate character of the Ce^{+3} $4f$ density (squeezed towards the x,y plane). This yields a $\langle\beta\Sigma_z\rangle \approx +0.17$ (of course this state is degenerate with the one with opposite spin). The large mixing between the two $4f$ states with the same $j_z = 5/2$ (45% from the positive spin state, $j = 7/2$, and 55%

from the negative spin state, $j = 5/2$) is responsible for this reverted spin moment.

At this stage, we can already test if the eq. (1.43) is satisfied. We know from RDFT, that the XC-field must be a transversal field; its source density must vanish everywhere. Once we have the non collinear self-consistent XC-field in principle at any point in space, we can calculate numerically its divergence. In cylindrical coordinates it reads:

$$\operatorname{div} \mathbf{B} = \frac{1}{\rho} \frac{\partial}{\partial \rho} (\rho B_\rho) + \frac{\partial}{\partial z} B_z \quad (3.2)$$

being $B_\phi = 0$ for symmetry reasons; ρ is the distance to the z axis.

In fig. 3.13 and 3.14 we show the non spherical and collinear self-consistent XC-field and its source density as calculated in Pb^+ . On the other hand, in fig. 3.15 and 3.16 we show the same quantities in the non spherical and non collinear case, again for Pb^+ (notice the similarity with fig. 1.1).

What is immediately clear after comparing the figures which show the XC-field source densities, it is that definitely LSDA does not automatically provide a transversal XC-field. This is in fact, not a surprise. The transversality condition to be fulfilled in all the space is a global requirement. There is no hope to have it from a local approximation. With figs. 3.14 and 3.16 we intended to show that a non collinear LSDA enhances the source densities with respect to the collinear one.

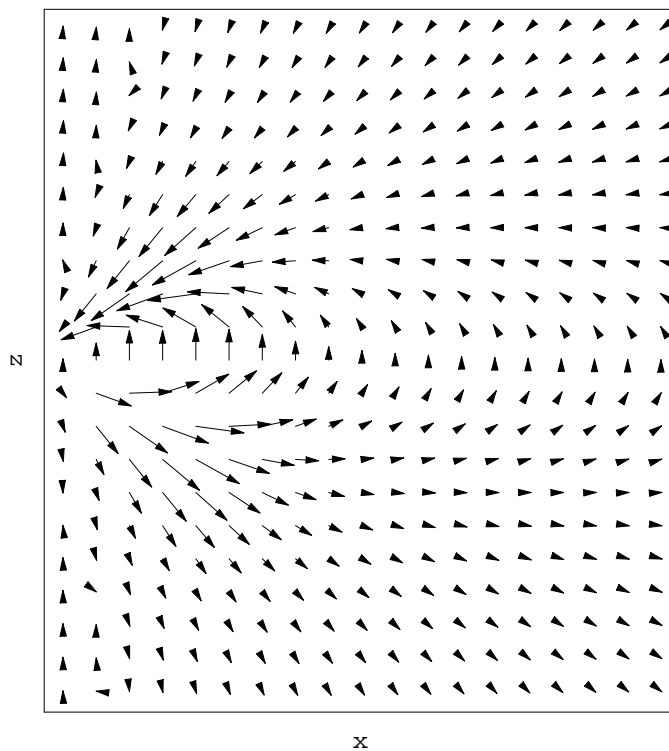


Figure 3.12: Non collinear self-consistent XC-field in Ce^{+3} . The picture is a cut in the x,z plane, with the nucleus at the middle of the left edge (nearby the label 'z'). Cylindrical symmetry is present such that the full three dimensional picture is obtained by rotating by 2π this picture along the left edge. Both edge lengths are 3.5 a.u. (twice the ion size). Arrows without a tail give of course, an idea of the direction of the field in each point, but can be associated to different (tiny) magnitudes. In the picture, the highly oblate shape of the Ce^{+3} $4f$ electron is also somewhat detectable.

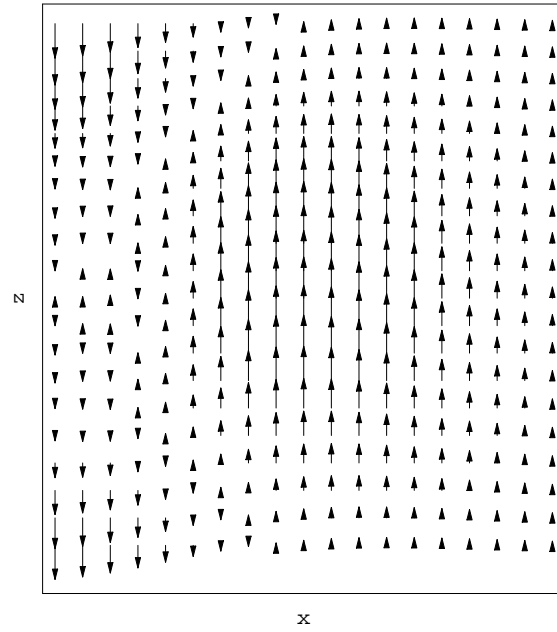


Figure 3.13: Non spherical and collinear XC-field in Pb^+ . Cf. fig. 3.12 for the caption. What changes here are the edge lengths of 5.5 a.u.

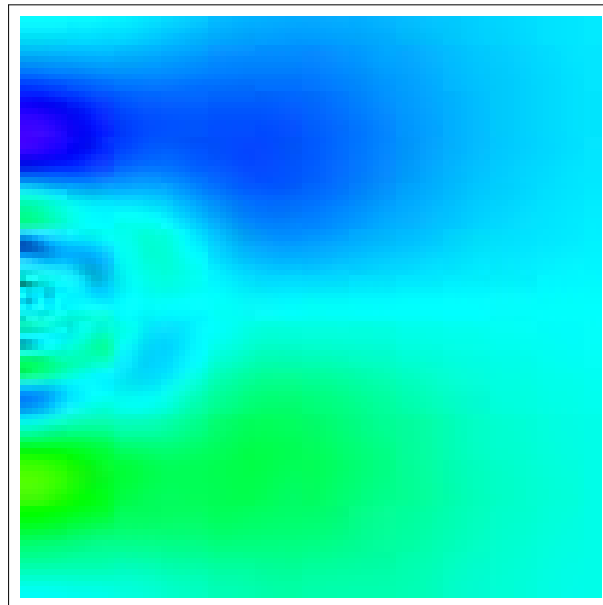


Figure 3.14: Non spherical and collinear XC-field source density in Pb^+ . Color legend is given in fig. 3.16. The nucleus is again at the middle of the left edge. Both edges measure 5.5 a.u.

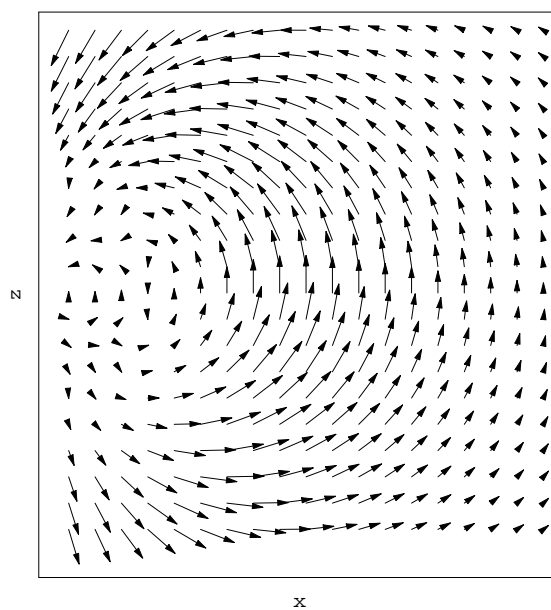


Figure 3.15: Non spherical and non collinear XC-field in Pb^+ . Cf. fig. 3.12 for the caption. What changes here are the edge lengths of 5.5 a.u. Notice the similarity with fig. 1.1.

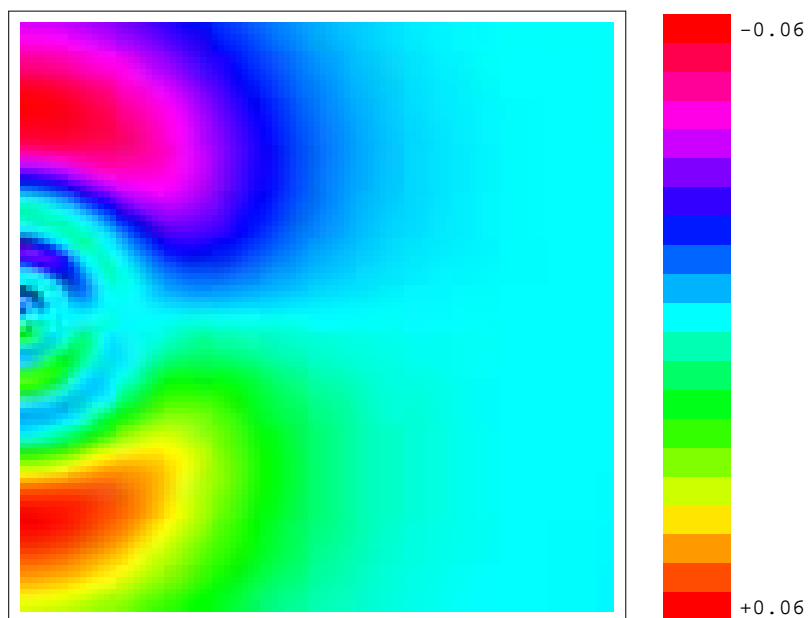


Figure 3.16: Non spherical and non collinear XC-field source density in Pb^+ . The nucleus lies at the middle of the left edge. The edge length is 5.5 a.u. The legend on the right explains the values in a.u. attributed to the colors.

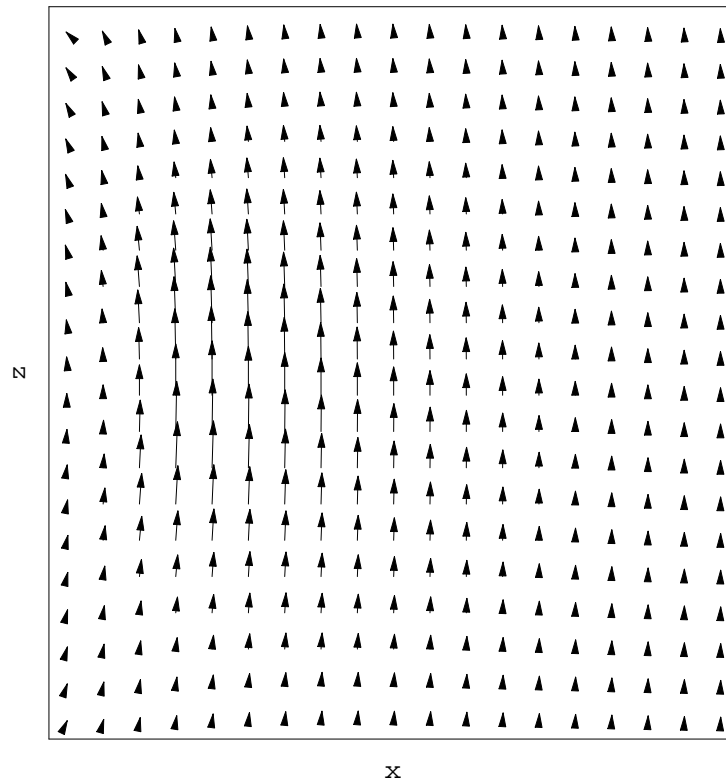


Figure 3.17: Non spherical and non collinear XC-field in C^+ . Cf. fig. 3.12 for the caption. What changes here are the edge lengths of 3.0 a.u. The XC-field is here 2 orders of magnitude larger than the $2p_{\frac{1}{2}}-2p_{\frac{3}{2}}$ spin-orbit splitting. Hence an high collinear situation is expected.

3.3 Transversal XC-field calculations

Once again, the variational method used in the previous two cases, the non spherical and non collinear ones, is used for solving the KSD equation now, in presence of a transversal XC-field. The non local procedure needed to achieve such a field was already explained in the previous chapter. As one can see from fig. 3.18 and fig. 3.19 compared with figs 3.17 and 3.15 respectively, the LSDA XC-field undergoes a big change. Also the magnitude of the XC-field changes: one can calculate the quantity

$$\frac{1}{N} \int d\mathbf{r} n(\mathbf{r}) |\mathbf{B}_{\text{XC}}| \quad (3.3)$$

for both the LSDA XC-field and transversal XC-field and obtain in the case of Pb^+ the values 0.002 and 0.036 a.u. respectively. The latter value assures us that we are not dealing with a spurious field which would arise as a numerical error due to the subtraction in eq. (2.46). In fig. 3.18, two regions can be noticed: nearby the nucleus an effective current density flowing inside the page generates a counterclockwise XC-field and vice versa nearby the right edge. The same occurs also in the XC-field of Pb^+ , but the second region is outside the drawn box and is not visible in fig. 3.19. Once more we stress the point that we have neglected the dependence of the XC-energy functional on the orbital magnetization density (SDFT).

We show also in fig. 3.20 the spin magnetization in Pb^+ arising from the transversal XC-field in fig. 3.19, because these two vectors do not have, in each point of the space, the same direction any more.

Anyway, as discovered for the non collinear case in the previous section, the contributions to the total energy due to a transversal XC-field are small and positive, in most of rare-earths below 5 mRy (cf. fig. 3.21). It seems also that this correction almost cancels the non collinear one displayed in fig. 3.9, so that in fact the final contribution of the intra-atomic non collinearity to the total energy is almost zero. This strongly elects the spin collinear approximation as a good approximation as far as total energy calculations are concerned.

Different is the situation with the total spin. Being a transversal field, originated only by vortices, the field lines must form a close path. This means that the XC-field and, presumably, the spin magnetization have to turn upside down somewhere. We see from fig. 3.19 that in fact in Pb^+ this occurs nearby the nucleus. We should expect a relevant influence on the average spin projection on the z axis. In Pb^+ indeed with a LSDA non collinear XC-field, one obtains $\langle \beta \Sigma_z \rangle \approx 0.33$, while with a transversal field $\langle \beta \Sigma_z \rangle \approx 0.25$. The spin reduction due to a transversal field, with respect to

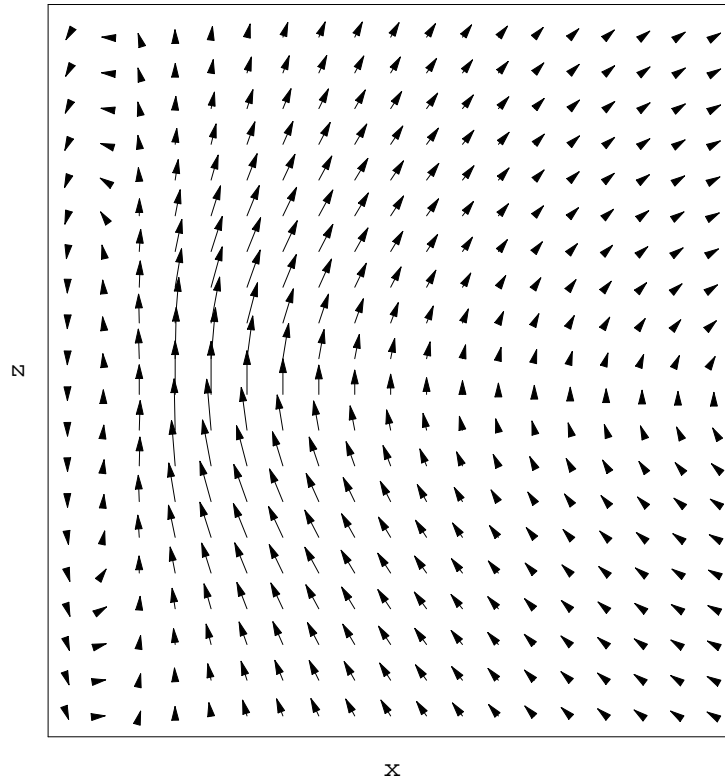


Figure 3.18: Source-free XC-field in C^+ . Cf. fig. 3.12 for the caption. What changes here are the edge lengths of 3.0 a.u.

the spherical case is shown in fig. 3.22 for rare earths. Note that now also in Gd^{+3} there is a spin reduction, despite its large collinearity parameter (cf. fig. 3.10), because of the XC-field reversion described above.

One possible way of checking our results on total spin is via magnetic x-ray circular dichroism (MXCD) experiments [49] or magnetic Compton scattering (MCS) experiments [50]. The former gives information on the orbital magnetization as well, and relies on some sum rules in order to separate the spin and orbital magnetic effects. The latter (MCS) gives informations on the spin part only [51] since, qualitatively speaking, using photon energies above 50 KeV (less than half an Ångström wave length), one probes only a small part of the electron clouds (core electron effects can be easily removed with some experimental tricks) and the orbital motion is not felt then. To our knowledge there are no experimental data available for gases or liquids, although MCS can be used to analyze them as well, the only experimental difficulty given by a substantial reduction of the scattered intensities.

A good candidate for a MCS experiment could be bismuth vapours in an aligning magnetic field (spherical approximated $\langle\beta\Sigma_z\rangle \approx 1.64$, transversal XC-field $\langle\beta\Sigma_z\rangle \approx 1.40$ corresponding to a 15% spin reduction).

Calculations on fcc Ni show the general trend of intra-atomic collinear LSDA to overestimate the atomic spin moment with respect to the MCS measured one [52]. This arises mainly at low momentum regions of the Compton profile ($p < 1$ a.u., i.e. $r > 1$ a.u.), where collinear LSDA predicts the existence of an unobserved positive peak. Fully non collinear or even transversal XC-field calculations for solid Ni would be necessary to understand if this fact can be addressed to a reversion of the XC-field in the interstitial regions and a subsequent spin moment reduction.

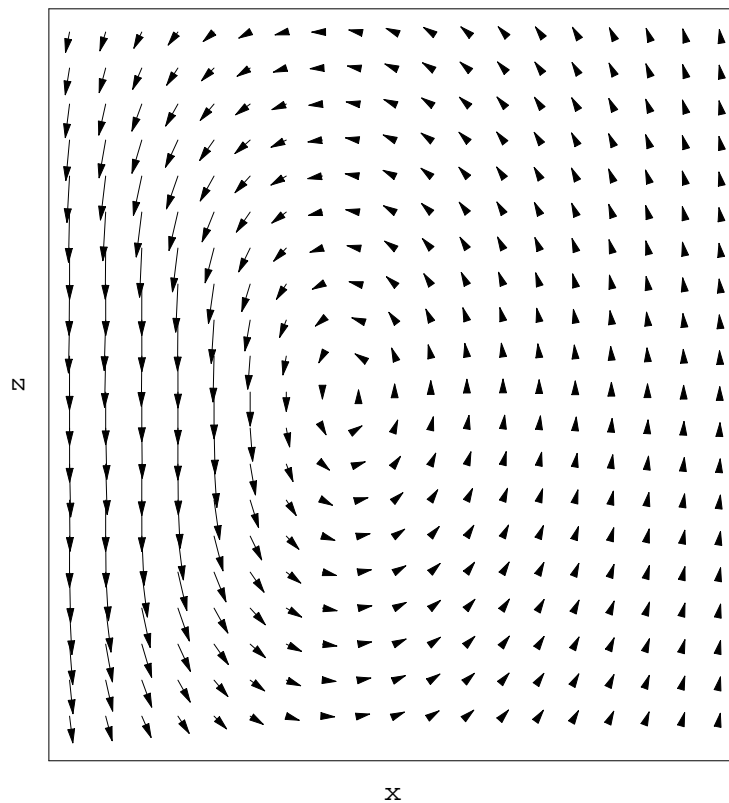


Figure 3.19: Source-free XC-field in Pb^+ . Cf. fig. 3.12 for the caption. What changes here are the edge lengths of 5.5 a.u.

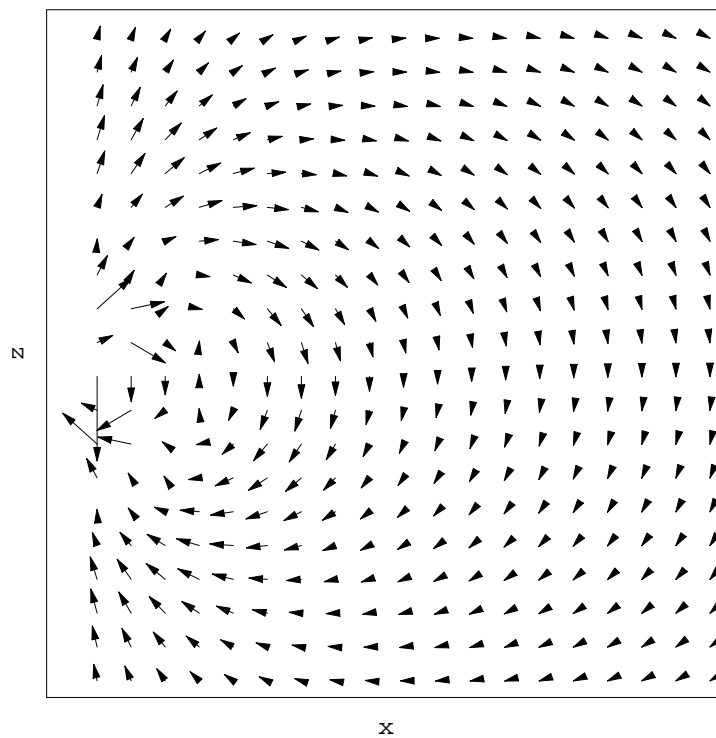


Figure 3.20: Spin magnetization arising from a source-free XC-field in Pb^+ . Cf. fig. 3.12 for the caption. What changes here are the edge lengths of 5.5 a.u.

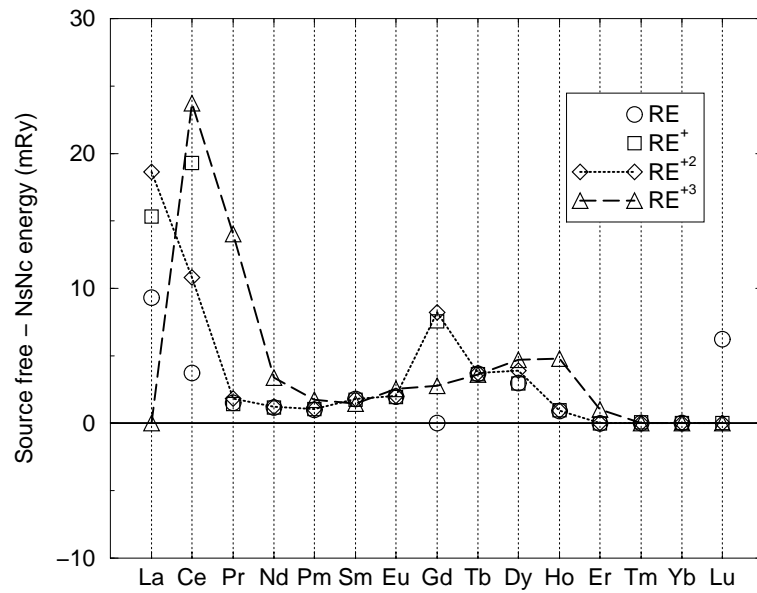


Figure 3.21: SIC-LSDA calculated [Source-free - non-spherical-noncollinear] total energy differences for rare-earths (RE) atoms and ions.

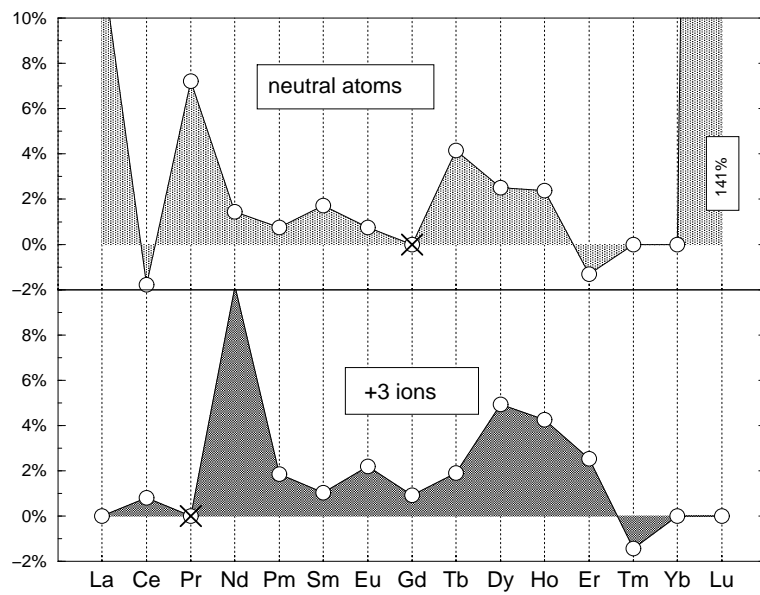


Figure 3.22: Percentual reduction with respect to the spherical approximation, of the z projection of the spin, driven in rare-earth atoms and +3 ions, by a source-free XC-field. Negative values correspond to an increase of s_z , instead. The value over 100% in Lu indicates a spin reversion. Data at crosses can be underestimated.

Chapter 4

Application of the spherical KSD equations

In this chapter, which can be considered as an appendix, we would like to show some results obtained using the spherically approximated functionals to calculate total energies and ground state densities. We have shown in the previous chapter how small the non spherical and non collinear corrections to the total energies are. So that in fact, the spherical approximation is a good approximation as far as complicated spin phenomenologies are not to be dealt with. There is in fact a lot of possible application of an atomic spherical four-component relativistic calculation. Here we show two of them, which to our opinion were the most interesting. Other works, such for example the calculation of Coulomb correlation energies for the whole set of lanthanides or f - d promotion energies also in lanthanides, were also carried out, but did not fit to the present manuscript.

4.1 Relativistic self interaction corrections

We have already discussed in section 1.7, the underlying theory behind the self interaction corrections. A supplementary term was subtracted *ad hoc* in the kinetic energy operator in eq. (1.64) in order to remove the non-physical self interaction of an electron with itself, arising if an approximate exchange-correlation functional is used:

$$\sum_{\alpha\sigma} (E_{\text{H}}[n_{\alpha\sigma}] + E_{\text{XC}}[n_{\uparrow} = n_{\alpha\sigma}, n_{\downarrow} = 0]). \quad (4.1)$$

Here, the orbitals were supposed fully polarized, i.e. the sum \sum_{σ} has only one non vanishing term. This led to an orbital dependent effective potential, which in a collinear approximation of the XC-field is written non-

relativistically as:

$$v_{\text{eff},\sigma\sigma'}^{\text{SIC},\alpha} = v_{\text{ext}} + v_{\text{H}} + v_{\text{XC}} + B_{\text{XC},z} \sigma_z - v_{\text{H}}^{\alpha} - v_{\text{XC}}^{\alpha} - B_{\text{XC},z}^{\alpha}. \quad (4.2)$$

where the term $B_{\text{XC},z}^{\alpha}$ appears as a scalar potential. Eventually, rearranging terms and switching to bispinor operators, one gets:

$$v_{\text{eff},\tau\tau'}^{\text{SIC},\alpha} = I_4 [v_{\text{ext}} + (v_{\text{H}} - v_{\text{H}}^{\alpha}) + (v_{\text{XC}} - v_{\text{XC}}^{\alpha})] + \beta \Sigma_z B_{\text{XC},z} - I_4 B_{\text{XC},z}^{\alpha} \quad (4.3)$$

where the new index τ covers all the four components.

We have assumed orbitals to be fully polarized, in particular with the spin projection along the positive z axis (had we assumed a negative polarization, being of course the exchange-correlation energy the same, the following argument would not change in contents), being the electron negative charged, one has that the $B_{\text{XC},z}^{\alpha}$ are *negative* quantities.

Suppose now to have a system containing only one electron, say a hydrogen-like atom. One would like to have an effective Hamiltonian with the potential energy given only by the external potential v_{ext} . In fact, the exchange-correlation scalar potential and the Hartree potential in eq. (4.3), cancel out. What still remains are the terms

$$I_4 v_{\text{ext}} + \beta \Sigma_z B - I_4 B^{\alpha}. \quad (4.4)$$

where B is a shortcut for $B_{\text{XC},z}$. The quantity B^{α} is generally not equal to B , just because an orbital cannot be fully spin polarized in a relativistic theory. This has two different reasons: the presence of non vanishing small components in the wave functions and the fact that one has eigenfunctions of j_z rather than Σ_z . Nevertheless, let's consider the case for the hydrogen $1s_{\frac{1}{2}}$ state, where the small component of the wave function is four orders of magnitude smaller than the large one and $j_z = \Sigma_z$. In this case $B^{\alpha} = -|B|$ and, focusing only on the last two terms, the previous expression becomes ($I_4 = \beta^2$)

$$\beta |B| \left(\frac{B}{|B|} \Sigma_z + \beta \right) \quad (4.5)$$

which explicitly means

$$2\beta B \begin{pmatrix} 1 & 0 & 0 & 0 \\ 0 & 0 & 0 & 0 \\ 0 & 0 & 0 & 0 \\ 0 & 0 & 0 & -1 \end{pmatrix} \quad \text{if } B > 0 \quad (4.6)$$

and

$$-2\beta B \begin{pmatrix} 0 & 0 & 0 & 0 \\ 0 & 1 & 0 & 0 \\ 0 & 0 & -1 & 0 \\ 0 & 0 & 0 & 0 \end{pmatrix} \quad \text{if } B < 0. \quad (4.7)$$

Since $B > 0$ if the state is in a spin down configuration ($j_z = -\frac{1}{2}$) and $B < 0$ if the state is in a spin up configuration ($j_z = +\frac{1}{2}$), even if the Hamiltonian contains the non vanishing terms (4.6, 4.7), they effectively give a vanishing contribution if evaluated on fully spin polarized states (for example in non relativistic states).

Consider now the hydrogen $2p_{\frac{1}{2}}$ state with $j_z = +\frac{1}{2}$. We already know from eq. (1.56) that if we neglect the small component contribution, the mean value of the spin magnetization projection is $-\frac{1}{6}$. Thus, this state is not fully spin polarized. Nevertheless, the XC-field B is sufficient to create a strong coupling between the state $2p_{\frac{1}{2}}$ and $2p_{\frac{3}{2}}$ with the same $j_z = +\frac{1}{2}$ because of the extremely small spin-orbit splitting (cf. table 2.2) and the state is erroneously fully polarized. Therefore, one achieves the spurious cancellation described in the previous paragraph and the eigenvalue is correct (apart from small component effects).

To summarize, using the SIC scheme of eq. (4.3) in one electron systems, one obtains the correct eigenvalues apart small component effects, but not the correct spin polarization, if the XC-field B is much greater than the spin-orbit splitting Δ_{SO} . If, on the contrary, the opposite is true and $B \ll \Delta_{\text{SO}}$, one has the correct spin polarization, but not the correct eigenvalues.

These two extreme cases are shown in table 4.1 and 4.2, where we show the mean spin polarization and energies of the first three states of hydrogen and Fm^{+99} ion respectively. The former table does not present particular features, apart the $2s_{\frac{1}{2}}$ LSDA state which has lower energy than the exact one. This is due to the exchange-correlation self interaction (LDA gives $E_{\text{LDA}} = -0.2484$ Ryd, incidentally equal to the LSDA $2p_{\frac{1}{2}}$). Note that the spin moment of the state $2p_{\frac{1}{2}}$, which should be $\frac{1}{3}$, is wrong.

More interesting is the table 4.2. From the first column one sees that the spin moment reduction due to the small components of the wave function

	$\langle\beta\Sigma_z\rangle_{\text{exact}}$	$\langle\beta\Sigma_z\rangle$	E_{exact} [Ryd]	ΔE_{LSDA} [Ryd]	ΔE_{SIC} [Ryd]
$1s_{\frac{1}{2}}$	1.000	1.000	-1.0000	0.0423	0.0000
$2s_{\frac{1}{2}}$	1.000	1.000	-0.2500	-0.0092	0.0000
$2p_{\frac{1}{2}}$	0.333	1.000	-0.2500	0.0016	0.0000

Table 4.1: Mean value of the spin magnetization and energies calculated within different approximations, for the first three states of Hydrogen. LSDA and SIC energies are shown as differences with respect to the exact analytically calculated value [41]. Spin magnetization gave the same result for each approximation.

	$\langle\beta\Sigma_z\rangle_{\text{exact}}$	$\langle\beta\Sigma_z\rangle$	E_{exact} [Ryd]	ΔE_{LSDA} [Ryd]	ΔE_{SIC} [Ryd]
$1s_{\frac{1}{2}}$	0.895	0.895	-11878.39	26.64	2.84
$2s_{\frac{1}{2}}$	0.973	0.973	-3097.31	1.89	0.34
$2p_{\frac{1}{2}}$	0.361	0.368	-3097.31	7.50	3.66

Table 4.2: First three states of the ion Fm^{+99} , i.e. one electron in a $-100/r$ potential. Cf. previous table caption.

is a remarkable 10% in the ground state, with a 3 Ryd error for the SIC energy and 3% in the $2s$ state. We find a 10% increase in the state $2p$, due again to the small component influence, and a 2% due to the non exact compensation of the XC-field. Since the small component effects on energies are almost the same for the $2s$ and $2p$ states, giving an energy shift of 0.3 Ryd as an estimation from the $2s$ row, the former non exact compensation of the XC-field for the $2p$ state results in an energy increase of about 3 Ryd.

The question is how much important are these XC-field non cancellation effects in heavy atoms with many electrons. The core levels are the most affected ones with an energy increase which is of few part per thousand. This corresponds to a slight increase of the electron core clouds radius, which could, in principle, affect indirectly also the outermost electrons. To be more precise, one should include finite nucleus effects, since they are corrections of the same order. The main difference is, of course, that the XC-field non cancellation effects modify the spin expectation value, whereas the former ones do not.

The ground philosophy of SIC should be to provide the exact quantum mechanical states for the limit case of one electron in an external potential. With this in mind we propose a simple generalization of the usual SIC scheme (1.64) which includes the possibility of partial orbital polarizations. The new SIC orbital dependent operator reads now:

$$\tilde{\Theta}[\hat{n}] = \min_{\{\varphi_\alpha\}} \left\{ \sum_{\alpha} \langle \varphi_\alpha | \mathcal{T} | \varphi_\alpha \rangle - E_{\text{H}}[n_\alpha] - E_{\text{XC}}[\hat{n}_\alpha] \left| \sum_{\alpha}^N \langle \mathbf{r} | \varphi_\alpha \rangle \langle \varphi_\alpha | \mathbf{r} \rangle = \hat{n}(\mathbf{r}); \langle \varphi_\alpha | \varphi_\beta \rangle = \delta_{\alpha\beta} \right. \right\}, \quad (4.8)$$

with \mathcal{T} the kinetic energy operator. The effective potential is now written in the collinear approximation as:

$$v_{\text{eff},\tau\tau'}^{\text{SIC},\alpha} = I_4 [v_{\text{ext}} + (v_{\text{H}} - v_{\text{H}}^\alpha) + (v_{\text{XC}} - v_{\text{XC}}^\alpha)] + \beta\Sigma_z (B_{\text{XC},z} - B_{\text{XC},z}^\alpha) \quad (4.9)$$

which actually reduces itself to the term v_{ext} in the case of a single electron system. Although the just introduced functional looks very appealing, it is

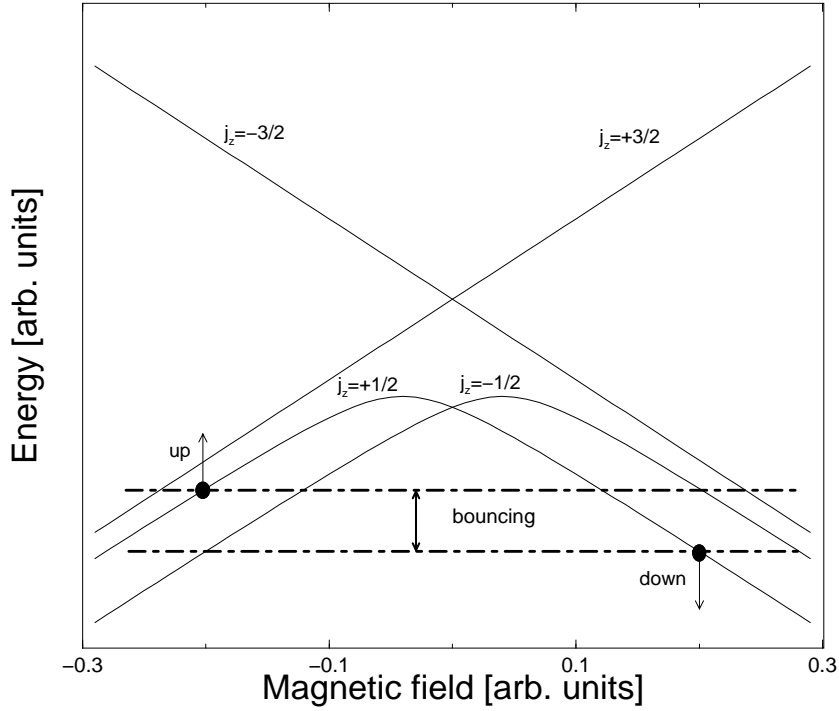


Figure 4.1: Some energy levels of an electron in a $-Z/r$ potential as a function of a homogeneous magnetic field coupled to the spin only according to the Hamiltonian (2.20). Let it be, for a qualitative understanding only, the effective XC-field generated by the electron itself. Suppose that the electron is in a spin down state depicted by the black dot on the right. At the next step, using the new suggested SIC, it will be on the left dot, reverting its spin and consequently the sign of its self XC-field. The system will bounce indefinitely between these two dots.

unfortunately not applicable to electrons in a Russel-Saunders coupling, if the latter ones are treated as in section 2.4. To clarify this last statement, consider picture 4.1. Therein, the energy levels $p_{\pm\frac{1}{2}}^*$ and $p_{\pm\frac{3}{2}}^*$ of an electron in a $-Z/r$ potential are shown as a function of an effective homogeneous XC-field directed along the z axis. The slope in each point gives the mean spin magnetization. Suppose now, to put one electron in the $p_{+\frac{1}{2}}^*$ state according to the aufbau principle (black dot on the right), having decided, yet, to have a positive magnetic field and having filled all levels below it. Hence, it is the only electron in an open shell. If the spin-orbit splitting is small compared to the exchange-correlation field, one has a Russel-Saunders coupling and the

electron is fully polarized. In this case one has

$$|B_{\text{XC},z}| \leq |B_{\text{XC},z}^\alpha| \quad \text{since} \quad |\zeta[\hat{n}^\alpha]| = \frac{|n_\uparrow - n_\downarrow|}{n} \leq |\zeta[\hat{n}^\alpha]| \approx 1 \quad (4.10)$$

and this means that the term $(B_{\text{XC},z} - B_{\text{XC},z}^\alpha)$ in the effective Hamiltonian will change sign at each step. As a result the solution will bounce between the two black dots without reaching a unique self-consistent state. All this will happen if the electron state is in a l - s coupling. If not, the electron will be in the region of figure (2.1) depicted as j - j coupling and the spin will have always the same sign. As a consequence, also the $B_{\text{XC},z}^\alpha$ will have the same sign and no bouncing will occur. One can easily estimate when one is in the previously mentioned condition:

The spin-orbit splitting between p^* states and p states can be expressed in a second order approximation in the fine-structure constant α (not to be confused with the orbital index used above) as $\Delta_{\text{SO}} = c_1 \alpha^2 \langle \frac{1}{r} \frac{d}{dr} U \rangle_p$. For one electron in a point like nuclear potential it becomes $\Delta_{\text{SO}} = c_1 Z \alpha^2 \langle \frac{1}{r^3} \rangle_p = c_1 Z^4 \alpha^2$, where c_1 carries all the multiplicative constants. According to eq. (1.60) $B_{\text{XC}} = |\frac{\delta \varepsilon_{\text{XC}}}{\delta \zeta}| \approx n^{\frac{1}{3}}$ where $n = |\psi|^2$. Since $\psi \approx e^{-Zr}$ is appreciable in a sphere of radius $1/Z$, the average density is one particle over this sphere volume, i.e. $\bar{n} \approx Z^3$. As a result $\bar{B}_{\text{XC}} \approx Z \rightarrow \bar{B}_{\text{XC}} = c_2 Z$. In a many electron case, just as an estimate, substitute Z with an effective Z_{eff} . There are no bouncing effects if $\frac{\Delta_{\text{SO}}}{B_{\text{XC}}^\alpha} = \frac{c_1}{c_2} \alpha^2 Z_{\text{eff}}^3 > 1$. With a direct calculation is possible to obtain the value of the multiplicative coefficient c_1/c_2 . For hydrogen $2p$ we find $\frac{c_1}{c_2} \approx 1.73$, while in the case of $2p \text{ Fm}^{+99}$ we get $\frac{c_1}{c_2} \approx 3.34$. As an average we take the value 2.5. The previous inequality becomes $Z_{\text{eff}} > (2.5 \alpha^{-2})^{\frac{1}{3}} \approx 36$

What we find is that for electrons which feel an effective nuclear charge greater than 36, namely core electrons, as well as for s electrons, it is possible to apply the new SIC scheme defined by the functional (4.8), without any convergence problem. An idea of the effects on total energies is given in tables 4.3, 4.4, 4.5. One can see, as expected, almost no effects in light atoms, but a large effect in heavy ions. In the Fm^{+46} the new-SIC gives a ground state which is 37.7 Ryd lower than the usual SIC; In the Fm^{+36} ion 38.2 Ryd. The difference between these two values (0.5 Ryd) gives an idea about the influence of the 10 electrons outside of the $[\text{Xe}]$ configuration. This value is extremely small and unimportant if compared with total energies values. The question is now, how important it is with respect to ionization energies.

In table 4.4 we calculate total energies for some heavy atoms and ions with

	El. configuration	E_{SIC} [Ryd]	$E_{\text{new-SIC}}$ [Ryd]
He	$1s^2$	-5.8389	-5.8389
Fm ⁺⁹⁸	$1s^2$	-23583.212	-23588.835
Li	[He] $2s^1$	-15.0106	-15.0106
Be	[He] $2s^2$	-29.3930	-29.3932
Fm ⁺⁴⁶	[Xe]	-66859.086	-66896.823
Fm ⁺³⁶	[Xe] $6s^2 p^6 7s^2$	-67588.187	-67626.431

Table 4.3: SIC vs new-SIC total energies.

	El. configuration	E_{SIC} [Ryd]	$E_{\text{hybrid-SIC}}$ [Ryd]
Ra	[Rn] $7s^2$	-50097.379	-50126.611
Ra ⁺	[Rn] $7s^1$	-50096.978	-50126.209
U	[Rn] $5f^3 6d^1 7s^2$	-56157.771	-56189.414
U ⁺	[Rn] $5f^4 7s^1$	-56157.357	-56188.999

Table 4.4: SIC vs hybrid-SIC total energies. The core electrons treated with the new SIC scheme were: 1s 2sp 3spd 4spd 5sp 6s.

	SIC [Ryd]	hybrid-SIC [Ryd]	Exp. [Ryd]
Ra	0.401	0.402	0.388
U	0.414	0.415	0.455

Table 4.5: SIC vs hybrid-SIC ionization energies. The core electrons treated with the new SIC scheme were: 1s 2sp 3spd 4spd 5sp 6s. Experimental data taken from <http://www.webelements.com>

an hybrid SIC, which performs the new-SIC scheme for core electrons and usual SIC for outer ones.

The corresponding first ionization energies are shown in table 4.5.

As one can see, using the new hybrid SIC yields practically no improvement on ionization energies. For this reason we shall not implement it in the following.

4.2 Photoemission cross sections

As a direct application of the spherical approximation to solve the Kohn-Sham-Dirac equations in connection with a self interaction corrected functional, we present the calculation of the cross section for the process of photoemission involving single isolated atoms. Qualitative conclusions will be presented for solids as well.

A photoemission process involving a single atom is depicted in figure 4.2.

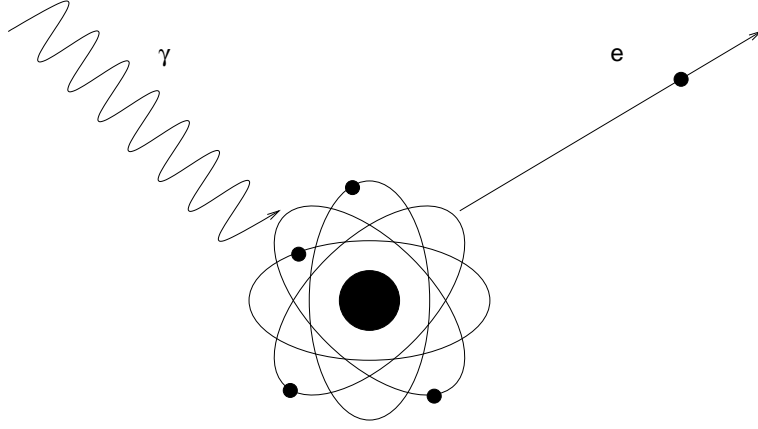


Figure 4.2: Sketch of a photoemission process in an atom. We shall consider only the process involving one incoming photon and one outgoing electron.

One photon with energy $h\nu$ interacts with the electronic cloud surrounding the atom and finally an electron is emitted in the continuum with a certain kinetic energy. Applying perturbation theory, in particular the Fermi golden rule, one can estimate the cross section of the process. Within the further dipole approximation [53], the cross section is proportional to the matrix element squared:

$$\sigma_{if} \propto h\nu \left| \int \psi_i^*(\mathbf{r}_1, \dots, \mathbf{r}_N) \sum_k^N \mathbf{r}_k \psi_f(\mathbf{r}_1, \dots, \mathbf{r}_N) d\mathbf{r}_1 \dots d\mathbf{r}_N \right|^2 \quad (4.11)$$

where the ψ_i and ψ_f are the wave functions of the initial and final state respectively. The initial state is constituted by an atom with N electrons, while the final state is composed by an ion with $N - 1$ electrons and one electron in the continuum. The initial wave function is normalized to unity, whereas the final one per unit energy range; thus:

$$\int |\psi_i|^2 d\mathbf{r}_1 \dots d\mathbf{r}_N = 1 \quad \text{and} \quad \int \psi_f^*(E) \psi_f(E') d\mathbf{r}_1 \dots d\mathbf{r}_N = \delta(E - E'). \quad (4.12)$$

If, in a crude estimate, ψ_i and ψ_f are both represented by single Slater determinants and no relaxation is allowed after ionization has taken place, then $N - 1$ of the orthonormal functions φ_k constituting the determinants are the same and the cross section can be written as:

$$\sigma_{if} \propto h\nu \left| \int \varphi_i^*(\mathbf{r}) \mathbf{r} \varphi_f(\mathbf{r}) d\mathbf{r} \right|^2, \quad (4.13)$$

where the φ_i is the orbital which was occupied in the initial state and due to the electromagnetic interaction turned into the final continuum state φ_f . One

can use as function φ_i the i -th KSD self interaction corrected orbital, while for the φ_f the wave function calculated with a certain energy in the continuum, in the same effective central potential felt by the φ_i . Using SIC adds a supplementary approximation given by the non orthogonality of the resulting SIC eigenfunctions. The assumption that the system remains unrelaxed after the ionization is already sufficiently crude to allow us to neglect these non orthogonality problems. The advantage of SIC over LSDA is that it is closer to the Hartree-Fock like methods used in Refs. [54, 55, 56], which we would like to discuss below, and it gives the correct asymptotic behaviour of the effective potential of an isolated atom at infinity, $v(r \rightarrow \infty) = -\frac{1}{r}$. Finally, taking into account that $h\nu = I_{nl} + \epsilon$ where I_{nl} is the ionization energy needed to expel an electron from the orbital with $i = (nl)$ and ϵ the outgoing electron kinetic energy, eq. (4.13) becomes:

$$\sigma_{nl}(\epsilon) \propto (\epsilon + I_{nl})[lR_{l-1}^2(\epsilon) + (l+1)R_{l+1}^2(\epsilon)] \quad (4.14)$$

with n and l indicating the principal and angular momentum quantum numbers respectively and the radial integrals

$$R_{l\pm 1} = \int_0^\infty P_{nl}(r) r P_{\epsilon, l\pm 1}(r) dr \quad P(r) \stackrel{\text{def}}{=} r\varphi(r). \quad (4.15)$$

Hence, the calculation of the cross section is reduced to the calculation of the matrix elements $R_{l\pm 1}$.

Let's fix our attention on the $4d$ shell in palladium. In figure 4.3 are plotted:

- The function $rP_{4d} = r^2\varphi_{4d}$ (warning: this is not the charge density);
- The function $P_{\epsilon, f}$ for $\epsilon = 187$ eV;
- The product of the previous two functions, i.e. the quantity inside the integral which defines R_f ;
- The integral $S_f(\epsilon, r) = \int_0^r r' P_{4d}(r') P_{\epsilon, f}(r') dr'$, with $R_f(\epsilon) = S_f(\epsilon, r \rightarrow \infty)$.

One can see from the picture that the integral $S_f(\epsilon, \infty)$ assumes a positive value for $\epsilon = 187$ eV. This is mainly due to the small positive region present in the $rP_{4d}(r)$ function nearby the nucleus, which in turn is caused by the presence of a node in the φ_{4d} wave function. For low electron kinetic energies, the function $P_{\epsilon, f}$ has of course a larger wave length and the integral is dominated by the negative region of P_{4d} . This means that $S_f(\epsilon = +0, \infty) < 0$. As a result, the $S_f(\epsilon, \infty)$ being continuous with respect to ϵ , there will be

a value of ϵ for which the matrix element R_f is zero and the cross section, depending on R_f^2 , will have a minimum. This is called the Cooper minimum, which appears whenever the atomic bound state has at least one radial node [54, 55]. In figure 4.4 the same functions of fig. 4.3 are shown for $\epsilon = 93$ eV, nearby the calculated Cooper minimum for palladium $4d$ electrons. The photoemission cross section σ_{4d} in palladium as a function of the electron kinetic energy is shown as in figure 4.5. What we are interested in, is the position of the Cooper minimum. That's why all multiplicative factors independent from ϵ were ignored in eq. (4.13). A complete table of cross section plots was provided by Yeh and Lindau [56] for all atoms from $Z=1$ up to $Z=103$ and it is still being used as a valid reference in the scientific community. In [56] all plots were calculated with Hartree-Fock methods, in particular no relativistic effects were considered. These relativistic effects could be very important in the $5f$ electrons of uranium, for example, since we saw that the position of the nodes are important for the matrix element (4.15) to change sign. Small shifts of the node position can produce a large shift in the calculated Cooper minimum. The node in the uranium $5f$ radial function occurs at 0.438 a.u. in the relativistic case, estimated using Kohn-Sham-Dirac wave functions, and at 0.430 a.u. in the non relativistic limit. It is indeed a small change, but to our experience also tiny changes in the wave functions can produce

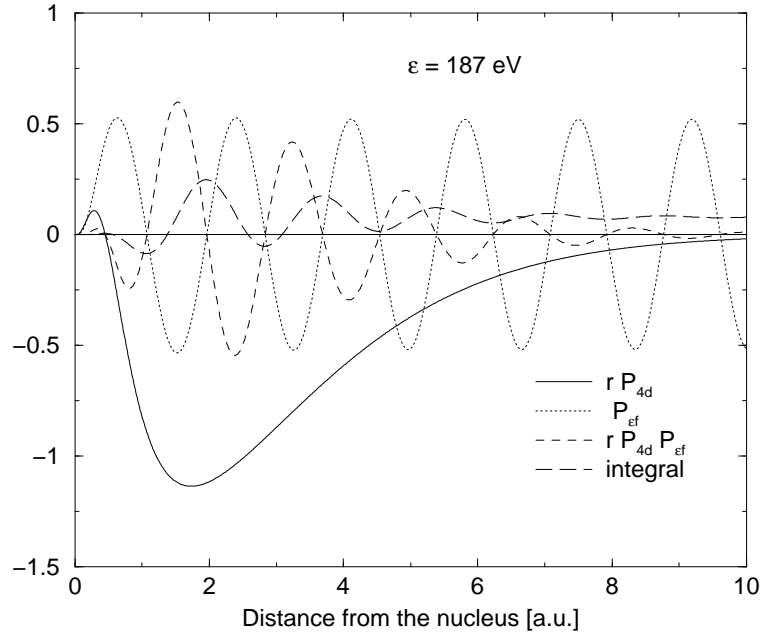


Figure 4.3: Pd ($4d$) and (ϵ, f) wave functions.

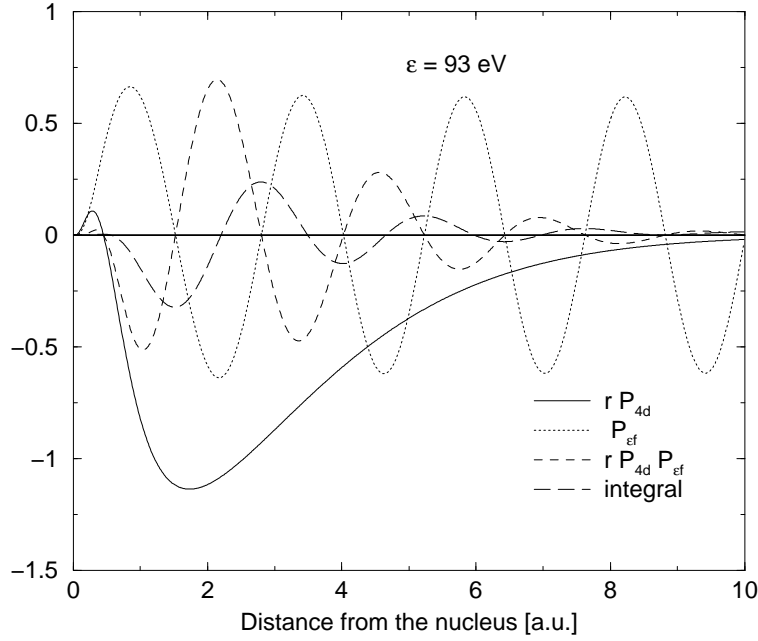


Figure 4.4: Pd ($4d$) and (ϵ, f) wave functions in proximity of the Cooper minimum.

large effects. Calculating the Cooper minimum for the uranium $5f$ states gives around 190 eV in the relativistic case and ca. 5 eV less in the non relativistic one. The reason for this slight change consists in the fact that also the (ϵ, d) and (ϵ, g) wave functions expand as a relativistic effect, such that the overall change of the matrix elements is small. One first important result we achieved is then: *the Yeh and Lindau tables [56] remain valid also if relativistic effects are introduced.*

Isolated atoms are of big pedagogical importance; noble gas systems can be treated as isolated atoms; another and perhaps more important question is what happens in solids. Here, the situation is more complex: overlap is present between valence orbitals belonging to different lattice sites, quantum states are usually described in terms of Bloch waves and the emitted electron can scatter through the lattice. Nevertheless the Yeh and Lindau tables are being used also for solids, whereat in most cases there is a good agreement found between the tabulated Cooper minimum and the observed one.

Recently [57], a new fcc phase of uranium, with an interatomic distance of ca. 3.2 Å, has been detected in ordered films, and in this case a Cooper minimum for the $5f$ shell around 90 eV has been observed [58] instead of the tabulated 200 eV. We already showed that such a large shift cannot be interpreted as a relativistic effect. A calculation with a relativistic layer

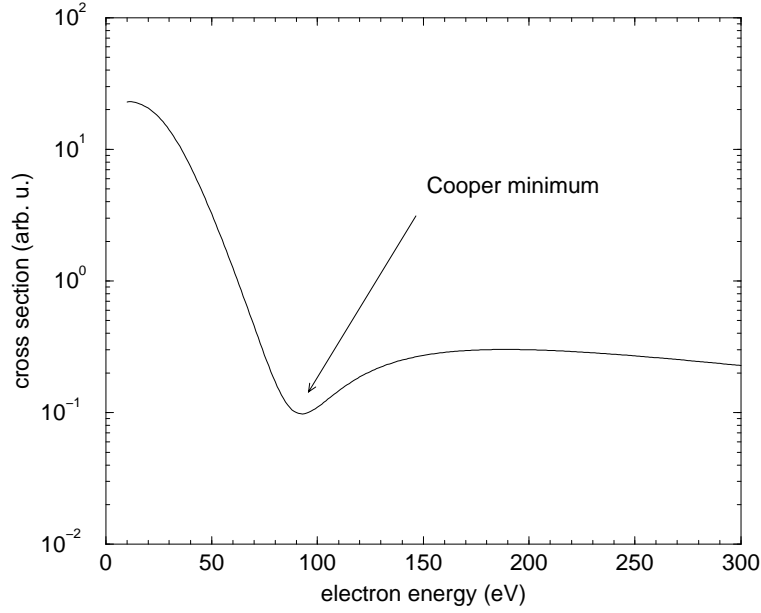


Figure 4.5: Calculated Pd ($4d$) photoemission cross section

KKR was performed by the authors of [58] and again a Cooper minimum around 90 eV was found. It was also possible to calculate the final states density of states and to exclude that this low energy minimum could be connected to a gap or a dip in the DOS. Moreover, calculations on various alloys and compounds containing uranium atoms yielded a similar low energy uranium $5f$ Cooper minimum. It is suggestive to consider this observation as a property of atoms embedded in a metallic surrounding, instead of believing in an accidental coincidence of matrix elements.

Would it be possible, then, to get a Cooper minimum of 90 eV for fcc uranium using some convenient approximation involving only radial isolated atomic wave functions?

Following an analogous approximation used in KKR methods, we inserted a cut-off in the integrals (4.15) such that the integration is performed up to an effective radius which lies half way to the first nearest neighbours. Wave function normalization constants may possibly change, but this will not affect the position of the minimum. In figure 4.6, we show the calculated photoemission cross section involving $5f$ electrons of uranium. The solid line is calculated without a cut-off, while the dotted one with a cut-off of 3.2 a.u. corresponding to half the interatomic distance in fcc uranium. The latter shows two minima at roughly 110 eV and 230 eV. One can also plot the calculated Cooper minima position as a function of the cut-off radius.

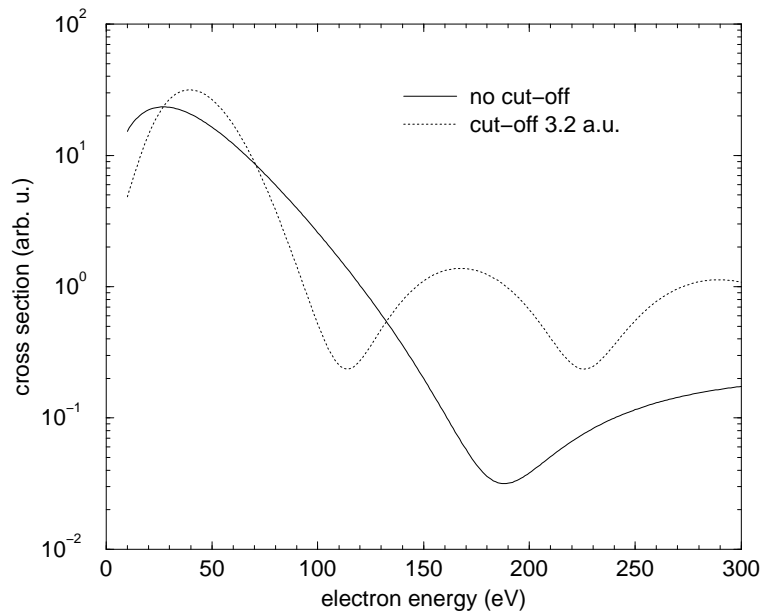


Figure 4.6: U ($5f$) photoemission cross section without an integration cut-off and with a cut-off of 3.2 a.u.

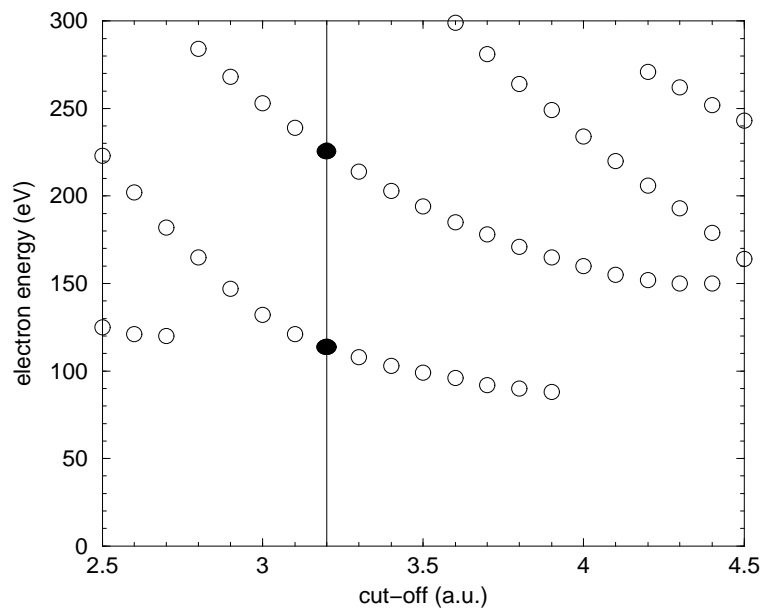


Figure 4.7: U ($5f$) Cooper minima position as a function of the radial cut-off. The black dots correspond to a cut-off of 3.2 a.u.

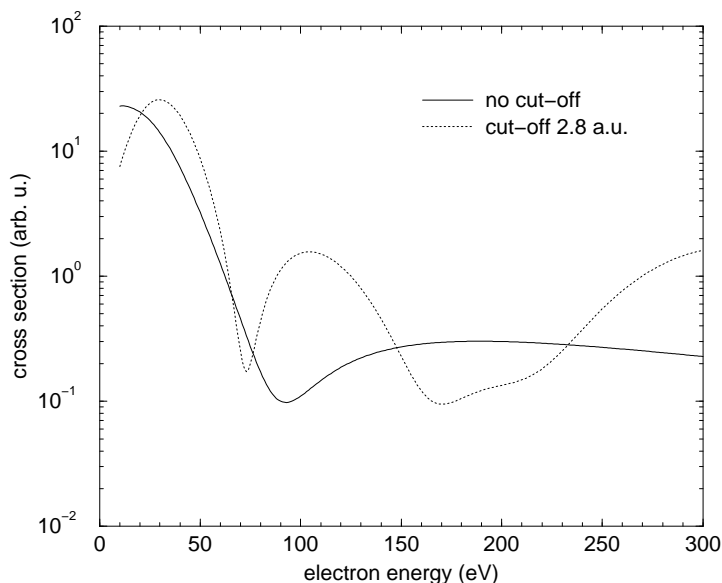


Figure 4.8: Pd ($4d$) photoemission cross section without an integration cut-off and with a cut-off of 2.8 a.u.

As a result the picture 4.7 is obtained. Note that increasing the cut-off value, causes the first minimum position to decrease. This feature can be explained qualitatively in this way: the effective cut-off should be a little bit bigger such to account, in an average way, for other than first neighbours and in fact the experimental value around 90 eV is obtained by a convenient choice of a cut-off radius between 3.6 and 4.0 a.u.

There is also an important new qualitative feature arising from the introduction of a cut-off radius in the calculation of the matrix elements (4.15), namely the presence of more than one minimum. We could explain qualitatively with our cut-off model, the negative energy shift of the Cooper minimum position, at least in uranium $5f$ electrons. It would be nice to have an experimental evidence for at least a second minimum as well, since it seems to be connected in our model to the mentioned energy shift. Having this in mind we performed the same calculations, as done for the uranium $5f$, for fcc palladium (interatomic distance ca. 2.8 Å) $4d$ electrons, which poses less experimental difficulties than uranium and can be, thus, easily investigated. The results are presented in the figures 4.8, 4.9. The experimental results obtained by Dr. S.L. Molodtsov are shown in fig. 4.10. Here, two minima are visible at position 50 eV and 130 eV incident photon energy, where the $4d$ ionization potential is ca. 8 eV. On the vertical axis the intensity of the emitted electrons, proportional to the cross section, has been plotted. The

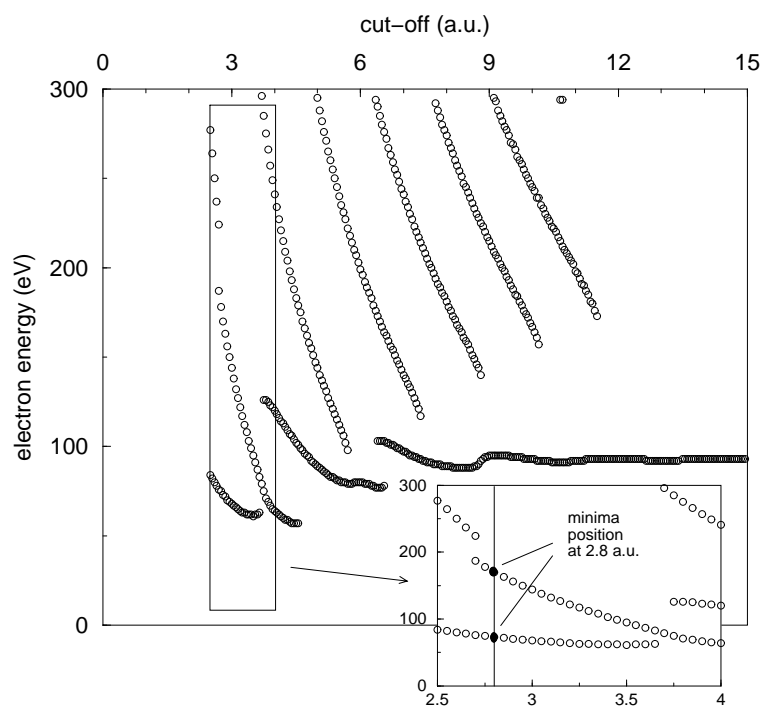


Figure 4.9: Pd ($4d$) Cooper minima position as a function of the radial cut-off. Black dots correspond to a cut-off equal to half the distance to the first neighbours.

experiment was performed on a 100 \AA fcc palladium layer on tantalum.

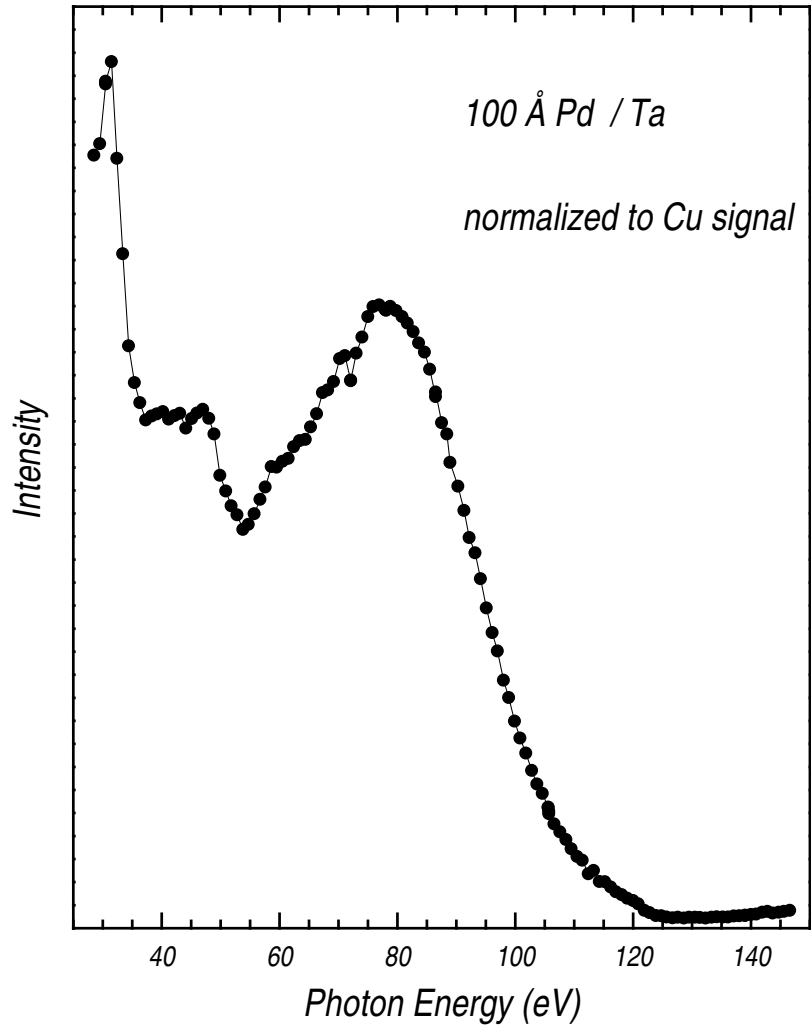


Figure 4.10: Pd ($4d$) experimental photoemission scattered electron intensity (proportional to the cross section of the process) [arb. u.].

Conclusions

The Density Functional Theory (DFT) is a fast tool which allows the calculation of ground state properties of inhomogeneous systems. Unfortunately the DFT must be used in connection with approximations of the exchange and correlation (XC) energy functional. One of these approximation, the simplest one, is the Local Spin Density Approximation (LSDA). The LSDA, despite its simplicity, has almost never been fully analyzed. It was, except in few rare cases in the literature [21, 22, 23], always used in connection with the intra-atomic spin collinearity approximation [59]. The vector spin density inside an atom was always considered parallel to a given axis. From a relativistic treatment of the theory (RDFT), which involves 4-vectors and 4-potentials, it comes out that the effective field which governs the behaviour of the vector spin density, the XC-field, must be a transversal field (its divergence must vanish identically). In the whole work the orbital momentum dependence of the XC-energy functional was neglected (Spin DFT). In a collinear approximation, as far as the field is not constant in space, the condition of transversality cannot be fulfilled. We focused our attention on isolated atoms and ions. What we found is that also considering a more general spin non collinear displacement, the LSDA does not provide a transversal field. It even enhances the source density locally, with respect to the collinear case. A local approximation cannot produce a transversal XC-field, for transversality in all the space is a global requirement. The good news is that total energies and ionization potentials are affected by non collinearity only marginally, i.e. its effect is very small with respect to other underlying approximation corrections. What is influenced in a more sensitive way is the total spin projection along the symmetry axis. In most cases we found a reduction of it. This effect is more evident in those atoms which have high spin-orbit effects on their open shells. Spin-orbit is in fact, the only way to mix the spin-up and spin-down part of the wave function, what generates spin non collinearity, in an isolated system within LSDA. Hence, we found a way to construct, by means of a non local procedure, an XC-transversal field. Again its effects on total energies were negligible, but the spin projection on the symmetry axis

is more quenched than in the non collinear LSDA. This is understandable, since a transversal field must revert its direction in the space. The total energy corrections given by the LSDA non collinear and transversal XC-field have comparable magnitudes but opposite sign. This scores an additional point in favor of the intra-atomic collinear approximation, which is simpler and faster to use, moreover.

Within the spherical and collinear approximation, some restrictions for the applicability of a relativistic self interaction scheme were presented. A fulfilled theoretic prevision on photo emission cross-sections in a solid closes this work.

Bibliography

- [1] E. Fermi, “Un metodo statistico per la determinazione di alcune proprietà dell’atomo”, *Rend. Accad. Naz. Lincei* **6**, 602 (1927).
- [2] L. H. Thomas, “The Calculation of Atomic Fields”, *Proc. Camb. Philos. Soc.* **23**, 542 (1927).
- [3] P. Hohenberg and W. Kohn, “Inhomogeneous Electron Gas”, *Phys. Rev.* **136**, 864 (1964).
- [4] W. Kohn and L. J. Sham, “Self-Consistent Equations Including Exchange and Correlation Effects”, *Phys. Rev.* **140**, 1133 (1965).
- [5] L. N. Oliveira, E. K. U. Gross and W. Kohn, “Density-functional Theory for superconductors”, *Phys. Rev. Lett.* **60**, 2430 (1988).
- [6] A. Griffin, “Rigorous density functional theory for inhomogeneous bose-condensed fluids”, *cond-mat/9511101* (1995).
- [7] M. Petersilka, U. J. Gossmann and E. K. U. Gross, “Excitation energies from time-dependent density-functional theory”, *Phys. Rev. Lett.* **76**, 1212 (1996).
- [8] G. Vignale and W. Kohn, “Current-Dependent Exchange-Correlation Potential for Dynamical Linear Response Theory”, *Phys. Rev. Lett.* **77**, 2037 (1996).
- [9] A. Gonzales, J. A. White, F. L. Roman, S. Velasco and R. Evans, “Density functional theory for small systems: Hard spheres in a closed spherical cavity”, *Phys. Rev. Lett.* **79**, 2466 (1997).
- [10] G. Vignale, C. A. Ullrich and S. Conti, “Time-dependent density functional theory beyond the adiabatic local density approximation”, *cond-mat/9706306* (1997).

- [11] K. Capelle, E. K. U. Gross and B. L. Györfy, “Theory of dichroism in the electromagnetic response of superconductors”, *Phys. Rev. Lett.* **78**, 3753 (1997).
- [12] M. S. S. Brooks, O. Eriksson, J. M. Wills and B. Johansson, “Density functional theory of crystal field quasiparticle excitations and the ab initio calculation of spin hamiltonian parameters”, *Phys. Rev. Lett.* **79**, 2546 (1997).
- [13] M. Städele, J. A. Majewski, P. Vogl and A. Görling, “Exact Kohn-Sham exchange potential in semiconductors”, *Phys. Rev. Lett.* **97**, 2089 (1997).
- [14] M. Seidl, J. P. Perdew and M. Levy, “Strictly correlated electrons in density-functional theory”, *Phys. Rev. A* **59**, 51 (1999).
- [15] N. Argaman and G. Makov, “Density Functional Theory — a brief introduction”, [physics/9806013](#) (1998).
- [16] W. Kohn, Y. Meir and D. E. Makarov, “van der Waals energies in density functional theory”, *Phys. Rev. Lett.* **80**, 4153 (1998).
- [17] O. Gunnarsson and B. I. Lundqvist, “Exchange and correlation in atoms, molecules, and solids by the spin-density-functional formalism”, *Phys. Rev. B* **13**, 4274 (1976).
- [18] R. M. Dreizler and E. K. U. Gross, *Density Functional Theory* (Springer-Verlag, Berlin, Heidelberg, New York, 1990).
- [19] H. Eschrig, *The Fundamentals of Density Functional Theory* (Teubner, Stuttgart, 1996).
- [20] J. P. Perdew, S. Kurt, A. Zupan and P. Blaha, “Accurate density functional with correct formal properties: a step beyond the generalized gradient approximation”, *Phys. Rev. Lett.* **82**, 2544 (1999).
- [21] L. Nordström and D. Singh, “Noncollinear Intra-atomic Magnetism”, *Phys. Rev. Lett.* **76**, 4420 (1996).
- [22] K. Knöpfle, L. M. Sandratskii and J. Kübler, “Symmetry properties of intra-atomic spin and angular momentum densities: application to U_3Sb_4 ”, *J. Phys.: Condens. Matter* **9**, 7095 (1997).
- [23] H. Eschrig and V. D. P. Servedio, “Relativistic Density Functional Approach to Open Shells”, *J. Comp. Chem.* **20**, 23 (1999).

- [24] G. Soff, "Theory of highly-ionized few-electron systems", *Z. Phys. D - Atom Mol Cl* **21 Suppl. S**, S7 (1991).
- [25] E. H. Lieb, "Density Functionals for Coulomb Systems", *Int. J. Quant. Chem.* **XXIV**, 243 (1983).
- [26] L. D. Landau and E. M. Lifshitz, *Quantum Mechanics* (Pergamon Press, London, 1958).
- [27] U. von Barth and L. Hedin, "A Local Exchange-Correlation Potential for the Spin Polarized Case: I", *J. Phys. C* **5**, 1629 (1972).
- [28] A. N. Kolmogorov and S. V. Fomin, *Elementi di teoria delle funzioni e di analisi funzionale* (Mir, Moskow, 1980).
- [29] A. K. Rajagopal and J. Callaway, "Inhomogeneous electron gas", *Phys. Rev. B* **7**, 1912 (1973).
- [30] A. H. MacDonald and S. H. Vosko, "A relativistic density functional formalism", *J. Phys. C* **12**, 2977 (1979).
- [31] G. Vignale and M. Rasolt, "Density-functional theory in strong magnetic fields", *Phys. Rev. Lett.* **59**, 2360 (1987).
- [32] H. Ebert, M. Bottoni and E. K. U. Gross, "Current density functional theory of spontaneously magnetised solids", *Europhys. Lett.* **40**, 545 (1997).
- [33] D. M. Ceperly and B. J. Alder, "Ground State of the Electron Gas by a Stochastic Method", *Phys. Rev. Lett.* **45**, 566 (1980).
- [34] J. P. Perdew and A. Zunger, "Self-interaction correction to density-functional approximations for many-electron systems", *Phys. Rev. B* **23**, 5048 (1981).
- [35] A. Svane, "Comment on "Self-interaction-corrected density-functional formalism"", *Phys. Rev. B* **51**, 7924 (1995).
- [36] F. E. Harris, "Hartree-like methods in electronic structure theory", *Int. J. Quantum Chem.* **13**, 189 (1978).
- [37] J. Forstreuter, L. Steinbeck, M. Richter and H. Eschrig, "Density-functional calculations for rare-earth atoms and ions", *Phys. Rev. B* **55**, 9415 (1997).

- [38] P. Pyykkö, “Relativistic effects in structural chemistry”, *Chem. Rev.* **88**, 563 (1988).
- [39] I. P. Grant, “Relativistic calculation of atomic structures”, *Adv. Phys.* **19**, 747 (1970).
- [40] S. D. Kenny, G. Rajagopal, R. J. Needs, M. J. G. W.-K. Leung, A. J. Williamson and W. M. C. Foulkes, “Quantum Monte Carlo calculations of the energy of the relativistic homogeneous electron gas”, *Phys. Rev. Lett.* **77**, 1099 (1996).
- [41] J. J. Sakurai, *Advanced quantum mechanics* (Addison-Wesley, Canada, 1987).
- [42] P. Cortona, S. Doniach and C. Sommers, “Relativistic extension of the spin-polarized local-density-functional theory: study of the electronic and magnetic properties of the rare-earth ions”, *Phys. Rev. A* **31**, 2842 (1985).
- [43] J. F. Janak and A. R. Williams, “Method for calculating wave functions in a non spherical potential”, *Phys. Rev. B* **23**, 6301 (1981).
- [44] W. Press, S. A. Teukolsky, W. T. Vetterling and B. P. Flannery, *Numerical Recipes in C. The art of scientific computing. 2nd edition.* (Cambridge University Press, Cambridge, 1995).
- [45] J. Forstreuter, *PhD Thesis* (TU Dresden, Germany, 1997).
- [46] C. P. Slichter, *Principles of magnetic resonance* (Springer-Verlag, New York, 1992).
- [47] R. Coehoorn, in *Supermagnets, Hard Magnetic Materials, Lecture notes NATO-ASI*, edited by G. J. Long and F. Grandjean (Kluwer Academic Pub., Dordrecht, 1991), p. 133.
- [48] R. M. Sternheimer, *Phys. Rev.* **95**, 736 (1954).
- [49] H. Ebert, in *Proceedings of an international workshop held at Herrsching, Germany, April 20-23, 1995*, edited by H. Ebert and G. Schütz (Springer, Germany, 1995), pp. 159–177.
- [50] S. Manninen, “Compton scattering: present status and future”, *J. Phys. Chem. Sol.* **61**, 335 (2000).

- [51] P. Carra, M. Fabrizio, G. Santoro and B. T. Thole, “Magnetic x-ray Compton scattering”, *Phys. Rev. B* **53**, R5994 (1996).
- [52] M. J. Cooper and J. A. Duffy, “Spin densities studied in momentum space”, *J. Phys. Chem. Sol.* **61**, 345 (2000).
- [53] H. Kuzmany, *Festkörper Spektroskopie* (Springer-Verlag, Berlin, 1990).
- [54] J. W. Cooper, “Photoionization from outer atomic subshells. A model study”, *Phys. Rev.* **128**, 681 (1962).
- [55] S. T. Manson and J. W. Cooper, “Photo-ionization in the soft x-ray range: Z dependence in a central-potential model”, *Phys. Rev.* **165**, 126 (1968).
- [56] J. J. Yeh and I. Lindau, “Atomic subshell photoionization cross sections and asymmetry parameters: $1 \leq Z \leq 103$ ”, *Atomic Data and Nuclear Data Tables* **32**, 1 (1985).
- [57] S. L. Molodtsov, J. Boysen, M. Richter, P. Segovia, C. Laubschat, S. A. Gorovikov, A. M. Ionov, G. V. Prudnikova and V. K. Adamchuk, “Dispersion of 5f electron states: Angle-resolved photoemission on ordered films of U metal”, *Phys. Rev. B* **57**, 13241 (1998).
- [58] S. L. Molodtsov and S. Halilov, “to be published”, *Phys. Rev. B* .
- [59] L. M. Sandratskii, “Noncollinear magnetism in itinerant-electron systems: theory and applications”, *Adv. Phys.* **47**, 91 (1998).

Acknowledgments

Before I came in this group I actually did not expect to find a second family. I was told, Germans are rather cold. Might be that physics is able to defrost souls. I've only found friendly people around, so it is very difficult to limit the number of people to thank (in fact, since this pamphlet has a finite weight, I managed. Didn't I?). Usually the acknowledgments in a thesis are not censored. One can write all likes, not only positive things, and who knows me can confirm that I would not hesitate to hunt false friends. The first one I would thank is myself. I feel I did a good work. I started from almost zero. It is very hard to survive in our society if you have no money. My dream was to study abroad. I managed.

A very special thank goes to Prof. H. Eschrig who believed in me at the very beginning and fed me with interesting and fruitful ideas.

To Dr. M. Richter I acknowledge many useful discussions, which somehow are contained in this work.

I am grateful to Prof. Dr. H. Ebert for providing his fully relativistic atomic code, which I used as a reference for the developed program.

Dr. P. Oppeneer was decisive for my understanding of MXCD experiments, which was necessary to conclude my thesis.

Thanks to Dr. J. Forstreuter who provided me some tools to start working.

Thanks to Dr. K. Koepernik who supported me psychologically at the beginning, to Dr. H. Rosner and Dr. T. Kraft for their friendship and the relaxing DOOM matches. Thanks to I. Chaplygin for his amusing mathematical puzzles.

A special thank goes also to my italian friends who made me feel like at home (they came into play for this work as well; who is happy produces better): C. Grazioli, A. Amici, P. De Los Rios.

Finally, I thank my **family**.

Versicherung

Hiermit versichere ich, daß ich die vorliegende Arbeit ohne unzulässige Hilfe Dritter und ohne Benutzung anderer als der angegebenen Hilfsmittel angefertigt habe. Die aus fremden Quellen direkt oder indirekt übernommenen Gedanken sind als solche kenntlich gemacht. Die Arbeit wurde bisher weder im Inland noch im Ausland in gleicher oder ähnlicher Form einer anderen Prüfungsbehörde vorgelegt.

Diese Dissertation wurde unter der Betreuung von Prof. Dr. H. Eschrig in der Arbeitsgruppe "Theorie komplexer und korrelierter Elektronensysteme" der Max-Planck-Gesellschaft, am Institut für Theoretische Physik der TU-Dresden und am Institut für Festkörper- und Werkstofforschung Dresden e. V. im Rahmen des Graduiertenkollegs "Struktur- und Korrelationseffekte in Festkörpern" an der Technischen Universität Dresden angefertigt.

Ich erkenne die Promotionsordnung der Fakultät Mathematik und Naturwissenschaften der TU Dresden an.

Dresden, den 29. Februar 2000

Vito D.P. Servedio